Targeting dendritic cells to improve antitumor immunity

Inauguraldissertation
zur
Erlangung der Würde eines Doktors der Philosophie
vorgelegt der
Philosophisch-Naturwissenschaftlichen Fakultät
der Universität Basel

von

Laura Fernández Rodríguez

Basel, 2024

Genehmigt von der Philosophisch-Naturwissenschaftlichen Fakultät auf Antrag von

Erstbetreuer: Prof. Dr. Alfred Zippelius; Zweitbetreuer: Prof. Dr. Jean Pieters; und externer Experte: Prof. Dr. Daniel Speiser.

Basel, den 20.09.2022

Prof. Dr. Marcel Mayor

Dekan

Table of Contents

1. Introduction

1.1. Cancer Immunology

Cancer is one of the world's leading causes of death, accounting for nearly 10 million deaths in 2020 (Ferlay et al., 2021). The accumulation of somatic mutations and epigenetic alterations result in the aberrant growth and proliferation of normal cells that ultimately can cause cancer (Hanahan & Weinberg, 2011; Takeshima & Ushijima, 2019). As a consequence of these genetic alterations, cancer cells can be recognized as non-self by the immune system, initiating cellular immune responses to eliminate the cells. Highly immunogenic cancer cell clones are prone to be eliminated in immunocompetent hosts, a process known as immunoediting (Schreiber et al., 2011). In this context, only poorly immunogenic variants survive and grow in the host leading to established tumors that the immune system can no longer eliminate. The immunoediting process comprises three phases: i) elimination, ii) equilibrium, and iii) escape or evasion. During the elimination phase, the immune system elicits cellular immune responses resulting in the elimination of the tumors. The second phase, equilibrium, is characterized by the survival of some cancer cells, which coexist with the immune system. Finally, specific mutations confer survival advantages to the tumor cells and can no longer be maintained under check by the immune system, eventually dominating the local tissue environment. This process is known as immune escape or evasion (Hanahan & Weinberg, 2011; Schreiber et al., 2011).

Nonetheless, immunogenic cancer cells may also escape the immune system control and establish tumors. For example, cancer cells secrete cytokines that can block the infiltration of dendritic cells (DCs), which recognize tumor-derived antigens and educate other cells to eliminate cancer cells, such as cytotoxic $CD8^+$ T cells (CTLs) and natural killer (NK) cells (Schreiber et al., 2011). In addition, the expression of immune checkpoint molecules in immune and cancer cells (i.e., programmed death 1 (PD-1) and its ligand PD-L1), and the presence of immunosuppressive inflammatory cells, including $CD4^+$ regulatory T cells (Tregs) and

myeloid-derived suppressor cells (MDSCs), contribute to an immunosuppressive microenvironment that ultimately leads to tumor progression (Gajewski et al., 2013; Saleh & Elkord, 2020a).

A successful immune response against cancer relies on the network linking innate and adaptive immunity. First, professional antigen-presenting cells (APCs), mainly DCs, sense, uptake, and traffic tumor antigens to the draining lymph nodes (dLNs). There, DCs prime both tumor-specific $CD4^+$ and $CD8^+$ T cells (Roberts et al., 2016). The activated $CD8^+$ T cells undergo differentiation and acquire cytotoxic effector functions, such as the production of granzymes, perforin, and cytokines, most prominently type II interferon (IFNγ) and tumor necrosis factor α (TNFα) (Chen & Mellman, 2013). These cells can then travel to the tumor, where cytotoxic $CD8^+$ T cells (CTLs) recognize and kill the cancer cells presenting the cognate peptides on the major histocompatibility complex (MHC) class I, resulting in the release of tumor antigens available again to DCs (Chen & Mellman, 2013). $CD4^+$ T are very plastic and undergo polarization into different cell subsets depending on the environmental signals (Patente et al., 2019). In a successful antitumor response, $CD4^+$ T cells recognize endogenously processed antigens presented in MHC-II by tumor cells and provide help to $CD8^+$ T cells (Friedman et al., 2012), or mediate the direct killing of the tumor (Quezada et al., 2010).

Interestingly, some DCs remain within the tumor microenvironment (TME), where they can promote antitumor immunity by supporting incoming T cells with survival signals (Di Pilato et al., 2021) and enabling them to perform their effector functions (Garris et al., 2018).

1.2. Dendritic cell subsets

While being highly conserved between mice and humans (Gerhard et al., 2021), tumor-infiltrating DCs are a sparse and heterogeneous population, which are divided into plasmacytoid DC (pDC) and cDC (Cabeza-Cabrerizo et al., 2021). An additional subset of cells, so-called monocyte-derived DCs (moDCs), are traditionally included in DC subsets. However, these cells arise from blood monocytes and are ontogenically distinct from DCs. Under inflammatory conditions, moDCs travel from the blood to the peripheral tissues, where they exert their functions (Guilliams et al., 2014; Villani et al., 2017). Nonetheless, moDCs generation is an *in vitro* tool for studying mouse conventional DCs, and we will further discuss them in the following chapters, along with the other DC subsets.

cDCs can be identified in mice by CD45, CD11c, and MHC-II expression and the lack of lineage markers characteristic of pDCs, T cells, NK, and B cells (Cabeza-Cabrerizo et al., 2021). cDCs can be further categorized into three transcriptionally distinct states: i) the $CD8\alpha^+$ and/or $CD103^+$ cDC1 subset in mice, corresponding to $CD141^+$ $CLEC9A^+$ $XCR1^+$ cDC1s in humans, ii) the $CD11b^+$ and/or Sirpα cDC2 subset in mice, and $CD1c^+$ cDC2s in humans, and most recently iii) DC3s, which are located in the TME and bear signatures specific for maturation (e.g., CD80, CD86, MHC-II), migration (CCR7), tumor control (IL-12) and also tumor suppression (PD-L1, PD-L2, CD200) (Garris et al., 2018; Maier et al., 2020; Zilionis et al., 2019). As mentioned before, DC3s receive other names, including mregDC (Maier et al., 2020), $LAMP3^+$ DC (Zhang et al., 2019), and $CCR7^+$ DC (Qian et al., 2020); however, all describe the same cellular state (Gerhard et al., 2021; Kvedaraite & Ginhoux, 2022).

Previously, common DC progenitors (CDPs) were thought to give rise to cDC1, cDC2, and pDCs. However, this is not entirely clear, and recent evidence suggests a different progenitor

for pDCs from the lymphoid lineage (Dress et al., 2019; Rodrigues et al., 2018). In mice, pDCs are identified by the expression of CD45, intermediate level of CD11c, B220, Ly6C, and sialic acid-binding immunoglobulin-like lectin H (Siglec-H). In humans, C-type lectin BDCA2, CD4, ILT3, CD68, and the IL-3 receptor α-subunit (CD123) are characteristic of pDCs.

1.3. Dendritic cells in antitumor immunity

DCs are a group of cells resident in almost all body tissues and specialized in the processing and presentation of antigens. Although they are rare within the tumors and dLN, DCs play a central role in initiating and regulating antigen-specific immunity and tolerance in cancer (Cabeza-Cabrerizo et al., 2021; Hildner et al., 2008). DCs can sense the environment surrounding them, detect changes, and quickly react to them, starting a maturation process that ultimately promotes immunity or induces tolerance depending on the ontogenically determined constraints and environmental signals (Cabeza-Cabrerizo et al., 2021; Kvedaraite & Ginhoux, 2022). DCs sense the environmental threats through pattern recognition receptors (PRRs) among other receptors and recognize damage-associated molecular patterns (DAMPs). DAMPs are host-derived motifs associated with cell death and tissue damage, for example, ATP, heat shock proteins (HSP), and high mobility group protein B1 (HMGB1) (Gallo & Gallucci, 2013). In addition, DCs, and particularly conventional DCs (cDCs), recognize and uptake tumor-associated antigens (TAA) from dead neoplastic cells or cellular debris. In non-viral tumors, these antigens include i) mutated antigens (such as mutations in the genes encoding for p53 and Ras proteins) (Gerstung et al., 2020; Robbins et al., 2013); ii) non-mutated antigens overexpressed by cancer cells (e.g., HER-2); and iii) cancer-germline antigens typically expressed by germ cells (ovary and testis) but silent in somatic cells (melanoma-associated antigens (MAGE), and NY-ESO-1) (Schreiber et al., 2011; Vigneron, 2015). The recognition of TAA and proinflammatory signals, including TNFα, IL-1β, CD40L,

and DAMP signals, induce the immunogenic maturation of cDCs. This is characterized by the upregulation of co-stimulatory molecules (e.g., CD80, CD86, and CD40), MHCI class I, T cell adhesion molecules (e.g., CD48 and CD58), MHC-II, and the inflammatory cytokines IL-1β, IL-6, IL-12, and TNFα (Gardner & Ruffell, 2016; Kvedaraite & Ginhoux, 2022; Mellman & Steinman, 2001). MHC class II molecules are sequestered in the endoplasmic reticulum (ER). The stimulatory signals trigger endosomal acidification, leading to the catabolism of tumor antigens and the MHC-II-associated invariant chain. These two steps are required to form the antigen-MHC-II complex in vesicles that then travel to the cell surface (Inaba et al., 2000; Turley et al., 2000). The maturation process is also accompanied by the upregulation of CCR7, which guide the DCs towards the dLN via lymphatic vessels to traffic tumor antigens and prime tumor-specific T cells (Roberts et al., 2016).

Matured DCs interact with T, B, and NK cells, providing immunomodulatory signals through cell-to-cell contact and cytokine secretion(Palucka & Banchereau, 2012). Full activation of naïve T cells requires three distinct signals from DCs: i) The interaction between peptide-MHC complexes in DCs and T cell receptors (TCRs)-CD3 complex in T cells; ii) the positive balance of co-stimulatory molecules over co-inhibitory molecules in the surface of DCs (including CD80, CD86, CD40, 4-1BBL, PD-L1/2) and T cells (CD28, CTLA-4, CD40L, 4-1BB, PD-1); and iii) the signaling provided by the cytokines released by DCs and T cells (Cabeza-Cabrerizo et al., 2021; Kvedaraite & Ginhoux, 2022; Schwartz, 2003; Sckisel et al., 2015). For example, IL-12 promotes the polarization of CD4 T cells towards IFNγ and TNF secreting $CD4^+$T helper cells (Th1), key players of $CD8^+$ T and NK cell-mediated tumor killing (Lasek et al., 2014).

Importantly, in the absence of stimuli, DCs induce peripheral tolerance. It is mediated mainly by two distinct mechanisms: i) clonal deletion of antigen-specific T cells, mediated by

Fas/FasL, TRAIL/TRAILR, and PD-1/PD-L1, and ii) the differentiation and expansion of $CD4^+$ $CD25^+$ $FoxP3^+$ regulatory T cells (Domogalla et al., 2017; Palucka & Banchereau, 2012). Therefore, although DC maturation can occur in tumors, it is often insufficient to render successful antitumor immunity.

1.3.1. cDC1

Both mouse and human cDC1 excel at inducing cellular immunity against tumors and intracellular pathogens, and their abundance and transcriptional signature are associated with better survival and responsiveness to ICI (Barry et al., 2018; Böttcher et al., 2018; Böttcher & Reis e Sousa, 2018; Spranger et al., 2017). cDC1s efficiently process and cross-present antigens through MHC-I and activate effector $CD8^+$ T cells (Broz et al., 2014). In addition, $CD103^+$ cDC1s were the only APC able to transport intact antigens to the LN and prime $CD8^+$ T cells in mouse melanoma models (Salmon et al., 2016). Although cDC2s also migrate to the dLN, it seems that the only cDCs able to deliver the intact tumor antigen to the dLN are cDC1. Moreover, it has been recently shown that cDC1 can support the polarization of $CD4^+$ T cells towards Th1 to provide help to tumor-specific $CD8^+$ T cells (Ferris et al., 2020).

Intratumoral DCs can also release cytokines to promote T cell infiltration. For example, cDC1s are the primary producers of the chemokine ligand CXCL9 and CXCL10, which attracts $CXCR3^+$ $CD8^+$ effector T cells and other cells expressing CXCR3 such as NK cells or ILC1 into tumors, promoting tumor clearance (Mikucki et al., 2015; Spranger et al., 2017; Wendel et al., 2008). Of note, in human melanoma metastasis, CXCL9, CXCL10, CXCL11, and CD8 T cell scores correlate with $XCR1^+$ DCs (Spranger et al., 2017). In addition, the presence of NK cells and $CD141^+$ cDC1 correlates with responsiveness to anti-PD-1 therapy in melanoma patients (Barry et al., 2018).

1.3.2. cDC2

cDC2 are more abundant and heterogeneous than cDC1. cDC2s are often described as potent drivers of $CD4^+$ helper T cells polarization (Binnewies et al., 2019; Cabeza-Cabrerizo et al., 2021). Also, mouse and human cDC2 have been described to activate cytotoxic $CD8^+$ T cells in the presence of TLR agonists (Desch et al., 2014; Mittag et al., 2011). Recent single-cell RNA sequencing data revealed two distinct cDC2 subsets in human blood: $CD5^+$ $CD163^-$ $CD14^-$ cDC2s and $CD5^-$ $CD163^+CD14^+$ cDC2s (Dutertre et al., 2019). The latter subpopulation was shown to prime naïve $CD8^+$ T cells into tissue-homing $CD103^+$ T cells under inflammatory conditions (Bourdely et al., 2020) and induced $CD4^+$ helper T cell response and IL-17 production (Segura et al., 2013). These cells are defined as inflammatory DCs, as they are present only under inflammatory conditions (Segura et al., 2013). It has been proposed that they evolve independently from CDPs, such as cDC1 and traditional cDC2 while depending on GM-CSF (Cytlak et al., 2020). However, the role of both cDC2 subpopulations in antitumor immunity needs to be further studied, as it likely depends on the tumor type.

1.3.3. DC3

Lastly, DC3s were first identified as tumor-associated DCs in lung adenocarcinoma (Zilionis et al., 2019) and have been found across many different cancer indications (Cheng et al., 2021; Maier et al., 2020; Qian et al., 2020; Zhang et al., 2019). DC3s are considered a cell state rather than a cell subset conserved across DC lineages. They are characterized by the expression of maturation (CD80, CD86, CD40), tumor control (IL-12), migration (CCR7), and immunosuppression (PD-L1). The latter likely limit their antitumor activity, and thus they were called "matured DCs enriched in immunoregulatory molecules" (mregDCs) (Maier et al., 2020). They likely derive from cDC1 and cDC2 in both humans and mice (Maier et al., 2020; Zilionis et al., 2019); however, it remains unclear how they acquire their regulation program

(Gerhard et al., 2021). Despite expressing CCR7, some of these cells stay in the tumor, supporting incoming T cells with survival signals (Di Pilato et al., 2021) and their effector functions (Garris et al., 2018). The LAMP3 marker, characteristic of DC3s, has been associated with better survival in patients across different cancer entities, including $HER2^+$ breast cancer (de Mingo Pulido et al., 2021), lung cancer (Germain et al., 2014), and metastatic melanoma (Movassagh et al., 2004).

1.3.4. Plasmacytoid dendritic cells

During viral infections, pDCs are specialized in the production of type I interferons (IFNs) (Swiecki & Colonna, 2015). In addition, they have been shown to rapidly initiate $CD8^+$ T cell responses (Di Pucchio et al., 2008). Also, upon TLR stimulation, pDCs can act as APCs mediating $CD4^+$ T cells activation, as similarly to cDCs, they also express MHC-II and co-stimulatory molecules, including CD80, CD86, and CD40 (Swiecki & Colonna, 2015). However, the antitumor immune response mediated by pDCs appears to be impaired in cancer (Koucký et al., 2019). Often, intratumoral pDCs are associated with poor prognosis (Jensen et al., 2012; Labidi-Galy et al., 2012; Sosa Cuevas et al., 2022).

1.4. The impact of tumor microenvironment in DCs

1.4.1. Inhibition of DC recruitment

The tumor microenvironment consists of cancer and non-cancer cells, including stromal cells, immune cells, and non-cellular components. The interaction of the cells residing in the TME and the secretion of extracellular matrix, cytokines, and chemokines contribute to establishing a local immunosuppressive milieu, allowing cancers to evade the control exerted by the immune system (Baghban et al., 2020). For example, tumor cells preferentially express

chemokines, including CCL2 and CCL22, to attract MDSCs and Treg cells, respectively, which contribute to the immunosuppressive environment (Nagarsheth et al., 2017).

It has been shown that β-catenin$^+$ tumors reduce CCL4 expression, a key chemokine in the recruitment of cDC1 into the tumor microenvironment, resulting in poor cDC1 infiltration and increased tumor growth (Spranger et al., 2015). In contrast, tumor-infiltrated NK cells, primarily resident CD49$^+$ NK, produce CCL5 which guides cDC1 infiltration within the TME, further supporting DC-CD8$^+$ T cell interactions and tumor control (Kirchhammer et al., 2022). However, a downside effect of CCL5 is that it can also promote the migration of macrophages and Tregs into the TME (Halama et al., 2016; Tan et al., 2009). In addition, NK cells can also produce XCL1 and FLT3L, influencing the cDC1 infiltration, positioning, and survival within the tumor microenvironment (Barry et al., 2018; Böttcher et al., 2018). However, tumor cells can inhibit NK survival and chemokine secretion by producing prostaglandin E_2 (PGE_2) and reducing the expression of chemokine receptors in cDC1 (Böttcher et al., 2018).

1.4.2. Impairment of intratumoral DC maturation

In addition to the presence of immunostimulatory TAA, the type of cell death and the local and systemic immune suppression caused by the tumor influence the degree of intratumoral DC maturation (Böttcher & Reis e Sousa, 2018; Gardner & Ruffell, 2016). For example, the DAMPs released during immunogenic cell death include the exposure of calreticulin and HSP on the cell surface, secretion of ATP, and release of HMGB1 (Fucikova et al., 2020). The recognition of nucleic acids released by tumor cells is mediated by HMGB1 (Yanai et al., 2009). This process is inhibited by T cell immunoglobulin mucin receptor 3 (Tim3), highly expressed in intratumoral DCs (Chiba et al., 2012), thus limiting the detection of dying cells by DCs. In addition, Tim3 inhibits the production of CXCL9 by XCR1$^+$ cDC1 (de Mingo

Pulido et al., 2021) and prevents the maintenance of $CD8^+$ effector and stem-like T cells by regulating the inflammasome activation (Dixon et al., 2021).

Several soluble factors secreted by tumor cells influence the maturation and differentiation of DCs, including the vascular endothelial growth factor (VEGF), TNF-β, IL-10, and IL-6 (Wculek et al., 2020)). For example, VEGF inhibits the differentiation and maturation of DCs by blocking NF-κB signaling in DC progenitor cells (Shi et al., 2014). Tumor-derived TGF-β mediate the downregulation of DC maturation markers CD80, CD86, and MHC-II, and the inhibition of proinflammatory cytokines IL-12, IL-1, TNFα, and IFN-α. Additionally, TGF-β inhibits the production of INFα by pDCs (Sisirak et al., 2012). Also, TGF-β induces an immunoregulatory program in DCs by promoting the release of TGF-β itself and influencing the polarization of DCs towards a regulatory phenotype. Regulatory DCs promote the differentiation of Tregs while suppressing the proliferation of effector T cells (Seeger et al., 2015). Both IL-10 and IL-6 are secreted by tumor and immune cells and inhibit the production of IL-12 production by DCs (Wculek et al., 2020).

1.4.3. PD-L1 immune checkpoint and DCs

In a steady state, DCs express the checkpoint molecule PD-L1, also known as B7-H1 and CD274. PD-L1 in DCs is further upregulated upon activation (Maier et al., 2020). PD-L1 is the ligand for PD-1, also known as CD279, predominantly expressed by antigen-stimulated T cells. Upon binding to PD-L1, PD-1 exerts inhibitory signals in T cells, suppressing T cell effector functions (activation, proliferation, and cytokine production) (Riley, 2009). However, PD-L1 can also interact in *cis* with CD80 on the surface of DCs (Zhao, Lee, et al., 2019). Whether the interaction PD-L1/CD80 leads to the upregulation of IL-6 or IFNγ similar to the interaction CD80/CD28 during DC/T cell engagement (Topalian et al., 2016), remains unknown. What

has been shown is that the interaction PD-L1/CD80 prevents PD-L1 from interacting with PD-1 (Sugiura et al., 2019; Zhao, Lee, et al., 2019), and loss of PD-L1 impedes CD80 upregulation by DCs (Lucas et al., 2020).

In addition to DCs, PD-L1 is expressed by cancer cells, macrophages, T and B cells, and endothelial cells, and its expression is tightly regulated by proinflammatory cytokines (Yamaguchi et al., 2022). PD-L1 expressed by DCs, despite being a minority of cells within the tumor microenvironment and being outnumbered by PD-L1^{+} macrophages, are critical regulators of T-cell immunity in cancer. Loss of PD-L1 in DCs, and not in macrophages leads to enhanced CD8^{+} T cell responses and impaired tumor growth in mice (Oh et al., 2020). Therefore, it is crucial to understand the contribution of immune checkpoint molecules in different cell subsets to design successful and targeted therapeutic approaches.

One major regulator of PD-L1 expression in the tumor microenvironment is IFNγ, secreted by cytotoxic T cells and NK cells (Garcia-Diaz et al., 2017). IFNγ is essential for successful antitumor immunity inhibiting the proliferation and inducing the apoptosis of cancer cells and, simultaneously, enhancing cytotoxic CD8+ T cell responses (Ni & Lu, 2018). This suggests that IFNγ-mediated upregulation of PD-L1 in tumors reflects a negative feedback loop due to the antitumor immune response orchestrated by T and NK cells. In addition to cytokines, TLR signaling upregulates PD-L1 expression in DCs (Lu, 2014).

PD-L1 also signals via its cytoplasmatic domain, a process known as reverse signaling (Lecis et al., 2019). While PD-L1 reverse signaling in cancer cells has been associated with epithelial to mesenchymal transition (EMT) in human esophageal cancer and tumor progression (Chen et al., 2017), little is known about reverse signaling in immune cells (Lecis et al., 2019; Tamburini, 2021). Interestingly, the loss of PD-L1 has been linked to reduced DC migration

towards the dLN during inflammation (Lucas et al., 2020). However, the exact mechanism remains unknown.

PD-L1 can also be secreted into the extracellular space or be translocated to the nucleus (W. Xiong et al., 2021). In tumor cells, nuclear PD-L1 was shown to interact with several transcription factors involved in immune-response-related genes, leading to the expression of other immune checkpoint molecules, including PD-L2 and V-domain immunoglobulin suppressor of T cell activation (VISTA) (Gao et al., 2020). Blocking the nuclear translocation of PD-L1 led to enhanced antitumor response to PD-1 blockade (Gao et al., 2020). However, the role of nuclear PD-L1 in immune cells, particularly in DCs, remains unsolved.

1.5. Cancer therapies

Over the last decade, many cancer therapies targeting the host immune system have emerged (Galluzzi et al., 2014). Monoclonal antibodies targeting CTLA-4 and the PD-1/PD-L1 axis, cancer vaccines, cell therapies, and oncolytic viruses are examples of such therapies (Tang et al., 2018; Wei et al., 2018). Targeting suppressive pathways affecting DCs and their direct activation unleash adaptive immunity and generate tumor-specific T cell responses (Wculek et al., 2020). Here, we focus on immunotherapies and chemotherapies modulating DCs to improve antitumor immunity.

1.5.1. Immunostimulatory chemotherapeutics

Originally, chemotherapeutics were designed to target malignant cells, limit their proliferation, or induce cell death. However, some of these anticancer agents interact with the host immune system and enhance antigen cross-presentation, induce DC maturation, or immunogenic tumor cell death (ICD), thereby reactivating pre-existing antitumor responses (Zitvogel et al., 2013).

Chemotherapy can induce direct or indirect DC activation. For example, anthracyclines can induce immunogenic cell death, which releases DAMPs and increases antigen availability within the TME to APCs, promoting antitumor T cell responses, in addition, to modulate the expression of PD-L1 in tumor cells (Michaud et al., 2011). Also, anthracyclines activate the expression of TLR3, induce the secretion of type I interferons, and release of CXCL10 (Emens & Middleton, 2015). Of note, it has been shown that chemotherapy results in the destabilization of the microtubules (i.e. ansamitocin-P3 or dolastatin-10) and not microtubule-stabilizing agents (MSA) (i.e. taxanes) were able to induce DC maturation leading to improved antitumor immunity in mice (Martin et al., 2014; Muller et al., 2014). Moreover, antibody-drug conjugates (ADCs) linking dolastatins and anti-CD30 antibodies showed durable objective responses with tumor regression in lymphoma patients (Ansell et al., 2022; Müller et al., 2014), showing the clinical relevance of such therapies. However, the mechanisms for the induction of DC maturation by microtubule-destabilizing agents (MDAs) remain elusive.

Microtubules are a very dynamic component of the cytoskeleton involved in maintaining cell structure, mitosis, and migration, providing a platform for intracellular transport of vesicles (Cirillo et al., 2017). The guanine nucleotide exchange factor-H1 (GEF-H1) binds to the microtubules in its inactive form. Upon microtubule perturbation, GEF-H1 dissociates from microtubules and becomes active, mediating the exchange of GDP and GTP on RhoA GTPases (Krendel et al., 2002; Matsuzawa et al., 2004), suggesting that this molecule can sense the destabilization of the microtubules. Several transcription factors are regulated by RhoA, including AP-1 and NF-κB (Kim et al., 2018). Interestingly, GEF-H1 has been shown to initiate intracellular signaling, leading to the release of proinflammatory cytokines in macrophages (Chiang et al., 2014), making GEF-H1 an attractive candidate responsible for DC maturation

upon microtubule destabilization. A detailed characterization of the immune activation pathways in DCs downstream of microtubule perturbation is one focus of this thesis, and we study whether GEF-H1 contributes to this process.

1.5.2. Immune checkpoint inhibitors and DCs

Therapeutic targeting of the immunosuppressive pathways driven by the interaction of immune checkpoint molecules and their ligands, amplifies basal antitumor responses initially primed by DCs (Ribas & Wolchok, 2018). As a result, immune checkpoint inhibitors (ICI) have had great success in clinical oncology. Multiple cancer entities have shown sustained and durable clinical responses, however only in a minority of patients (Shen & Zhao, 2018).

CTLA-4 mAb

Antibodies targeting cytotoxic T lymphocyte antigen 4 (CTLA-4) and the PD-1/PD-L1 axis have been approved for several cancer entities (Hargadon et al., 2018). The co-inhibitory receptor CTLA-4 is upregulated in T cells following TCR engagement, binding with greater affinity than its co-stimulatory counterpart CD28 to CD80/CD86 expressed in DCs. Furthermore, CTLA-4 transduced negative signals in effector T cells through phosphatases limiting T cell activation during primary and memory immune responses (Hargadon et al., 2018; Qureshi et al., 2011; Rowshanravan et al., 2018). Monoclonal antibodies (mAbs) targeting CTLA-4 promotes T cell effector functions and reduce Treg-associated immunosuppression (Liu & Zheng, 2020). Intratumoral Treg cells express high levels of surface CTLA-4. It has been shown that in mice, anti-CTLA-4 mAb treatment leads to Treg depletion in an Fc-dependent manner, resulting in an intratumoral increase of T effector to Treg cell ratio (Teff/Treg), essential for the therapeutic efficacy of the compound (Selby et al., 2013; Simpson et al., 2013). However, the depletion of Tregs during anti-CTLA-4 treatment in

patients is controversial and not entirely clear (Arce Vargas et al., 2018; Gan et al., 2022; Sharma et al., 2019).

PD-1/PD-L1 mAb

In addition to CTLA-4 mAb, mAbs that modulate the PD-1/PD-L1 axis are widely and successfully used in cancer patients (Schachter et al., 2017). Several mAbs targeting PD-1 (i.e., pembrolizumab and nivolumab) and PD-L1 (atezolizumab and durvalumab) have become a standard of care in the treatment of melanoma, non-small cell lung cancer (NSCLC), head and neck squamous cell carcinoma (HNSCC), mismatch repair-deficient (dMMR) and microsatellite-instable (MSI-H) colorectal cancer among others(Pan et al., 2020). In addition, pembrolizumab has been approved for any tumor presenting high microsatellite instability (MSI-H) or mismatch repair deficient (dMMR) (Pan et al., 2020; Robert, 2020; Yamaguchi et al., 2022). However, despite the unprecedented clinical efficacy of these monoclonal antibodies, the majority of patients develop primary or acquired resistance (Sharma et al., 2017). CTLA-4 and PD-1 mAbs seem to target non-redundant pathways (Wei et al., 2019) and their combination or combination with chemotherapy and targeted therapies have been used to treat patients otherwise refractory to other treatments (Bashraheel et al., 2020; Blank et al., 2018; Hellmann et al., 2018).

While a complete understanding of the mechanisms that contribute to efficacy and resistance is still lacking, there are several limitations of using blocking antibodies targeting immune checkpoint molecules. For example, some mAbs present a poor tissue permeability leading to limited activity. Also, the antibody-receptor complexes can be internalized from the cell surface by intratumoral host cells, such as macrophages, a process mediated by the Fc receptor (Arlauckas et al., 2017; H. Jin et al., 2021), thereby reducing antibody bioavailability and consequently overall efficacy. Furthermore, mAbs are directed only toward cell-surface

receptors on the target cells (Imai & Takaoka, 2006). Thus, multiple approaches, including small molecules and antisense oligonucleotides (ASOs), are being explored to overcome these challenges and develop more efficient therapeutic modalities targeting the PD-1/PD-L1 axis (Yamaguchi et al., 2022).

Numerous antibodies and small molecules targeting other putative immune checkpoints, including LAG3, TIM3, TIGIT, CD39, and CD73, to disrupt the negative interactions between T cells and tumor cells, or myeloid cells and T cells, are currently under preclinical and clinical development (Perrot et al., 2019; Qin et al., 2019). A deeper understanding of the mechanisms underlying the activity of ICI is fundamental for further improvement of the therapies.

1.5.3. Small molecules

As described above, tumor cells can influence the maturation of intratumoral DCs. For example, the secretion of IL-10, IL6, and VEGF expression lead to the hyperactivation of STAT3 signaling, promoting tumor growth and inhibiting DC-mediated antitumor response (Zou et al., 2020). Several compounds, including small molecules and antisense oligonucleotides, targeting STAT3 are under development in preclinical and clinical trials (Zou et al., 2020). A study showed that the STAT3 inhibitor JSI-124 reversed the suboptimal DC function in cancer (Nefedova et al., 2005). Furthermore, its combination with a TLR agonist increased antitumor efficacy in a murine melanoma tumor model (Molavi et al., 2008). In humans, the inhibition of STAT3 has a weak effect on DC dysfunction, but the co-inhibition with the mitogen-activated protein kinase (MAPK), also involved in IL-10, IL-6 and VEGF signaling, restores the differentiation and immunostimulatory capacity of DCs (Oosterhoff et al., 2012).

1.5.4. Antisense oligonucleotides

Antisense oligonucleotides represent a new strategy for cancer immunotherapy. First, they recruit the enzyme RNase H upon binding to the target pre-mRNA, leading to efficient degradation (Gagliardi & Ashizawa, 2021). Second, the targeting of pre-mRNA allows the downregulation of targets present in different cellular locations (e.g., intracellular, secreted and surface) (Jaschinski et al., 2015). For example, preclinical and clinical studies used second generation ASOs to target STAT3 in neuroblastoma (Odate et al., 2017) and leukemia (Shastri et al., 2018). Also, the combination of a CD39-targeting ASO with an anti-PD-1 mAb improves antitumor responses in preclinical models (Kashyap et al., 2019).

In addition, due to their DNA-based chemical structure, ASOs can mimic microbial infections and elicit immune stimulation by activating PRRs. For instance, Toll-like receptor 9 (TLR9) is a PRR expressed by different types of immune cells including DCs and is activated by extracellular DNA, especially DNA-containing unmethylated CpG motifs frequently present in bacterial DNA (Hemmi et al., 2000). Intratumoral administration of CpG-based ASOs, triggering TLR9, have shown promising results in preclinical (Humbert et al., 2018; Nierkens et al., 2009; Sato-Kaneko et al., 2017) and clinical studies (Ribas et al., 2021). The treatment with the TLR9 agonist vidutolimod in combination with pembrolizumab showed therapeutic benefit in metastatic melanoma patients resistant to anti-PD-1 antibodies (Ribas et al., 2021). Presumably, their efficacy may rely on the alteration of local inflammation, modifying the tumor microenvironment. However, the mechanism is not yet understood. The second part of this thesis aims to overcome PD-1/PD-L1 mAb limited therapeutic efficacy using an ASO-based therapeutic strategy with the dual capacity to trigger DC activation and modulate PD-L1 expression in mice.

1.5.5. Cancer Vaccines

Cancer vaccines based on DCs relies on the ability of these cells to recognize, internalize, process and present antigens derived from tumors to T cells, inducting cytotoxic T cell immune responses and long-lasting tumor control or eradication. Distinct stimuli and spatial location leads to different immune responses elicited by DCs (Filin et al., 2021).

Ex vivo-generation of cancer vaccination consist in the reinfusion of isolated DCs previously pulsed with tumor antigens or tumor lysates and stimulated *ex vivo* or inducing the uptake of tumor-antigens by DCs *in vivo* (Palucka & Banchereau, 2012). For example, Sipuleucel-T is an FDA approved DC vaccine, that showed improved overall survival in patients with advanced prostate cancer (Higano et al., 2009; Kantoff et al., 2010). However, the benefit of DC vaccinations is limited.

The source of DCs, the selection of tumor antigens and stimuli are essential for the clinical success of DC-based vaccines. In most preclinical studies DCs used for vaccinations are derived from bone marrow, and for most clinical trials monocyte-derived DCs are used. These subsets are believed to be counterparts of inflammatory DCs rather than resident DCs, lacking strong T cell stimulatory capacity (Filin et al., 2021; Gu et al., 2020; Kvedaraite & Ginhoux, 2022). The use of tolerogenic and dysfunctional DCs contribute to the limited success of DC-vaccination studies. It might be worth attempting to derive alternative DCs resembling lymphoid-tissue resident DCs.

2. Aim of the project

Dendritic cells play a central role in initiating and regulating antigen-specific immunity in cancer. However, they are influenced by the tumor microenvironment, and often DC maturation is insufficient, leading to poor antitumor immunity (Corrales et al., 2017). Despite the major advances in recent years, the current clinical success of cancer therapies is limited, and most patients who initially respond to the treatment later develop intrinsic or acquired resistance (Sharma et al., 2017). In this thesis, we aim to better understand and improve cancer therapies targeting DCs, which are a promising strategy to enhance antitumor immunity. To do so, we first aim to study the downstream molecular mechanisms that leads to effective DC maturation during immunostimulatory chemotherapies, specifically microtubule-destabilizing agents. Secondly, we aim to improve the limited therapeutic efficacy of anti-PD-L1 mAb by using an ASO-based strategy with the dual capacity of triggering DC activation via TLR engagement and control of PD-L1.

3. Results and discussion

3.1. GEFH1 signaling upon microtubule destabilization is required for dendritic cell activation and specific anti-tumor responsesPD-L1 ASO

Abhishek S Kashyap[1,2*], Laura Fernandez-Rodriguez[1#], Yun Zhao[2#], Gianni Monaco[1], Marcel P Trefny[1], Naohiro Yoshida[2], Kea Martin[1,6], Ashwani Sharma[3], Natacha Olieric[3], Pankaj Shah[2], Michal Stanczak[1], Nicole Kirchhammer[1], Sung-Moo Park[2], Sebastien Wieckowski[1,7], Heinz Laubli[1,4], Rachid Zagani[2], Benjamin Kasenda[4], Michel O Steinmetz[3,5], Hans-Christian Reinecker[2#*], Alfred Zippelius[1,4#*]

# equal contribution

[1]Department of Biomedicine, University Hospital Basel and University of Basel, 4031 Basel, Switzerland
[2]Gastrointestinal Unit and Center for the Study of Inflammatory Bowel Disease, Massachusetts General Hospital, Harvard Medical School, 02114 Boston, USA
[3]Laboratory of Biomolecular Research, Division of Biology and Chemistry, Paul Scherrer Institut, 5232 Villigen, Switzerland
[4]Medical Oncology, University Hospital Basel, 4031 Basel, Switzerland
[5]University of Basel, Biozentrum, CH-4056 Basel, Switzerland
[6]current address: Novartis Institute of Biomedical Research, 4002 Basel, Switzerland
[7]current address: Vaximm AG, 4057 Basel, Switzerland

Lead contact: Alfred Zippelius: alfred.zippelius@usb.ch

* Address correspondence to:

Alfred Zippelius: alfred.zippelius@usb.ch

Hans-Christian Reinecker: hans-christian_reinecker@hms.harvard.edu

Abhishek Kashyap: abhishek.kashyap@unibas.ch

Adapted from the publication: Kashyap, A. S., Fernandez-Rodriguez, L., Zhao, Y., Monaco, G., Trefny, M. P., Yoshida, N., ... & Zippelius, A. (2019). GEF-H1 signaling upon microtubule destabilization is required for dendritic cell activation and specific anti-tumor responses. Cell reports, 28(13), 3367-3380.

DOI: https://doi.org/10.1016/j.celrep.2019.08.057

3.1.1. Summary

Dendritic cell (DC) activation is a critical step for antitumor T cell responses. Certain chemotherapeutics can influence DC function. Here we demonstrate that chemotherapy capable of microtubule destabilization has direct effects on DC function; namely, it induces potent DC maturation and elicits antitumor immunity. Guanine nucleotide exchange factor-H1 (GEF-H1) is specifically released upon microtubule destabilization and is required for DC activation. In response to chemotherapy, GEF-H1 drives a distinct cell signaling program in DCs dominated by the c-Jun N-terminal kinase (JNK) pathway and AP-1/ATF transcriptional response for control of innate and adaptive immune responses. Microtubule destabilization, and subsequent GEF-H1 signaling, enhances cross-presentation of tumor antigens to $CD8^+$ T cells. In absence of GEF-H1, antitumor immunity is hampered. In cancer patients, high expression of the GEF-H1 immune gene signature is associated with prolonged survival. Our study identifies an alternate intracellular axis in DCs induced upon microtubule destabilization in which GEF-H1 promotes protective antitumor immunity.

3.1.2. Introduction

Because of their efficient antigen processing and presentation machinery, antigen-presenting cells, such as dendritic cells (DCs), play a central role in the initiation and regulation of specific antitumor immunity (Melief, 2008). DC maturation is necessary for antigen processing and to provide costimulatory signals to T cells (Mildner & Jung, 2014). Although DC maturation may occur in tumors, it is often insufficient to induce potent immunity and hindered by suppressive mechanisms within tumors (Corrales et al., 2017). Furthermore, in contrast to mature or activated DCs, immature DCs are tolerogenic, immunosuppressive, and lead to deficient antitumor immunity (Gardner & Ruffell, 2016). Bypassing suppressive pathways or directly activating DCs can unleash adaptive immunity through cross-presentation of tumor antigen to generate tumor-specific T cell responses (Wei et al., 2018). Hence, the therapeutic targeting of DC maturation or activation processes is a promising strategy to enhance antitumor immunity.

DC maturation is conventionally known to be a consequence of the engagement of pattern recognition receptors (PRRs, including Toll-like receptors (TLRs) and nucleotide-binding domain, leucine rich containing (NLRs)) and/or the CD40-CD40L axis (Gardner & Ruffell, 2016; Kawai & Akira, 2011). The perturbation of microtubules has emerged as an exciting and promising medical concept that potently triggers DC maturation (Muller et al., 2015). As a therapeutic consequence, the targeted delivery of microtubule-destabilizing agents (MDAs) can induce potent anticancer adaptive immunity, which can be boosted by immune checkpoint inhibitors. Specifically, antibody drug conjugates (ADCs) incorporating MDAs, such as the maytansine DM1 (trastuzumab emtansine) or the auristatin monomethyl auristatin E (MMAE) (brentuximab vedotin), activate DCs (Muller et al., 2015; Muller et al., 2014) and are of high clinical relevance (Connors et al., 2018; Verma et al., 2012; von Minckwitz et al., 2019; Younes et al., 2010). This DC activation enhances the capture of tumor antigens and the production of proinflammatory cytokines, which improves the intratumoral infiltration of tumor antigen-

specific effector T cell populations and therapeutic synergy with immune checkpoint inhibitors (Muller et al., 2015). MDAs administered as free drugs, such as vinblastine (Tanaka et al., 2009), colchicine (Mizumoto et al., 2007), ansamitocin-P3 (Martin et al., 2014), and dolastatin-10 (Muller et al., 2014), have a similar capacity to induce DC maturation and T cell-dependent tumor control. However, the distinct immune activation pathways in DCs operational downstream of microtubule destabilization remain elusive.

Guanine nucleotide exchange factor-H1 (GEF-H1), encoded by the Arhgef2 gene, is a member of the Dbl family of guanine nucleotide exchange factors (GEFs) that is sequestered on microtubules (Meiri et al., 2012), and is linked to the activation of Rho guanosine triphosphatases (GTPases) (Krendel et al., 2002). GEF-H1 is implicated in numerous cellular processes, such as cell motility and polarization (Fine et al., 2016), cell-cycle regulation, epithelial barrier permeability, and cancer (Birkenfeld et al., 2008). GEF-H1 contributes to immune signaling in macrophages during anti-viral host defense responses (Chiang et al., 2014) and intracellular pathogen recognition (Fukazawa et al., 2008; Zhao et al., 2012; Zhao, Zagani, et al., 2019). How GEF-H1 is released and controls cellular functions in response to changing microtubule dynamics, especially in antigen-presenting cells, remains unclear as yet.

Here, we investigated the consequence of perturbing microtubule dynamics in DCs and focus on the distinct downstream molecular and cellular mechanisms that control DC maturation and antigen presentation to T cells. Collectively, we identify GEF-H1 as a key alternate axis in DC maturation, which is induced after microtubule destabilization. We found that through the microtubule release of GEF-H1, MDAs can induce immune responses that normally require host defense activation by microbial PRRs. Activation of GEF-H1 signaling by MDAs induced

cross-presentation of antigens to drive specific $CD8^+$ T cell responses during anticancer chemotherapy.

3.1.3. Results

Microtubule destabilization leads to phenotypic and functional maturation of DCs

MDAs administered as free drugs or delivered as ADCs boost antitumor immune responses by inducing the full spectrum of DC maturation and the release of proinflammatory cytokines (Martin et al., 2014; Muller et al., 2014). To confirm a class effect of microtubule-targeting agents, we tested various MDAs and microtubule-stabilizing agents (MSAs) for their capacity to induce DC maturation based on the upregulation of cell surface CD80 and CD86. The MDAs ansamitocin-P3, MMAE, plinabulin, and eribulin all potently induce activation of the immature DC cell line SP37A3. In contrast, the MSAs epothilone-A and peloruside derivative CW190, as well as taxanes, namely, docetaxel and paclitaxel, had no DC-stimulatory effects (Figure 1A; Figure S1A). The targeting of different tubulin-binding sites by MDAs did not correlate with the potency of DC activation (Figure 1A).

Treatment of SP37A3 cells with ansamitocin-P3 induced significant production of proinflammatory cytokines interleukin (IL)-1b, IL-6, and IL-12 at doses greater than 100 nM (Figure 1B). In addition, exposure to ansamitocin-P3 induced the expression of the costimulatory molecules CD80, CD86, and CD40 (Figure 1C; Figure S1B). The dosing used for the MDAs favorably compares with the dosing used in clinics (patient dosing data available for plinabulin and vincristine; (Mita et al., 2010; Yang et al., 2018)). DC viability was not reduced compared with vehicle at all concentrations of ansamitocin-P3 tested (Figure S1C). Taxane and etoposide (a topoisomerase inhibitor that does not target microtubules) did not induce DC maturation (Figures 1A–1C), indicating specificity to MDAs. Moreover, this

indicates that microtubule destabilization was sufficient for DC maturation even in the absence of PRR ligands such as lipopolysaccharide (LPS). Similar induction of DC maturation was observed in freshly isolated splenic DCs specifically upon exposure to MDAs ansamitocin-P3 and plinabulin in a dose-dependent manner and was comparable to LPS-induced DC maturation (Figures 1D and 1E; Figure S1D). Furthermore, ansamitocin-P3 treatment of bone marrow-derived DCs (BMDCs) from Zbtb46-GFP reporter mice led to the differentiation of classical DCs (cDCs), as measured by the induction of the transcription factor Zbtb46 (Satpathy et al., 2012) (Figure 1F). Accordingly, taxane had no effect on promoting cDC differentiation (Figure 1F).

To assess the activation of antigen-specific T cell responses, SP37A3 cells were pretreated with ansamitocin-P3 or taxane, loaded with ovalbumin (OVA) and cocultured with labeled CD8 and CD4 T cells isolated from OT-I and OT-II T cell receptor (TCR) transgenic mice, respectively. Treatment of DCs with ansamitocin-P3, but not taxane, led to robust CD8 and CD4 T cell proliferation (Figure 1G). This suggested that microtubule destabilization alone promotes DC maturation, leading to both major histocompatibility complex (MHC) class I and MHC class II antigen presentation.

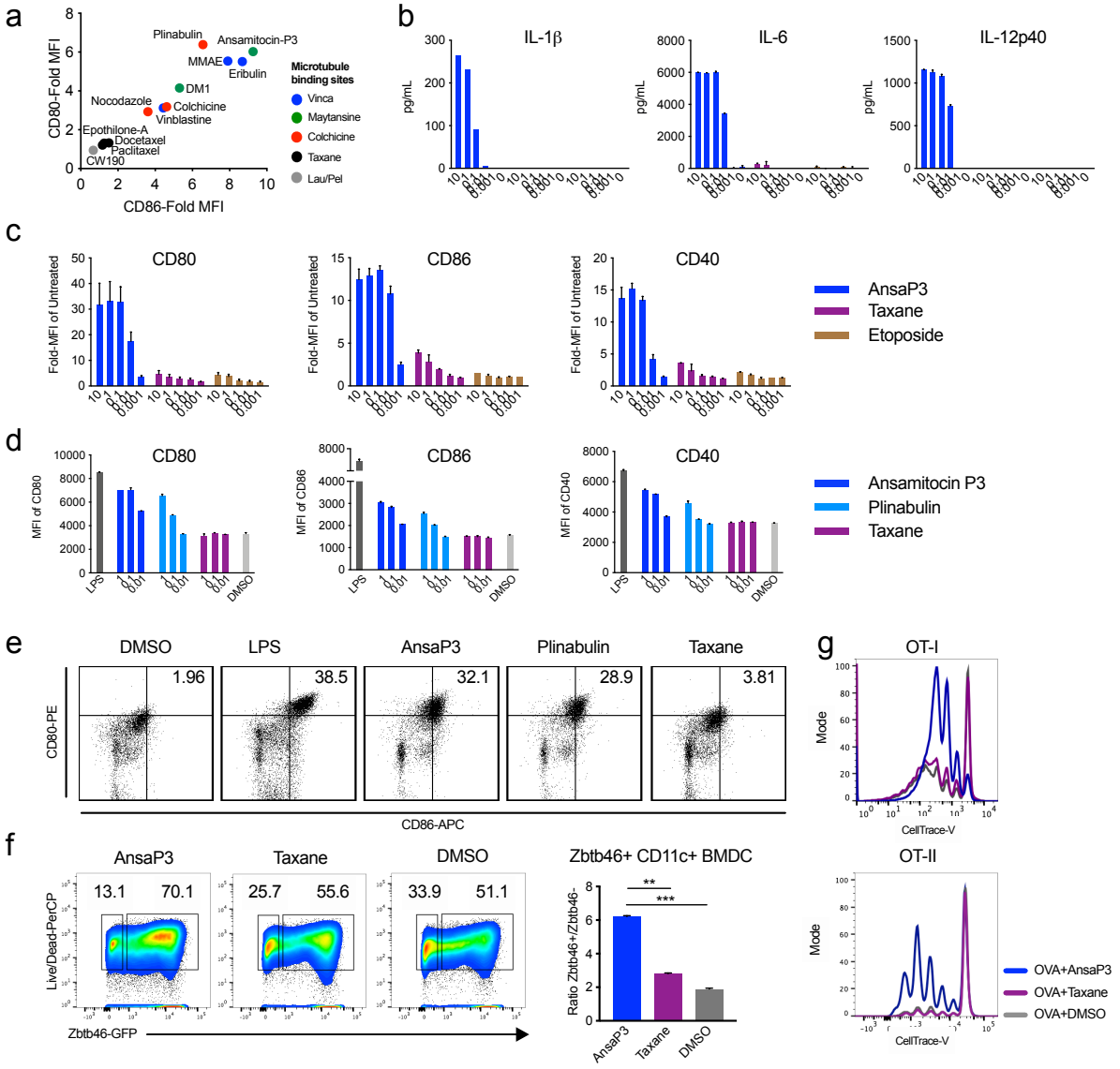

Figure 1. Microtubule destabilization, but not stabilization, induces DC maturation (A) SP37A3 cells were treated with various drugs at 100 nM or LPS at 500 ng/mL. CD80 and CD86 expression was assessed after 20 h using flow cytometry and expressed as fold-mean fluorescence intensity (MFI) of 0.1% DMSO. n = 3 biological replicates. **(B)** Quantification of cytokines (in picograms per milliliter) using ELISA from supernatant of SP37A3 cells treated for 20 h at indicated concentrations (in micromolars). n = 2 biological replicates. **(C)** Surface expression of CD80, CD86, and CD40 on cells from (B) was assessed using flow cytometry. **(D)** Splenic DCs from C57BL/6N mice were treated with LPS (200 ng/mL), ansamitocin-P3, plinabulin, and taxane at indicated doses (in nanomolars), or 0.1% DMSO. The MFI of CD80, CD86, and CD40 was assessed after 20 h by flow cytometry. n = 2 biological replicates. **(E)** Dot plots and percentage of CD80 and CD86 double-positive cells from live CD11c+MHC-II+ DCs from (D) are depicted. Representative plots from four biological replicates are indicated. **(F)** BMDCs from Zbtb46-GFP mice were cultured with ansamitocin-P3, taxane, or 0.1% DMSO for 24 h, and Zbtb46 expression (GFP) was assessed by flow cytometry (gating: CD11c+MHCII+GFP+). The bar graph represents the ratio of Zbtb46hi versus Zbtb46low cells. **p < 0.01, ***p < 0.001; n = 3 mice. **(G)** SP37A3 cells pretreated with 100 nM ansamitocin-P3, taxane, or 0.1% DMSO were pulsed with OVA protein and cocultured with OT-I (1:20 DC:T cell) or OT-II (1:15 DC:T cell) T cells labeled with CellTrace violet dye. Dye dilution in OT-I/OT-II cells was assessed using flow cytometry after 72 h. Representative overlapping histograms are presented. Experiment was repeated three times with similar results. Error bars represent SD. See also Figure S1.

Microtubule destabilization by MDAs releases and activates GEF-H1

Microtubule-associated GEF-H1 can initiate intracellular signaling, leading to the release of proinflammatory cytokines in macrophages (Chiang et al., 2014). We therefore investigated whether GEF-H1 was responsible for DC maturation upon microtubule destabilization. Using COS-7 fibroblasts overexpressing GEF-H1-GFP, we demonstrated the release of GEF-H1 from the microtubule network as early as 15 min upon treatment with ansamitocin-P3 (Figure 2A, arrowheads; Video S1). The release of GEF-H1 did not occur upon microtubule stabilization by taxane (Figure 2A). GEF-H1 is reported to bind to microtubules through interaction with the dynein motor complex (Meiri et al., 2012).

It has been proposed that the zinc-finger motif-containing C1 domain, the pleckstrin homology (PH) domain, and the coiled-coil domain of GEF-H1 are involved in microtubule binding (Glaven et al., 1999; Krendel et al., 2002). To test the possibility that GEF-H1 (Figure S2A) binds directly to microtubules, we sought to perform a biochemical experiment with purified proteins. We thus cloned a construct in which we fused the C1, PH, and the coiled-coil domain of GCN4 (denoted GEF-H1-C1-PH-GCN4) (see STAR Methods). Using a standard in vitro microtubule pelleting assay, we demonstrate that GEF-H1-C1-PH-GCN4 binds in a specific manner to microtubules (Figure 2B; Figure S2B). This finding suggests that GEF-H1 can interact directly with microtubules and is released from this binding upon treatment with MDAs.

The MDA-specific release of GEF-H1 from microtubules was subsequently confirmed in BMDCs treated with ansamitocin-P3 using coimmunoprecipitation. A decreased amount of a-tubulin observed in western blotting was correlated with reduced binding of GEF-H1 to microtubules (Figure 2C). Furthermore, ansamitocin-P3, but not taxane, treatment of BMDCs rapidly dephosphorylated GEF-H1 within 30 min (Figure 2D), a critical step associated with

the activation and release of GEF-H1 from microtubules (Chiang et al., 2014; Meiri et al., 2012). GEF-H1 re-phosphorylated within 60 min of treatment with ansamitocin-P3, suggesting the involvement of certain kinases that need to be further investigated. Lack of phosphorylated and total GEF-H1 was noted in BMDCs of GEF-H1-deficient (GEF-H1$^{-/-}$) mice (Figure 2D). GEF-H1 activation is known to be accompanied by the activation of Ras homolog gene family, member A (RhoA)-guanosine diphosphate (GDP) (Matsuzawa et al., 2004). The transient activation of GEF-H1 was observed to lead to the accumulation of RhoA-guanosine triphosphate (GTP) within 30 min of ansamitocin-P3 treatment (Figures S2C and S2D). The inhibition of RhoA using CCG-1423 prevented ansamitocin-P3-induced DC activation in a dose-dependent manner (Figure S2E).

Ansamitocin-P3 treatment of BMDCs derived from TLR4$^{-/-}$, TRIF$^{-/-}$, and NALP3$^{-/-}$ mice demonstrated that DC maturation in response to microtubule disruption occurred independent of TLR4, TRIF$^{-/-}$, or NLRP3 inflammasome activation (Figures S2F–S2H). Altogether, destabilization of microtubules was sufficient to induce potent DC maturation, wherein GEF-H1 release induced a potent downstream signaling pathways to promote DC subspecification and maturation.

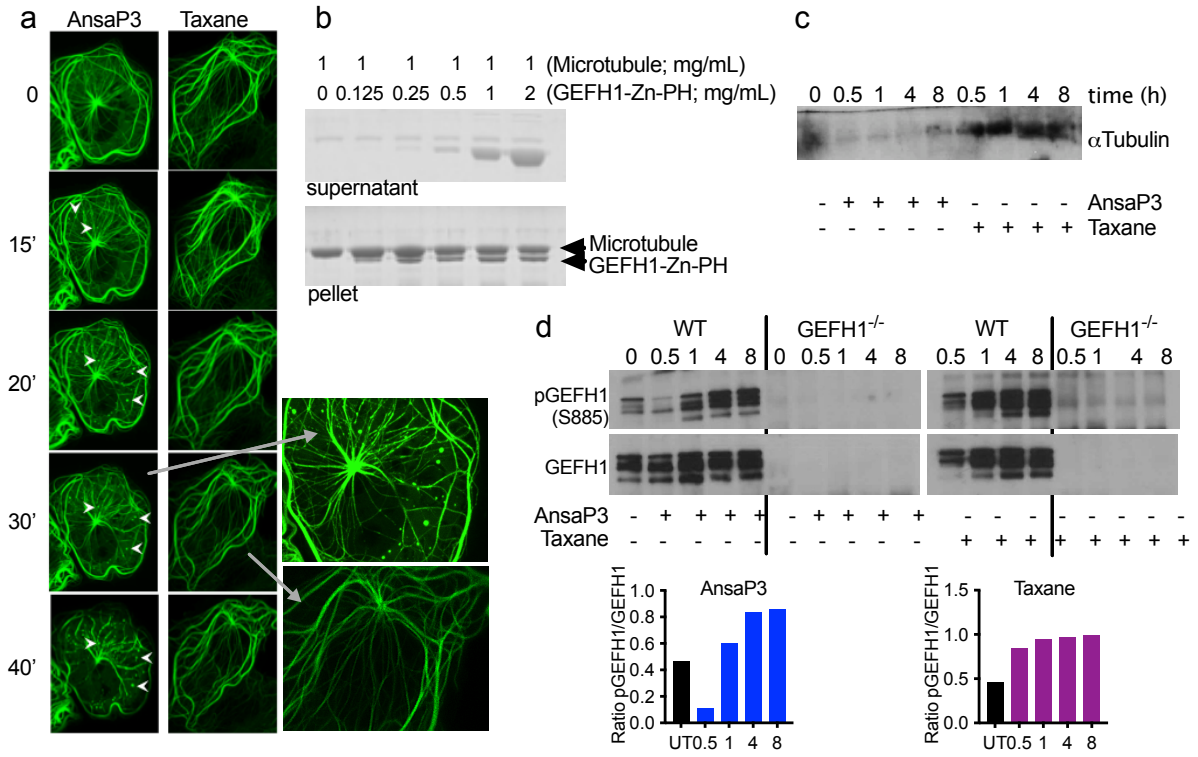

Figure 2. GEF-H1 release and activation upon microtubule destabilization. (A) COS-7 fibroblasts were transfected with GEF-H1-GFP plasmid and imaged upon treatment with 1 mM ansamitocin-P3 or taxane using confocal live cell microscopy. Time is depicted in minutes. Arrowheads indicate GEF-H1 delocalization. Scale bar, 40 mm. **(B)** Coomassie-stained SDS-PAGE showing the cosedimentation of microtubules (1 mg/mL) with increasing concentration of GEF-H1-C1-PH-GCN4 (upper blot, supernatant fractions; lower blot, pellet fractions). **(C)** GEF-H1 was immunoprecipitated from WT BMDCs treated with ansamitocin-P3 or taxane (100 nM) for indicated time points (in hours) and was probed for a-tubulin.**(D)** Lysates obtained from (C) were probed for phosphorylated and total GEF-H1. GEF-H1 activation was quantified using densitometry and depicted as the ratio of phosphorylated GEF-H1 (pGEF-H1) to total GEF-H1. The experiment was repeated twice with comparable results. See also Figure S2 and Video S1.

GEF-H1-dependent transcriptional programs signal microtubule destabilization for the activation of DCs

To gain insights into the GEF-H1-dependent molecular mechanisms activated upon destabilization of microtubules, we performed high-resolution RNA sequencing (RNA-seq). We used duplicate samples of RNA isolated from BMDCs of GEF-H1$^{-/-}$ and wild-type (WT) mice pre-treated for 5 h with ansamitocin-P3. Microtubule destabilization induced a significant GEF-H1-dependent inflammatory response with the expression of genes such as *Il1a*, *Il1b*, *Il6*, *cd80*, *cd14*, and chemokines associated with nuclear factor kB (NF-kB)/AP-1 activation (Table S1). This gene signature was synonymous with innate immune activation in response to

microbial stimuli. Principal component analysis (PCA) of normalized expression revealed that control and ansamitocin-P3-treated WT DCs segregate into distinct quartiles, whereas the control and treated DCs lacking GEF-H1 remained in the same quartile (Figure 3A). The lack of transcriptional changes in GEF-H1 lacking DCs was also revealed in pairwise comparisons, in which GEF-H1$^{-/-}$ DCs lack most ansamitocin-P3-induced transcriptional changes (Figure 3C). Furthermore, hierarchical clustering (Seqmonk; Babraham Bioinformatics) of ansamitocin-P3-regulated genes revealed that a significant proportion of the ansamitocin-P3-induced transcriptional response required GEF-H1 (Figure 3C). Of the 984 regulated genes with more than 2-fold upon microtubule destabilization in WT DCs (also seen in Figure 3B), GEF-H1 was required for inhibition of 362 or induction of 469 transcripts (Figure 3C, clusters I and III; Table S2). This suggested that changes in gene expression occurring downstream of microtubule destabilization critically depended on the presence of GEF-H1. Nevertheless, we detected minor proportion of GEF-H1-independent changes to the destabilization of microtubules within two additional clusters of 68 and 81 transcripts (Figure 3C, clusters II and IV; Table S2) that remained either decreased or elevated in both WT or GEF-H1$^{-/-}$ treated DCs (Figure 3C).

For gene set enrichment analyses (GSEAs) of GEF-H1-dependent transcriptional activation, genes were ranked on their dependence on GEF-H1 and their extent of regulation upon microtubule destabilization. GSEAs revealed that GEF-H1 controlled a microtubule destabilization-induced innate immune transcriptional signature normally associated with proinflammatory host defenses. The top three significant Hallmark biogroups included tumor necrosis factor alpha (TNFα) signaling (overlap of 187 genes; normalized enrichment score [NES] = 1.53), inflammatory response (overlap of 168 genes; NES = 1.42), and IL-6-JAK-STAT3 signaling (overlap of 77 genes; NES = 1.40) (Figure 3D; Figure S3A). These contain

major innate immune regulators such as *Il1a*, *Il1b*, *Il6*, *cd80*, *tnfsf4*, *tnfsf15*, *nfkb1*, *jun*, and the GEF-H1 interactor *ripk2* (Figure S3A). The GEF-H1-dependent genes significantly enriched for the transcription factor motif biogroup of ATF3 (over- lap of 165 genes; NES = 1.26), CEBPB (overlap of 176 genes; NES = 1.25), AP-1 (overlap of 163 genes; NES = 1.23), and serum response factor (SRF)-binding site gene sets (Figure 3D; Fig- ure S3B). Both AP-1 (dimer of c-Jun/c-Fos) and CEBPB (interacts with c-Jun, c-Fos, and NF-kB) belong to the activating transcription factor (ATF) family of transcription factors and are predominantly involved in the regulation of proinflammatory responses(Huber et al., 2012; Thompson et al., 2009).

To retrieve the most pivotal and central genes within the GEF-H1-dependent gene signature (Figure 3C, clusters I and III) (831 genes), we performed co-expression enrichment analysis (van Dam et al., 2012). The genes were ranked according to their overall co-expression within the signature, and the top 80 genes were selected, expression of which across treatments was represented as a heatmap in Figure 3E (and Table S3). The selected genes were assumed to be the central and most fundamental genes involved in the GEF-H1 signaling program in response to MDAs. Using co-expression analyses, we also mapped the top 15 transcription factors co-expressed with these 831 genes (Figure 3F). The top 3 belonged to the AP-1/ATF family, which also confirmed the results obtained with GSEAs (Figure 3D) in this independent and unbiased analysis. In addition, we performed an integrated system for motif activity response analysis (ISMARA) to determine the activity of transcription factor motifs in a genome-wide analysis (Balwierz et al., 2014). These analyses revealed JunB/Junc/Fos transcription factors (AP-1 transcription factor complex) are the dominant GEF-H1-dependent signaling output of ansamitocin-P3 (Figure 3G; Table S4). Altogether, the transcriptome analyses of BMDCs

treated with MDA revealed that GEF-H1 controlled most proinflammatory gene expression signatures that signaled microtubule destabilization in DCs.

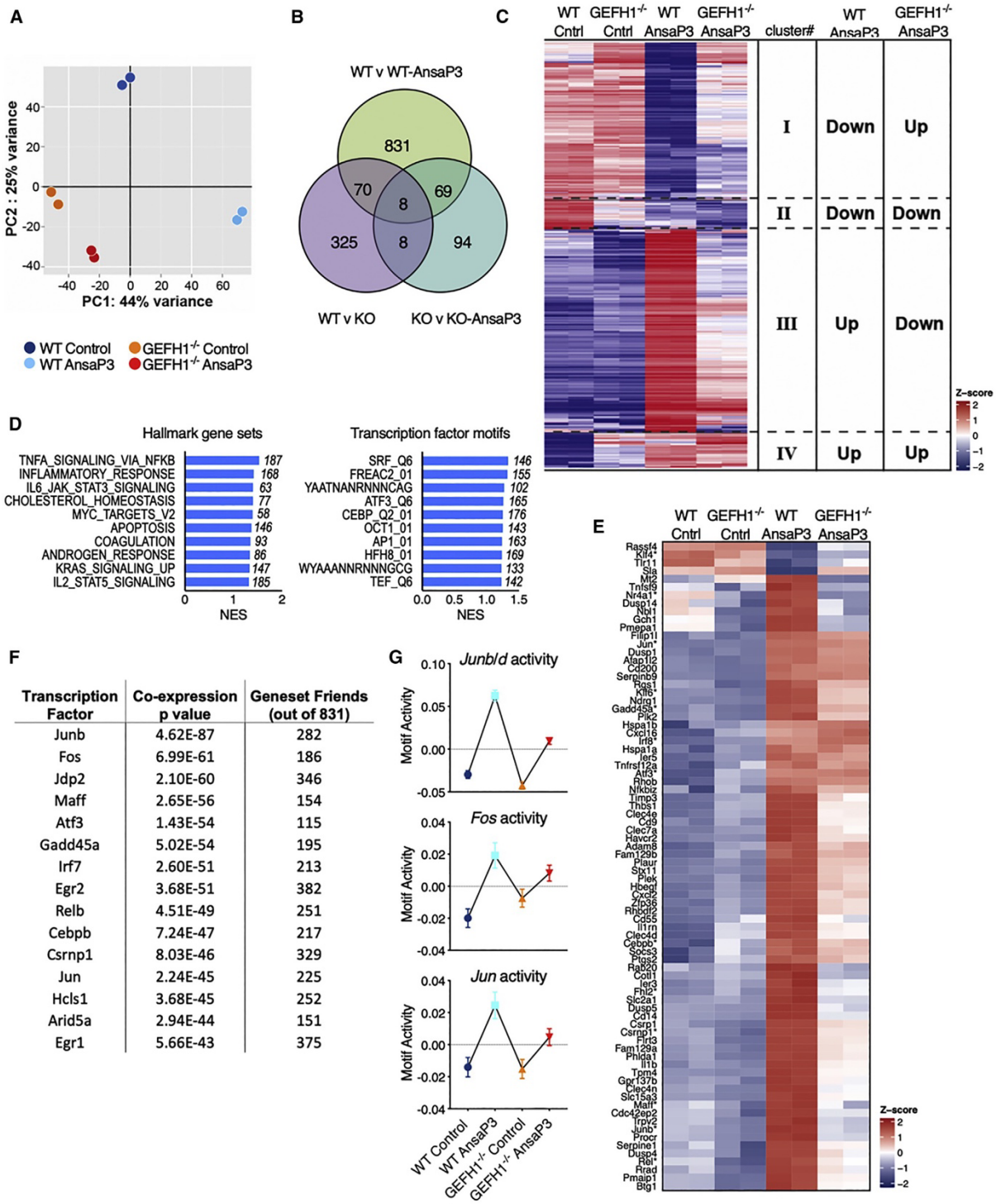

Transcription Factor	Co-expression p value	Geneset Friends (out of 831)
Junb	4.62E-87	282
Fos	6.99E-61	186
Jdp2	2.10E-60	346
Maff	2.65E-56	154
Atf3	1.43E-54	115
Gadd45a	5.02E-54	195
Irf7	2.60E-51	213
Egr2	3.68E-51	382
Relb	4.51E-49	251
Cebpb	7.24E-47	217
Csrnp1	8.03E-46	329
Jun	2.24E-45	225
Hcls1	3.68E-45	252
Arid5a	2.94E-44	151
Egr1	5.66E-43	375

Figure 3. Transcriptional profiling of WT and GEF-H1-deficient BMDCs subjected to microtubule destabilization. (A) Principal component analyses of expression values color coded by treatment groups. **(B)** Venn diagram of differentially expressed genes in indicated pairwise comparisons (false discovery rate [FDR] <

0.05 and log fold change [logFC] > 1). Knockout (KO) denotes GEF-H1$^{-/-}$ BMDCs. **(C)** Heatmap of genes differentially expressed ($p < 0.01$, FDR < 0.05, and logFC > 1) in WT BMDCs treated with and without ansamitocin-P3 represented across all indicated samples (duplicates per sample). Hierarchical clustering separated genes into 4 clusters. These were either GEF-H1 dependent (clusters I and III) or GEF-H1 independent (clusters II and IV). **(D)** Top gene sets enriched in the GEF-H1-dependent ansamitocin-P3 treatment response performed using the Broad Institute GSEA method for the Hallmark and C3 transcription factor motif gene set collections. Shown are the top 10 gene sets containing at least 50 overlapping genes ordered by their normalized enrichment scores (NESs). The number of overlapping genes within each gene set is indicated. **(E)** Top 80 genes and their scaled, centered log fragments per kilobase million (logFPKM) values selected from the gene signature comprising cluster I and III in (C) retrieved from the co-expression enrichment analysis using GeneFriends. Asterisks indicate transcription factors. **(F)** Top 15 transcription factors that are coexpressed with the gene signature of (E) were mapped using GeneFriends. In all cases, heatmaps indicate scaled, centered logFPKM values across all samples. **(G)** ISMARA analyses of transcription factor motif activity across the four samples. JunB, JunD, Jun, and Fos were the top regulated transcription factors. Error bars represent SD. See also Figure S3 and Tables S1, S2, S3, and S4.

Microtubule destabilization and release of GEF-H1 leads to c-Jun and Interferon Response Factor (IRF) activation

To identify the precise signaling events that mediate GEF-H1-dependent immune activation, we assessed the activation status of key transcription factors (IRF3, IRF5, STAT1, p65 NF-kB, and c- Jun) and cell signaling intermediates (ERK1/2, c-Jun N-terminal kinase (JNK), and p38 mitogen-activated protein kinase (MAPK)) in WT and GEF-H1$^{-/-}$ BMDCs. We found GEF-H1 is required for the activation of the transcription factors c-Jun, p65 NF-kB, IRF3, and IRF5 and the signaling intermediates JNK and ERK1/ 2 upon ansamitocin-P3-induced microtubule destabilization (Figures 4A and 4C; Figure S4A). The activation of IRF5, c-Jun, and JNK by GEF-H1 specifically occurred as a consequence of microtubule destabilization. In contrast, stabilization of microtubules by taxane resulted in GEF-H1-independent activation of STAT1, NF-kB, and ERK1/2 (Figures 4A and 4C; Figure S4A).

The cellular response to ansamitocin-P3 was further characterized by the GEF-H1-dependent activation of MKK4, an upstream kinase for JNK activation (Figures 4B and 4C). MKK3, which is not involved in the activation of JNK (Derijard et al., 1995), remains inactive in response to ansamitocin-P3 (Figure S4A). Microtubule stabilization by taxane did not activate either MKK3 or MKK4. We found the activation of the JNK pathway was critical for DC

maturation, because the JNK inhibitor SP600125 blocked CD80 and CD86 expression in response to stimulation with the MDAs ansamitocin-P3 and plinabulin (Figure 4D; Figure S4B). Altogether, we found that microtubule destabilization initiated profound innate immune responses in DCs that normally signal innate immune activation for host defenses.

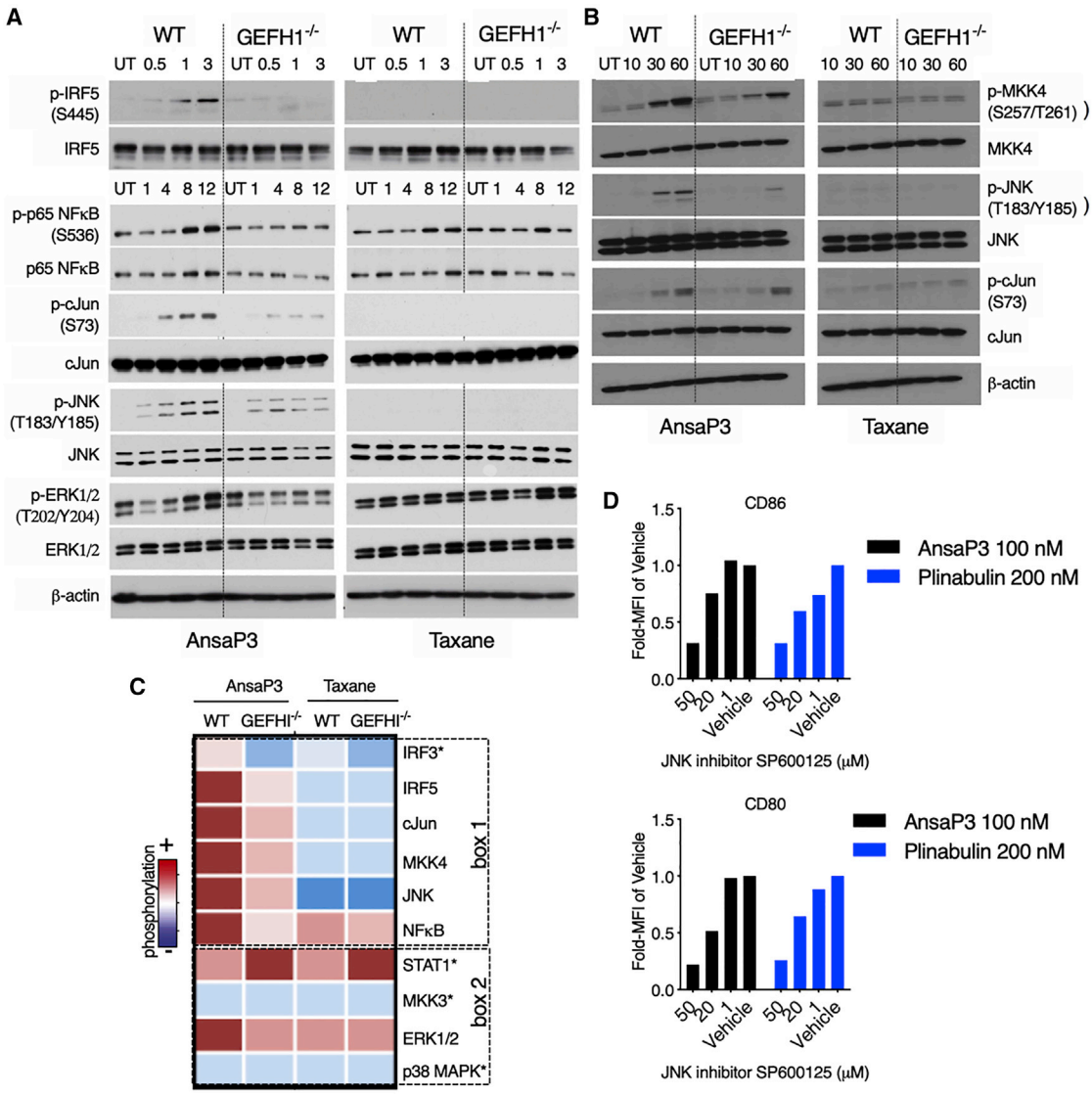

Figure 4. Differential activation of cell signaling intermediates upon microtubule destabilization and stabilization. (A and B) Lysates from WT or GEF-H1$^{-/-}$ BMDCs treated for specified time points with ansamitocin-P3 or taxane (both 100 nM) were probed for the indicated phosphorylated proteins. Time points are indicated in hours in (A) and in minutes in (B). Blots were stripped and re-probed for the respective total proteins. **(C)** Qualitative intensity map of phosphorylation profile (from A and B) of the various signaling intermediates is represented across the outlined BMDC samples. Box 1 represents signaling intermediates activated uniquely in response to ansamitocin-P3 in a GEF-H1-dependent manner. Non-specifically activated or nonactivated proteins are represented in box 2. Blots with an asterisk are in Figure S4. **(D)** DCs were preincubated with the indicated concentrations of the JNK inhibitor SP600125 or vehicle (0.5% DMSO) for 2 h, after which they were exposed to MDAs ansamitocin-P3 (100 nM) or plinabulin (200 nM) for 20 h. Data are represented as fold change in MFI

of CD80 and CD86 compared with vehicle-treated cells. n = 3 technical replicates. The experiment was performed twice with similar results. See also Figure S4.

GEF-H1 Signaling Is Required for DC Maturation upon Microtubule Destabilization

We next determined whether GEF-H1-mediated signals were responsible for directing DC function in response to microtubule destabilization. Compared with WT, GEF-H1$^{-/-}$ BMDCs stimulated with ansamitocin-P3 failed to induce mRNA expression of cytokines *Il1b*, *Il6*, and *Il12a* (Figure 5A) and costimulatory molecules CD80 and CD86 (Figure 5B). Both WT and GEF-H1$^{-/-}$ BMDCs failed to mature in response to the MSA taxane (Figure 5B). DC maturation that occurred in response to an additional MDA, dolastatin-10, also depended on GEF-H1 (Figure 5C; Figure S5A). As an additional control, we generated a XS106 DC cell line lacking GEF-H1 expression by CRISPR/ Cas9 targeting. In the absence of GEF-H1, CD80 and CD86 protein expression remained uninduced in response to MDAs ansamitocin-P3 as well as plinabulin (Figure 5D; Figure S5B), even over extended periods of up to 72 h (Figures S5C and S5D).

To assess in vivo DC maturation upon microtubule destabilization, we injected ansamitocin-P3, LPS, or vehicle (DMSO) into the earflap of WT and GEF-H1$^{-/-}$ mice. In WT mice, ansamitocin-P3 induces significantly higher expression of CD80 and CD86 in isolated DCs compared with GEF-H1$^{-/-}$ mice (Figure 5E; Figure S5E). However, GEF-H1 absence had minimal impact on LPS-induced DC activation in vivo (Figure 5E). Altogether, our results indicated that GEF-H1 is required for the maturation of DCs by MDAs that facilitate microtubule polarization.

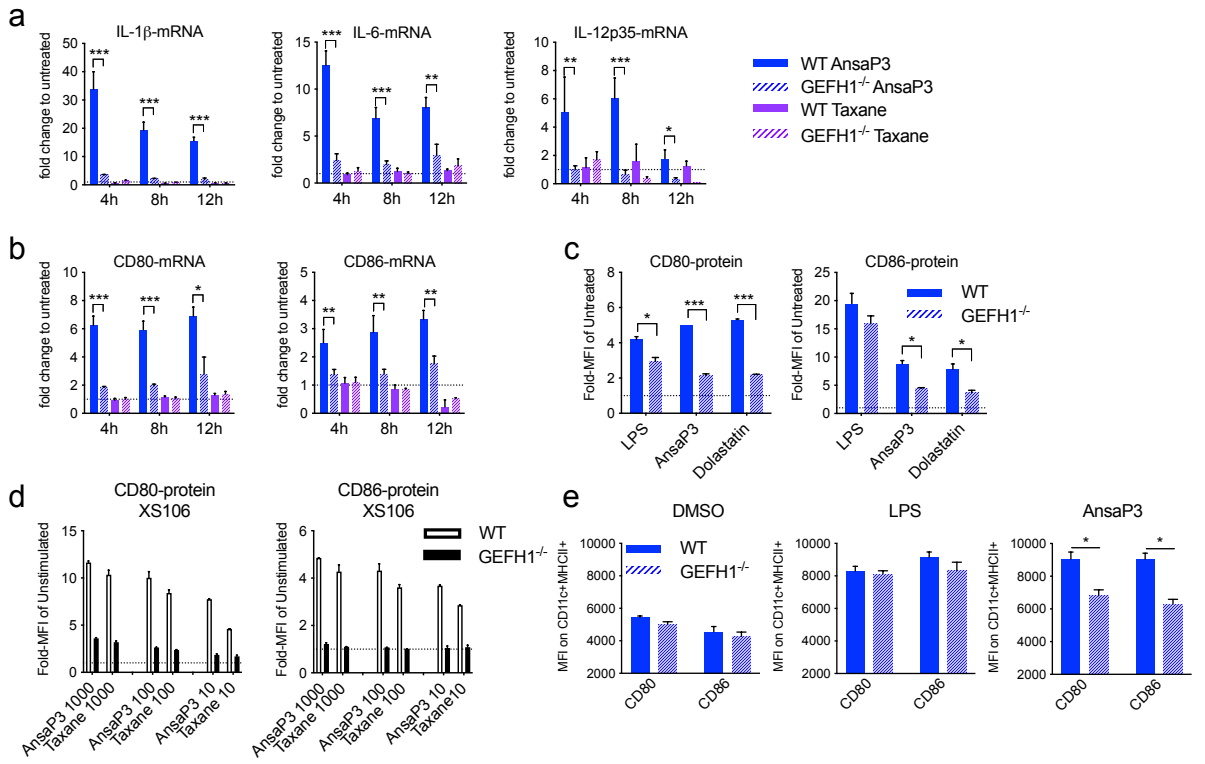

Figure 5. Involvement of GEF-H1 in microtubule destabilization-induced DC activation. (A–C) WT and GEF-H1$^{-/-}$ BMDCs treated with ansamitocin-P3 or taxane (both 100 nM) were assessed for expression of cytokines and DC activation markers using qPCR (A and B) at indicated time points or using flow cytometry (C) 20 h after treatment. **(D)** CD80 and CD86 expression was assessed by flow cytometry in WT or GEF-H1$^{-/-}$ XS106 cells treated at indicated doses (in nanomolars) for 20 h. **(E)** Ansamitocin-P3 (4 mg), LPS (8 mg), or vehicle alone (1.5% DMSO) was injected in the earflaps of WT and GEF-H1$^{-/-}$ mice. CD80 and CD86 expression after 20 h on in situ intradermal CD11c^{+}MHC-II^{+} DCs was analyzed by flow cytometry. In all cases, asterisks indicate statistical comparison between WT and GEF-H1$^{-/-}$. *p < 0.05, **p < 0.01, ***p < 0.001. Data in (A)–(D) are from three biological repeats and in (E) are from two biological repeats (technical repeats R 6). Error bars represent SD. See also Figure S5.

GEF-H1 signaling controls CD8 T cell activation upon DC maturation by MDAs

We next determined the role of GEF-H1 signaling in DCs for the induction of antigen-specific T cell responses. We adoptively transferred labeled CD8 and CD4 T cells, respectively, isolated from OT-I and OT-II transgenic mice, into congenic WT or GEF-H1$^{-/-}$ recipient mice. We measured the proliferation of T cells in the draining lymph node following immunization with ansamitocin-P3 or LPS in the presence of full-length OVA protein (Figure 6A). In WT animals, ansamitocin-P3 was as potent as LPS in significantly enhancing OT-I (Figures 6B and 6C) and OT-II (Figures 6F and 6G) T cell proliferation. Similar effects for WT BMDCs are observed

in vitro (Figures S6A and S6B). However, we noticed a profound reduction of proliferating, adoptively transferred OT-I T cells in GEF-H1$^{-/-}$ mice after immunization with ansamitocin-P3, although GEF-H1$^{-/-}$ mice were able to sustain LPS-induced OT-I T cell proliferation (Figures 6B and 6C). This selective effect on CD8 T cell proliferation in GEF- H1$^{-/-}$ mice, suggesting deficits in antigen cross-presentation, was confirmed in vitro using co-culture experiments of OT-I CD8 T cells with BMDCs derived from GEF-H1$^{-/-}$ and WT mice (Figures S6A and S6B). To specifically investigate the impact of GEF-H1 on antigen processing versus antigen presentation during cross-priming of CD8 T cells, we immunized ansamitocin-P3- or LPS-treated GEF-H1$^{-/-}$ and WT mice with the OT-I OVA257–264 peptide (Daniels et al., 2006) (Figures 6D and 6E). Upon peptide immunization, OT-I CD8 T cells were equally proliferative in both WT and GEF-H1$^{-/-}$ mice treated with ansamitocin-P3. This suggests that the intracellular antigen processing machinery of antigen cross-priming, not the extracellular antigen presentation, requires intact GEF-H1 signaling. Altogether, these data indicated that GEF-H1 was specifically required for efficient MHC class I-mediated CD8 T cell activation, because OT-II cells still underwent substantial proliferation after immunization with ansamitocin-P3 or LPS in GEF-H1$^{-/-}$ mice (Figures 6F and 6G).

GEF-H1 signaling controls ectopic tumor growth and promotes antitumor immunity of MDAs

We next investigated the role of GEF-H1 in tumor rejection. It is known that ansamitocin-P3 treatment of immunocompetent C57BL/6N WT mice bearing MC38 tumors leads to significant tumor control, which depends on DCs and T cells (Martin et al., 2014). Herein, we show that MC38 tumors grow faster in GEF-H1$^{-/-}$ mice compared with WT mice, although no significant differences in survival to endpoint were observed. In addition, the significantly larger tumors

observed in ansamitocin- P3-treated GEF-H1$^{-/-}$ compared with WT mice suggests that GEF-H1 regulates the antitumor efficacy of ansamitocin-P3 (Figure 6H).

Given the indication of a direct role of GEF-H1 in anti-tumor immune responses, we used The Cancer Genome Atlas (TCGA) to investigate the prognostic relevance in cancer patients of the proinflammatory GEF-H1-dependent immune signature obtained from Figure 3 (and outlined in Table S5). In at least three tumor types—melanoma, head and neck cancer, and uterine cancer—increased expression of the GEF-H1-dependent genes was associated with better overall survival (Figure 6I; Figures S6C and S6D). In addition, increased CD8A expression was noted in patients with higher expression of the GEF-H1 immune gene signature (Figure S6E). This suggests that the GEF-H1-dependent proinflammatory gene signature induced upon microtubule destabilization in DCs maybe prognostic, because it correlated with improved intratumoral T cell infiltration. Collectively, our findings indicated that GEF-H1 plays a critical role in initiating antitumor immunity, particularly upon treatment with MDAs such as ansamitocin-P3, and establishes a framework to guide the development of microtubule-targeting strategies.

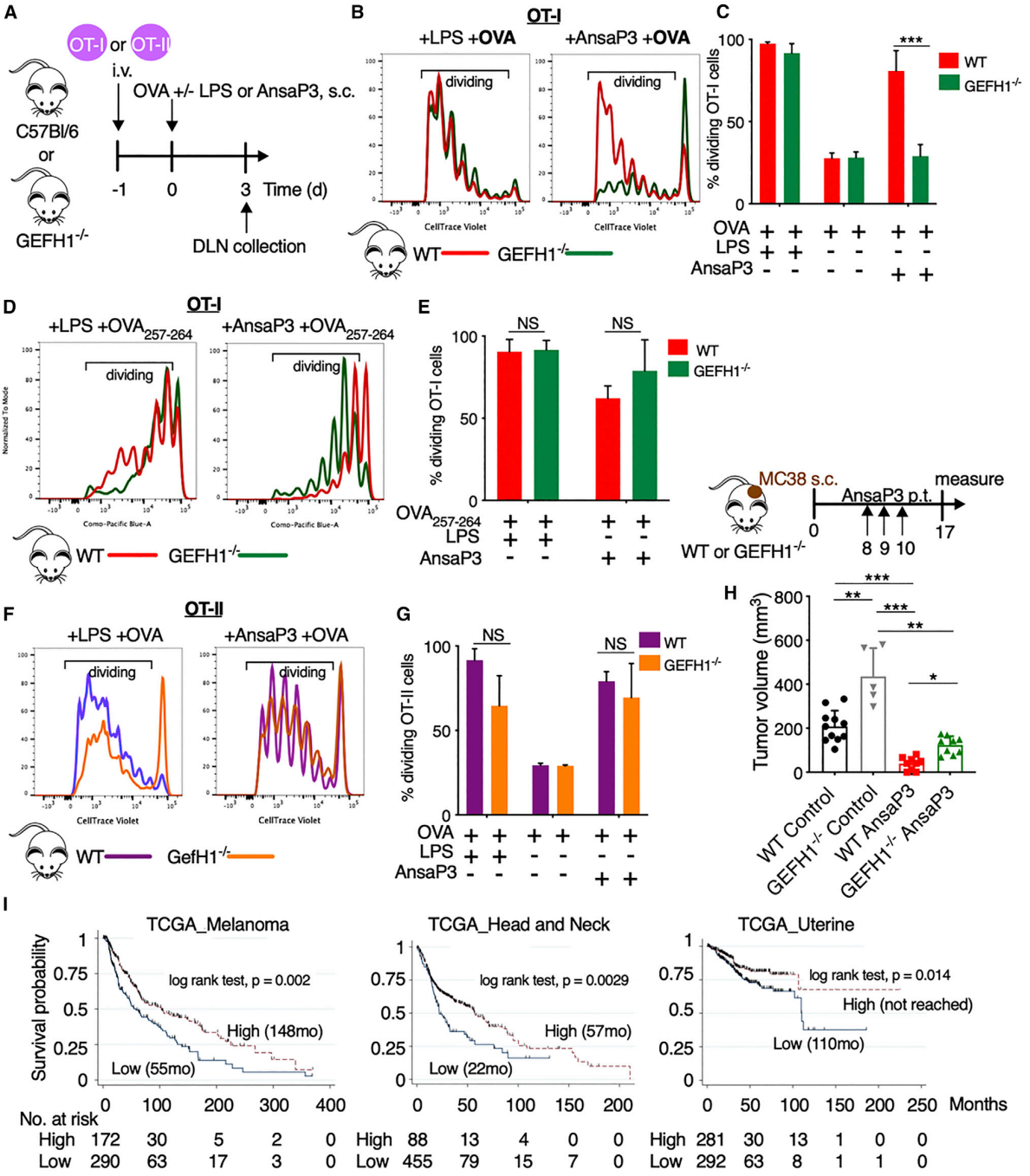

Figure 6. Assessment of GEF-H1 in T Cell expansion and antitumor immunity. (A) Experimental setup for **(B)–(G).** CellTrace violet-labeled CD8/CD4 T cells of OT-I/OT-II transgenic mice, respectively, were adoptively transferred into WT or GEF-H1$^{-/-}$ recipient mice. After 24 h, mice were immunized with 25 mg OVA or the OT-I OVA257–264 peptide (SIITFEKL) via tail base in the presence of ansamitocin-P3 (4 mg/mouse), LPS (25 mg/mouse), or vehicle (0.5% DMSO). Proliferation of donor-derived OT-I CD8 and OT-II CD4 T cells was assessed by flow cytometry 3 days after immunization. **(B, D, and F)** Representative histograms indicate overlap of CellTrace violet dye dilution of donor OT-I (B and D) or OT-II (F) T cells isolated from draining lymph nodes (DLNs) of WT and GEF-H1$^{-/-}$ recipient mice. **(C, E, and G)** Percentage of proliferating (dividing) OT-I (C and E) and OT-II (G) is calculated based on events within the gates as per (B), (D), and (F). ns, not significant ($p > 0.05$), ***$p < 0.001$. Data are obtained from three biological repeats (n = 9 mice). **(H)** Tumor volume (at day 17 after cell injection) of MC38 tumor-bearing WT or GEF-H1$^{-/-}$ mice after peri-tumoral (p.t.) injection (on days 8, 9, and 10) of vehicle (2% DMSO) or ansamitocin-P3 (0.3 mg/kg). Only animals bearing homogeneous tumors across all groups (between 50 and 70 mm3) before treatment start were included in the experiment. *$p < 0.05$, ***$p < 0.001$. Each data point represents a mouse. **(I)** Kaplan-Meier survival plot from TCGA analyses in patients stratified by the GEF-H1 immune signature high and low based on the cutoff of 14 log2 FPKM as per Figure S6C

(high, median log2 FPKM > 14; low, median log2 FPKM < 14). The number of patients at risk within the stratified groups is depicted at each time point. Error bars represent SD. See also Figure S6 and Table S5.

3.1.4. Discussion

Here we demonstrate that GEF-H1 is essential for the induction of an innate immune activation pathway upon treatment with microtubule-targeting chemotherapy that can restore antitumor immunosurveillance. Upon destabilization of microtubules, GEF-H1 is responsible for cell-intrinsic immune activation that leads to DC differentiation to cDCs with the ability to process and present antigens, as well as activate T cells. The specificity of the GEF-H1 pathway for DC activation is reserved for chemotherapies that destabilize microtubules (e.g., ansamitocin-P3, colchicine, and vinca alkaloids) and is not used for microtubule-stabilizing chemotherapies (e.g., paclitaxel and docetaxel).

Microtubules are highly dynamic cytoskeletal filamentous polymers composed of αβ-tubulin heterodimers and are the cellular targets of numerous chemotherapy drugs that either stabilize or destabilize microtubules (Jordan & Wilson, 2004). The latter typically bind to the vinca site (vinblastine, eribulin, and MMAE), to the colchicine site (colchicine, nocodazole, and plinabulin), or to the maytansine site on tubulin (ansamitocin- P3 and DM1) (Gigant et al., 2005; Prota et al., 2014; Ravelli et al., 2004; Steinmetz & Prota, 2018). Drugs with microtubule-destabilizing activity dominate the payloads within ADCs; most ADCs in clinical trials are conjugated to MMAE, mono-methyl auristatin F (MMAF), DM1, or DM4 (Beck et al., 2017). Non-targeted novel microtubule-destabilizing drugs such as plinabulin have demonstrated durable clinical responses (Mohanlal et al., 2016). In addition to their tumor cytotoxicity, drugs altering microtubule dynamics are known to improve DC function (Martin et al., 2014; Mizumoto et al., 2005). Although such DC stimulatory effects are reserved for drugs with microtubule-destabilizing activity irrespective of their distinct tubulin-binding sites,

intrinsic parameters such as cell permeability, compound stability, and expression of drug efflux pumps (Dumontet & Jordan, 2010) may influence their DC activation capacity.

Here, we demonstrate that a GEF-H1 variant comprising the C1, PH, and coiled-coil domains binds directly to microtubules, which upon action of MDAs on microtubules, is expected to be released and activated to induce DC maturational changes. In addition to microtubule-targeting drugs, anthracycline and its derivatives are known to promote DC maturation (Zitvogel et al., 2013). Anthracycline chemotherapies induce an immunogenic cell death (ICD) program in tumor cells, including the release of damage-associated molecular patterns (DAMPs), which are subsequently sensed by complementary PRRs, especially TLR4 expressed on DCs (Zitvogel et al., 2013). Antitumor immunity observed with anthracycline chemotherapy is mechanistically distinct from the microtubule-destabilizing chemotherapy reported herein. The latter is primarily mediated through its direct action on DCs and thus employs alternate mechanisms distinct from ICD. We observed no significant impact of the lack of TLR4, TRIF, or NALP3 on DC maturational changes upon microtubule destabilization. Upregulation of CD40, CD86, and MHC class II occurred independently of MyD88, a cytosolic adaptor protein shared by most TLRs (Müller et al., 2014). However, the intracellular GEF-H1 signaling was critical in initiating DC maturation upon microtubule destabilization and induction of immune responses such as proinflammatory cytokine production (e.g., IL-1, IL-6, and IL-12) that otherwise require extracellular and intracellular microbial pattern recognition. These findings are in agreement with a specific function of GEF-H1 in microtubule-dependent signaling of intracellular nucleic acid detection pathways, while extracellular pattern recognition through TLRs occurs independent of microtubules (Chiang et al., 2014).

In line with our finding and in contrast to the critical role of PRRs in mediating immunological responses to anthracycline chemotherapies, mice deficient in TLR or IL-1 receptor signaling display no defect in spontaneous or radiation-induced T cell responses against tumors (Deng et al., 2014; Woo et al., 2014). These findings suggest an alternate pathway leading to effective DC activation, which may be advantageous to engage, particularly in the tumor microenvironment. In addition, the activation of IRF5 and NF-kB suggests that the MDAs investigated here can initiate a GEF-H1-dependent innate immune pathway that is activated in response to microbial peptidoglycans (Zhao, Zagani, et al., 2019).

Though agonists of PRRs are in clinical development mainly as adjuncts to cancer immunotherapy strategies (Shekarian et al., 2017), chronic activation of TLRs may induce protumorigenic effects (Pandey et al., 2015). Furthermore, PRR expression is specific for distinct DC subsets, which results in variable responsiveness to PRR targeting depending on DC infiltration profiles (Gilliet et al., 2008). Hence, careful investigation of alternate pathways that lead to DC activation and effective antitumor immunity such as the ones proposed herein are of high relevance in the landscape of immune oncology.

We used RNA-seq to better characterize the intracellular signaling pathways and transcriptional responses upon microtubule destabilization in DCs. RNA-seq analyses revealed the extent and specificity of the GEF-H1-dependent immune response in DCs in the context of microtubule destabilization. Gene enrichment analysis associated the regulated gene clusters with inflammatory signaling and the control of adaptive T cell-mediated immune responses. The involvement of the AP-1 transcription family, particularly c-Jun, in the treatment response was independently identified in our gene expression analyses, unbiased co-expression analyses, and protein phosphorylation or activation experiments. c-Jun is part of the dimeric transcription

factor AP-1 complexes that assemble from members of the Jun (c-Jun, JunB, and JunD), Fos (c-Fos, FosB, Fra-1, and Fra-2), ATF, and MAF protein families (Karin et al., 1997). Its upstream signaling regulators, namely, RhoA, MKK4, and JNK1/2, were seen in our study to feed into the AP-1 transcriptional response in a GEF-H1-dependent manner. Although AP-1 activation is also a hallmark for pathogen recognition path- ways, DC activation upon treatment with microtubule-destabilizing chemotherapy was independent of PRRs. The SRF transcription factor (TF) motif, the highest enriched gene set in our GSEAs, is regulated by the Rho family GTPases, including RhoA, Rac, and Cdc42 (Hill et al., 1995), which are downstream substrates of GEF-H1. This is known to affect cytoskeletal dynamics, including actin, which may alter antigen processing and T cell priming.

However, animals lacking GEF-H1 signaling were unable to efficiently cross-present antigens to CD8 T cells upon microtubule destabilization and consequently were more refractory to therapy-induced anti-tumor immunity. This is surprising, because GEF-H1 is implicated in the differentiation of DCs in the Trif-GEF-H1-RhoB pathway involved in MHC class II expression (Kamon et al., 2006). Because MHC class I-specific OVA257–264 peptide presentation was not impaired in GEF-H1$^{-/-}$ DCs, the precise mechanism by which GEF-H1 controls antigen processing in DCs will need to be further investigated. Nevertheless, there is evidence for the role of GEF-H1 in membrane trafficking and recycling (Arnette et al., 2016), wherein the loss of GEF-H1 impaired recycling endosomes and the post-Golgi secretory vesicles (Ullrich et al., 1996). This indicates that the intracellular machinery used for antigen cross-presentation upon microtubule destabilization is hampered in the absence of GEF-H1. Altered CD8 T cell expansion after full-length OVA immunization, but not after OVA peptide immunization, indicates that GEF-H1$^{-/-}$ DCs have impaired intracellular antigen processing capabilities that are required for cross-presentation.

The more rapid growth of untreated MC38 tumors in GEF- $H1^{-/-}$ animals in the early phase of tumor immune control, i.e., when the tumor burden is low, indicates that the GEF-H1 axis may be involved in the early events that control tumor immunity, DC activation, and tumor antigen presentation. Thus, microtubule-based control mechanisms may exist that naturally govern DC maturation that are amplified by MDAs. The clinical relevance of the GEF-H1 immune pathway is supported by our TCGA analysis, which shows a significant association of CD8A to the GEF-H1 immune gene signature in patients with melanoma, head and neck cancer, and uterine cancer. This suggests that tumors with active GEF-H1 signaling have improved antitumor immunity, resulting in decreased risk of death. Better definition of the predictive potential of this pathway would require a TCGA dataset from patients treated with microtubule-destabilizing chemotherapy. In addition, because selection criteria for patient data available in TCGA are unknown, it is not possible to account for potential confounding factors that may have biased this analysis using standard statistical analysis techniques (McShane et al., 2005). Our findings identify GEF-H1-dependent immune activation events in DCs that could be harnessed for the design of immunotherapy approaches extending beyond microtubule-targeting chemotherapy. For instance, radiotherapy, which is exceedingly being used and combined with immunotherapy (Marciscano et al., 2018), is known to influence tubulin content and cause microtubule destabilization (Woloschak et al., 1990; Zaremba & Irwin, 1981), which may thereby directly activate GEF-H1 to boost DC function.

In summary, we demonstrate that an alternate cell-intrinsic pathway of DC maturation is induced upon microtubule destabilization by GEF-H1 that is capable of reinstating and enhancing antitumor immune responses. DC activation by the GEF-H1 pathway may be used

to overcome the immune tolerant tumor environment and improve the utility of current immune check- point blockade and personalized cancer vaccinations.

3.1.5. Material and methods

KEY RESOURCES TABLE

REAGENT or RESOURCE	SOURCE	IDENTIFIER
Antibodies		
Rabbit monoclonal phospho JNK (Thr183/Tyr185) (81E11)	Cell Signaling	Cat# 4668
Rabbit Anti-Mouse JNK	Cell Signaling	Cat# 9252
Rabbit Anti-Mouse phospho p65-NFκB (93H1)	Cell Signaling	Cat# 3033
Rabbit Anti-Mouse p65-NFκB (D14E12)	Cell Signaling	Cat# 8242
Rabbit Anti-Mouse phospho ERK1/2 (D13.14.4E)	Cell Signaling	Cat# 4370
Rabbit Anti-Mouse ERK1/2 (137F5)	Cell Signaling	Cat# 4695
Rabbit Anti-Mouse phospho p38-MAPK (12F10)	Cell Signaling	Cat# 4511
Rabbit Anti-Mouse p38 MAPK (D13E1)	Cell Signaling	Cat# 8690
Rabbit Anti-Mouse phospho MKK4 (C36C11)	Cell Signaling	Cat# 4514
Rabbit Anti-Mouse MKK4	Cell Signaling	Cat# 9152
Rabbit Anti-Mouse phospho MKK3 (D8E9)	Cell Signaling	Cat# 12280
Rabbit Anti-Mouse MKK3 (D4C3)	Cell Signaling	Cat# 8535
Rabbit Anti-Mouse phospho c-Jun (D47G9)	Cell Signaling	Cat# 3270
Rabbit Anti-Mouse c-Jun (60A8)	Cell Signaling	Cat# 9165
Rabbit Anti-Mouse phospho IRF3 (4D4G)	Cell Signaling	Cat# 4947
Rabbit Anti-Mouse IRF3 (D83B9)	Cell Signaling	Cat# 4302
Rabbit Anti-Mouse phospho STAT1 (58D6)	Cell Signaling	Cat# 9167
Rabbit Anti-Mouse STAT1	Cell Signaling	Cat# 9172
Mouse anti-β-actin (8H10D10)	Cell Signaling	Cat# 3700
Rabbit Anti-phospho GEFH1	Abcam	Cat# ab74156
Rabbit Anti-IRF5	Abcam	Cat# ab21689
Rabbit Anti-alpha Tubulin	Abcam	Cat# ab15246
Sheep Anti-Mouse GEFH1 antibody	Exalpha Biologicals	Cat# X1089P
Anti-phospho IRF5 (Ser-445)	NeoBiolab (MA, USA)	N/A
Zombie UV™ Fixable Viability Kit	BioLegend	Cat# 423107
Anti-Mouse TCRVb5-APC (clone MR9-4) (1:200 dilution)	BioLegend	Cat# 139505
Anti-Mouse MHCII (I-A/I-E)-BV510 (clone M5/144.15.2) (1:200 dilution)	BioLegend	Cat# 107636
Anti-Mouse CD11b-APC-Cy7 (clone M1/70) (1:200 dilution)	BioLegend	Cat# 101226
Anti-Mouse CD86-APC (clone GL-1) (1:300 dilution)	BioLegend	Cat# 105012
Anti-Mouse CD80-PE (clone 16-10A1) (1:300 dilution)	BioLegend	Cat# 104707
Anti-Mouse CD45-APC-Cy7 (clone 30-F11) (1:300 dilution)	BioLegend	Cat# 103116
Anti-Mouse CD40-BV421 (clone 3/23) (1:200 dilution)	BD Biosciences	Cat# 562846

Anti-Mouse CD11-c-Pe-Cy7 (clone HL3) (1:200 dilution)	BD Biosciences	Cat# 561022
Bacterial and Virus Strains		
pSpCas9(BB)-2A-GFP (PX458) vector	Ran FA et al., 2013	Addgene Plasmid; Cat# 48138
GEFH1-C1-PH-GCN4 construct	This paper	N/A
GEFH1 sgRNA-pSpCas9(BB)-2A-GFP	This paper	N/A
Chemicals, Peptides, and Recombinant Proteins		
Ansamitocin-P3	Cayman chemicals	Cat# 20538
Dolastatin-10	National Cancer Institute	N/A
Vinblastine	National Cancer Institute	N/A
Colchicine	Sigma Aldrich	Cat# C9754
Nocodazole	Sigma Aldrich	Cat# M1404
Etoposide	Sigma Aldrich	CAS: 33419-42-0
Hyaluronidase	Sigma-Aldrich	Cat# H6354
DNAse type IV	Sigma-Aldrich	Cat# D5025; CAS: 9003-98-9
Dimethyl sulfoxide (DMSO)	Sigma-Aldrich	Cat# D2650; CAS: 67-68-5
Epothilone-A	Santa Cruz Biotechnology	Sc-207628; CAS: 152044-53-6
Docetaxel	Selleckchem	Cat# S1148
Paclitaxel	Cayman Chemicals	Cat# 10461; *CAS: 33069-62-4*
CW190	Prof. Altmnann, ETH Zurich	N/A
Accutase	Sigma Aldrich	A6964
EndoFit Endotoxin-free ovalbumin protein	InVivo Gen	vac-pova-100
Lipopolysaccharide from Escherichia coli 0111:B4	InVivo Gen	Ultrapure LPS, E. coli 0111:B4
Collagenase Type 4	Worthington	Cat# LS004189
CellTrace Violet	Molecular Probes	Cat# C34557
Phosphatase Inhibitor (PhosSTOP)	Roche	Cat# 4906845001
Protein G Plus/Protein A Agarose	Calbiochem	Cat# IP0414ML
SDS-PAGE sample buffer	Bio-Rad	Cat# 1610747
ECL Western Blotting Detection reagents	GE Healthcare	Cat# GERPN2209
Plinabulin	BeyondSpring Pharmaceuticals	N/A
Eribulin	Eisai Co. Ltd	N/A
MMAE	Seattle Genetics	N/A
DM1	Concortis Biosystems	N/A
Critical Commercial Assays		
EasySep™ Mouse CD11c Positive Selection Kit II	STEMCELL Technologies	Cat #18780
IL-1β Mouse ELISA kit	eBioscience	Cat# BMS6002
IL-6 Mouse ELISA kit	eBioscience	Cat# BMS603-2

IL-12 Mouse ELISA kit	eBioscience	Cat# BMS616
IC Fixation buffer	eBioscience	Cat# 00-8222-49
Mouse CD4+ T Cell Isolation Kit	Miltenyi Biotec	Cat# 130-104-454
Mouse CD8a+ T Cell Isolation Kit	Miltenyi Biotec	Cat# 130-104-075
RNeasy kit	Qiagen	Cat#74104
iScript cDNA synthesis kit	Bio-Rad	Cat#1708890
SsoAdvanced Universal SYBR Green supermix kit	Bio-Rad	Cat# 172-5270
TruSeq Stranded mRNA sample preparation kit	Illumina	Cat# 20020594
Kapa Biosystems library quantification kit	Roche	N/A
Experimental Models: Cell Lines		
COS-7 fibroblasts cells	American Type Culture Collection (ATCC)	N/A
SP37A3 (immature dendritic cell line)	Merck KGaA	
XS106 cell line	Professor Akira Takashima, University of Texas, USA	N/A
NS47 fibroblast cell line	Professor Akira Takashima, University of Texas, USA	N/A
XS106 GEFH1$^{-/-}$	This paper	N/A
E.coli Bl21 (DE3) cells	NEB Biolabs	Cat# C2527I
Experimental Models: Organisms/Strains		
Mouse: C57BL/6NRj wild type	In house	N/A
Mouse: OT-I (B6.129S6-*Rag2*^{tm1Fwa} Tg(TcraTcrb)1100Mjb)	In house	N/A
Mouse: OT-II (B6.129S6 *Rag2*^{tm1Fwa} Tg(TcraTcrb)425Cbn)	In house	N/A
Mouse: 129S.Zbtb46^{tm1Kmm}/J	The Jackson Laboratories	Stock No: 000690
Mouse: GEFH1$^{-/-}$ (B6.Arhgef2<tm1Hcr>)	In house	N/A
Oligonucleotides		
Primer Il1b-Forward: GCAACTGTTCCTGAACTCAACT	Microsynth	N/A
Primer Il6-Forward: CCTAGTTGTGATTCTTTCGATGCT	Microsynth	N/A
Primer Il12a-Forward: AGACATCACACGGGACCAAAC	Microsynth	N/A
Primer IL12b-Forward: TGGTTTGCCATCGTTTTGCTG	Microsynth	N/A
Primer CD80-Forward: TCGTCTTTCACAAGTGTCTTCAG	Microsynth	N/A
Primer CD86-Forward: GAAGCCGAATCAGCCTAGC	Microsynth	N/A
Primer Gapdh-Forward: TGACCTCAACTACATGGTCTACA	Microsynth	N/A
GEFH1 guide RNA_1: GCACATGGTCATGCCGGAGA	Microsynth	N/A
GEFH1 guide RNA_2: GACAAGGTAGGAGTCAGCCT	Microsynth	N/A
Software and Algorithms		
Volocity	PerkinElmer	N/A
NIS-Elements imaging software	Nikon	N/A
ISMARA	https://ismara.unibas.ch	N/A
GraphPad Prism 7	GraphPad Software	N/A
FlowJo	https://www.flowjo.com/	N/A

Blc2fastq2 Conversion software	https://support.illumina.com/sequencing/sequencing_software/bcl2fastq-conversion-software.html	N/A
Cuffdiff version 1.05	https://software.broadinstitute.org/cancer/software/genepattern/modules/docs/Cuffdiff/7	N/A
Seqmonk	https://www.bioinformatics.babraham.ac.uk/projects/seqmonk/	N/A
STAR (2.5.2a)	Devred, F. et al. 2010	N/A
edgeR Bioconductor Package in R	https://www.r-project.org	N/A
R package ComplexHeatmap	https://bioconductor.org/packages/release/bioc/html/ComplexHeatmap.html	N/A
HCOP: Orthology Predictions Search	http://www.genenames.org/cgi-bin/hcop at 8.9.17	N/A
GSEA java application	http://www.broad.mit.edu/gsea/)	N/A
LM22 matrix	Newman, A.M. et al 2015	N/A
R package TCGAbiolinks	Colaprico, A. et al 2016	N/A
Cox regression analyses	Sauerbrei, W., Royston, P. & Binder, H. 2007	N/A

Lead contact and materials availability

Further information and requests for plasmids (GEFH1-C1-PH-GCN4 and GEFH1 sgRNA-pSpCas9(BB)-2A-GFP) and mouse cell lines (XS106 GEFH1$^{-/-}$) generated in this paper and other resources and reagents should be directed to and will be fulfilled by the Lead Contact, Alfred Zippelius (alfred.zippelius@usb.ch).

Experimental models and subject details

Animals

C57BL/6N wild type, OT-I and OT-II TCR transgenic mice were bred in-house either at University Hospital Basel, Switzerland or Massachusetts General Hospital (MGH), USA. In case of unavailability mice were also obtained from Jackson Laboratories (USA) or Janvier Labs (France). GEFH1$^{-/-}$ mice on C57BL/6N background were generated as previously published (Chiang et al., 2014) and were bred at MGH. 129S.Zbtb46-GFP reporter mice (obtained from Jackson Laboratories) were also bred at MGH. Both males and females were used and no difference was observed on the results. All mice used were 8- to 16-week-old, housed under specific pathogen-free conditions. All animals were maintained under a strict 12 h light cycle (lights on at 5:00 a.m. and off at 5:00 p.m.), and given food and water available *ad libitum*. All animal experiments were performed in accordance with Swiss federal regulations (Basel Kantonal licence numbers: 2370, 2589 and 2408) and the Subcommittee on Research Animal Care at MGH.

Cell Lines

COS-7 fibroblast cells were purchased from American Type Culture Collection (ATCC), maintained in DMEM supplemented with 10% fetal bovine serum (FBS) and 0.5% penicillin-streptomycin (P/S; Gibco) mixture. The immature mouse DC cell line SP37A3 (kindly provided by Merck KGaA) was cultured in Iscove's Modified Dulbecco's Medium (IMDM; Sigma) supplemented with 10% heat-inactivated FBS (PAA), sodium pyruvate (Gibco), P/S, L-glutamine mix (Gibco), MEM nonessential amino acids (Sigma), and with 20 ng/mL recombinant mouse GM-CSF and 20 ng/mL recombinant mouse M-CSF (both Peprotech). XS106 cell line (kind gift from Professor Akira Takashima, University of Texas South-Western, TX, USA) is a long-established DC line derived from the epidermis of newborn mice

56 and are better suited for lipid/viral transfection compared to SP37A3 cells. These cells were cultured in RPMI-1640 medium supplemented with 10% FBS and 0.5% P/S. The medium was further supplemented with 20 ng/mL murine recombinant GM-CSF and 5% (v/v) culture supernatant derived from the NS47 fibroblast cell line. The NS-47 cell line was cultured in RPMI-1640 complete medium. All cells were cultured at 37° in a 5% CO2/air atmosphere. GEFH1 deficient XS106 cells were created using CRISPR/Cas9 mediated gene editing. Two guide RNAs (GCACATGGTCATGCCGGAGA and GACAAGGTAGGAGTCAGCCT) were designed using the online tool e-crisp.org, synthesized by Microsynth (Switzerland) and cloned into the pSpCas9(BB)-2A-GFP (PX458) vector (Addgene plasmid #48138). After transient transfection, XS106 cells were single cell sorted according to GFP expression, expanded and subsequently screened for GEFH1 expression by western blot.

Primary Cell Culture

Bone marrow derived DCs were generated by plating 5 million bone marrow cells freshly isolated from tibia and femur of C57BL/6N mice into 10 cm dishes. RPMI-1640 supplemented with 10% heat inactivated FCS, 0.5% P/S, GM-CSF (10 ng/mL; Peprotech) and IL-4 (10 ng/mL; Peprotech) was used to culture the BM cells. On day 6, floating and loosely attached cells were collected representing the BMDCs. Briefly, spleens were collected and cut into fine pieces and digested with Collagenase type D (1 mg/ml, Roche) and DNase I (40 µg/ml, Roche) in RPMI 10% FCS for 40 minutes at 37°C. Single cell suspensions were obtained by passing the digested tissue through a 70 □m strainer using ice-cold PBS supplemented with 0.5 mM EDTA and 2% FCS. The DCs were isolated by immunomagnetic CD11c+ positive selection according to manufacturer's protocol (StemCell Technologies). The purity of the splenic DCs was also assessed by flow cytometry and was typically between 80-90%.

Method Details

Reagents and Antibodies

Anti-cancer agents namely, ansamitocin-P3 (Cayman Chemicals), plinabulin (kindly provided by BeyondSpring Pharmaceuticals), eribulin (kindly provided by Eisai Co. Ltd), MMAE (kindly provided by Seattle Genetics), DM1 (Concortis Biosystems), colchicine (Sigma Aldrich), vinblastine (National Cancer Institute), nocodazole (Sigma Aldrich), dolastatin-10 (National Cancer Institute), epothilone-A (Santa Cruz Biotechnology), docetaxel (Selleckchem), paclitaxel (Cayman Chemicals), CW190 (Prof. Altmnann, ETH Zurich) and etoposide (Sigma Aldrich) were dissolved in 100% DMSO (10 mM stock) and tested at various concentrations with a final maximum DMSO concentration of 0.1%. Endotoxin-free ovalbumin (OVA) protein (EndoFit) was purchased from InvivoGen. Lipopolysaccharide (LPS) from Escherichia coli 0111:B4 was purchased from InvivoGen. The following antibodies for immunoblotting were obtained from Cell Signaling: phospho JNK (81E11), JNK, phospho p65-NFκB (93H1), p65-NFκB (D14E12), phospho ERK1/2 (D13.14.4E), ERK1/2 (137F5), phospho p38-MAPK (12F10), p38 MAPK (D13E1), phospho MKK4 (C36C11), MKK4, phospho MKK3 (D8E9), MKK3 (D4C3), phospho c-Jun (D47G9), c-Jun (60A8), phospho IRF3 (4D4G), IRF3 (D83B9), IRF5 phospho STAT1 (58D6), STAT1 (cat no. 9172), and β-actin (8H10D10). Antibodies for phospho GEFH1 (ab74156), anti-IRF5 (ab21689) and αTubulin were purchased from Abcam. Anti-GEFH1 antibody (x1089p) was purchased from Exalpha Biologicals. The anti-IRF5 phosphorylated at Ser 445 was produced by NeoBiolab (MA, USA) by immunizing rabbits with a synthetic peptide (IRLQIPS^{445}NPDLC). Plasmids encoding GFP-GEFH1 (pCMV6-AC-GFP-hGEFH1) were purchased from OriGene.

Stimulation of Murine DCs In Vitro

Pre-seeded day 6 BMDCs (80,000 cells/well of 96-well plate), freshly isolated splenic DCs (160,000 cells/well of 96-well plate), murine SP37A3 DC cells or murine XS106 DC cells (80,000 cells/well of 96-well plate) were incubated with microtubule targeting agents or LPS at the indicated concentrations. After 20 hours, unless otherwise stated, the DCs were harvested using PBS/EDTA detachment and their phenotype was assessed either by flow cytometry or ELISA.

Measurement of Cytokine Production

IL-1β, IL-6, and IL-12 in supernatants of murine DC cultures pre- and post-stimulation were detected by standard sandwich ELISA procedures using commercially available kits (eBioscience) following manufacturer's instructions.

Analyses of mRNA Expression

Murine BMDCs were isolated and treated as described above. Qiagen RNeasy kit was used for the extraction of RNA. cDNA was synthesized using the iScript cDNA synthesis kit (Bio-Rad) following which SsoAdvanced Universal SYBR Green supermix kit (Bio-Rad) was used for real-time qPCR (Bio-Rad CFX96 Real-Time PCR Detection System) according to the manufacturer's specifications. The value obtained for each gene was normalized to that of the *GAPDH* gene. Primers used were as follows (all 5' to 3'). Il1b-F: GCAACTGTTCCTGAACTCAACT, IL1b-R: ATCTTTTGGGGTCCGTCAACT; Il6-F: CCTAGTTGTGATTCTTTCGATGCT, Il6-R: ACAGACATCCCCAGTCTCATATTT; Il12a-F: AGACATCACACGGGACCAAAC, Il12a-R: CCAGGCAACTCTCGTTCTTGT; IL12b-F: TGGTTTGCCATCGTTTTGCTG, IL12b-R: ACAGGTGAGGTTCACTGTTTCT; CD80-F: TCGTCTTTCACAAGTGTCTTCAG, CD80-R: TTGCCAGTAGATTCGGTCTTC;

CD86-F: GAAGCCGAATCAGCCTAGC, CD86-R: CAGCGTTACTATCCCGCTCT; Gapdh-F: TGACCTCAACTACATGGTCTACA, Gapdh-R: CTTCCCATTCTCGGCCTTG.

Immunoprecipitation and Immunoblotting

To assess phosphorylated and total GEFH1, day 6 BMDCs treated with ansamitocin-P3 (100 nM) or taxane (100 nM) at indicated time points were lysed using NP-40 buffer (1% NP-40, 20 mM Tris-HCl at pH 7.4, 150 mM NaCl, 2 mM EDTA, 2 mM EGTA, 4 mM Na_3VO_4, 40 mM NaF) containing protease and phosphatase inhibitors (Complete Mini tablet; Roche). Lysates were used for direct assessment by Western blotting or for GEFH1 immunoprecipitation. For immunoprecipitation, lysates were incubated with protein G plus agarose (Calbiochem) at 4°C for 30 minutes and pre-cleared. Pre-cleared lysates were incubated with anti-GEFH1 antibody (1:200) at 4°C overnight followed by incubation with agarose beads at 4°C for 4 hours. Precipitated proteins were collected by centrifugation and washed 3 times in washing buffer (0.5% NP-40, 20 mM Tris-HCl at pH 7.4, 150 mM NaCl, 2 mM EDTA, 2 mM EGTA, 4 mM Na_3VO_4, 40 mM NaF). After washing, proteins were boiled with SDS-PAGE sample buffer at 95°C for 10 minutes and detected by Western blotting. Membranes were blocked with 5% non-fat dry milk in Tris-buffered saline (TBS) at room temperature for 1 hour and incubated with primary antibodies against the phosphorylated protein diluted in blocking solution to a ratio of 1:1000 at 4°C overnight. After washing in TBS with 0.05% Tween-20 (TBS-T), membranes were incubated with appropriate horseradish peroxidase conjugated secondary antibody diluted in blocking buffer for 1 hour at room temperature. Blots were washed 3 times with TBS-T and hybridized bands were detected by Amersham ECL Western blotting detection reagent (GE Healthcare). The blots probed for the phosphorylated proteins were stripped and re-probed with antibodies for the respective total proteins.

Confocal Live Cell Imaging

COS-7 fibroblasts pre-seeded into 4-well chamber slides (LabTek) were transfected with 1 μg of the GFP-GEFH1 plasmid using Lipofectamine 3000. Live cells were imaged 20 hours post transfection with a Nikon A1R-A1 confocal microscope. Images were acquired immediately upon the addition of ansamitocin-P3 (1 μM) or taxane (1 μM). Image acquisition was carried out with NIS-Elements imaging software (Nikon) followed by analyses by Volocity (PerkinElmer).

Cloning and Production of GEFH1 Constructs

The human GEFH1 (Uniprot Q92974-1) C1 (residues 28-100) and PH domains (residues 439-589) were initially cloned in isolation into a pET-based bacterial expression vector containing an N-terminal thioredoxin-6xHis cleavable tag using a restriction free positive selection method (Olieric et al., 2010). The GEFH1-C1-PH-GCN4 construct was assembled by homologous recombination using overlapping PCR fragments by fusing in frame the leucine zipper coiled-coil domain of the yeast transcriptional activator GCN4 (O'Shea et al., 1991) C-terminally to the PH domain. All clones were verified by sequencing.

Protein samples were produced by overexpression in *E. coli* Bl21(DE3) cells. Protein purification was performed by immobilized metal-affinity chromatography (IMAC) on HisTrap HP Ni^{2+} Sepharose columns (GE Healthcare) according to the manufacturer's instructions. Processed protein samples were concentrated and processed on a HiLoad Superdex 200 16/60 size exclusion chromatography column (GE Healthcare) equilibrated in 50 mM Tris HCl, pH 7.5, supplemented with 150 mM NaCl and 2 mM DTT. Protein fractions were analyzed by Coomasie stained SDS-PAGE. Fractions containing the target protein were

pooled and concentrated by ultrafiltration. Protein concentrations were estimated by UV absorbance at 280 nm.

In vitro Microtubule Pelleting Assay

Microtubule binding of GEFH1 variants was performed by a standard microtubule co-sedimentation assay (Devred et al., 2010). Briefly, tubulin at 2 mg/mL in BRB80 buffer (80 mM PIPES-KOH, pH 6.8, 1 mM $MgCl_2$, 1 mM EGTA) supplemented with 0.5 mM GTP and 1.25 mM DTT was incubated at 4°C for 5 minutes followed by incubation at 37°C for 10 minutes. Taxol was added to the reaction mix in a step wise manner (0.1, 1, and 10 μM) to induce microtubule formation. Taxol-stabilized microtubules were mixed with test proteins (ranging from 0.125 to 2 mg/mL). The reaction mixture was added on top of a Taxol-glycerol cushion (2X BRB80, 40% glycerol, 20 μM taxane). After high-speed centrifugation (80,000 rpm, 30 min, 30°C), the microtubule-rich pellet fraction was separated from the supernatant fraction. Each fraction was analysed on 12% SDS-PAGE followed by Coomasie staining.

Flow Cytometry

Flow cytometry was performed on cell lines, BMDCs or cells isolated from spleen, lymph nodes or skin. Single cell suspensions were washed with PBS and stained with the fixable live/dead UV Zombie dye (BioLegend). Cells were then blocked with Fc receptor-blocking anti-CD16/32 antibody (clone 2.4G2; 1:100) for 20 minutes at 4 °C and stained for cell surface antigens using the following fluorophore-conjugated anti-murine antibodies for 20 minutes at 4 °C: CD11c-PE-Cy7 (clone HL3; 1:200), MHCII-BV510 (clone M5/144.15.2; 1:200), CD11b-APC-Cy7 (clone M1/70; 1:200), CD86-APC (clone GL-1; 1:300), CD80-PE (clone 16-10A1; 1:300), CD45-APC-Cy7 (clone 30-F11; 1:300), CD40-BV421 (clone 3/23; 1:200), TCRVb5-APC (clone MR9-4; 1:200). Washing and antibody incubations were performed in

FACS buffer (PBS, 0.5 mM EDTA, 2% FCS). Cells were either fixed with IC fix buffer (eBioscience) for 20 minutes or were directly acquired on LSR Fortessa or FACS Aria III (both BD Bioscience).

In vitro Stimulation of OVA-Specific OT-I and OT-II T Cells

SP37A3 cells or day 6 BMDCs were pulsed for 1 hour with OVA full-length protein (0.1 mg/mL) before activation with ansamitocin-P3 (100 nM), taxane (100 nM) or LPS (100 ng/mL) and added at the indicated ratios to CD8 or CD4 T cells purified (by magnetic selection; Miltenyi Biotec) from spleen and LN of OT-I/OT-II transgenic mice (2 x10^5 total cells/well, 96-well round bottomed plate). The CD8 and CD4 T cells were loaded with the proliferation dye CellTrace Violet (Molecular Probes) before co-culture following manufacturer's instructions. Proliferation was assessed after 3 days using flow cytometry.

In vivo Activation of Skin DCs

Ansamitocin-P3 (4 µg/ear) or LPS (8 µg/ear) or Vehicle (1.5% DMSO) was injected intradermally into the ears of C57BL/6N WT or GEFH1$^{-/-}$ mice. Analysis was performed after 24 hours using flow cytometry. Epidermal sheets were digested with Accutase (Sigma), collagenase IV (Worthington), hyaluronidase (Sigma), and DNAse type IV (Sigma). Single-cell suspensions were prepared and stained with anti-CD45, anti-CD11c, anti-MHC-II, anti-CD86 and anti-CD80 antibodies. Dead cells were excluded using Zombie UV dye (BioLegend).

In Vivo Stimulation of Antigen-Specific CD8 and CD4 T Cells

CD8 and CD4 T cells from LNs and spleen of naïve OT-I and OT-II transgenic mice, respectively, were purified using magnetic separation (Miltenyi Biotec) and labeled with CellTrace Violet (Molecular Probes) following manufacturer's instructions. Two million CD8 or CD4 T cells were adoptively transferred i.v. into C57BL/6N WT or GEFH1$^{-/-}$ mice. After 24 hours, mice were immunized via tail-base injection with full length OVA protein (25 µg/mouse) together with ansamitocin-P3 (4 µg/mouse) or LPS (25 µg/mouse) or vehicle (0.5% DMSO). Three days after immunization draining lymph nodes (iliac, axial and inguinal) were collected and proliferation of the adoptively transferred OT-I CD8 and OT-II CD4 T cells was assessed by flow cytometry.

In Vivo Tumor Challenge and Treatment Protocol

C57BL/6N WT or C57BL/6N GEFH1$^{-/-}$ mice were injected subcutaneously into the right flank with 500,000 syngeneic MC38 cells suspended in phenol red-free DMEM (without additives). Mice bearing palpable MC38 tumors received peri-tumoral injection of 50 µL ansamitocin-P3 (0.3 mg/kg) or vehicle (2% DMSO) on days 8, 9 and 10 post tumor challenge. Tumor volume was calculated according to the formula: D /2*d*d, with D and d being the longest and shortest tumor diameter in mm, respectively.

RNAseq and GSEA Analyses

RNA was isolated from C57BL/6N WT and GEFH1$^{-/-}$ DCs using RNeasy Micro kit (Qiagen) following the manufacturer's instructions. Libraries were synthesized using Illumina TruSeq Stranded mRNA sample preparation kit from 500 ng of purified total RNA and indexed adaptors according to the manufacturer's protocol (Illumina). The final dsDNA libraries were quantified by Qubit fluorometer, Agilent Tapestation 2200, and RT-qPCR using the Kapa

Biosystems library quantification kit according to manufacturer's protocols. Pooled libraries were subjected to 35-bp paired-end sequencing according to the manufacturer's protocol (Illumina NextSeq 500). Targeted sequencing depth was 25 million paired-end reads per sample. Blc2fastq2 Conversion software (Illumina) was used to generate de-multiplexed Fastq files.

Expression values were normalized as Fragments per Kilobase Million reads after correction for gene length (FPKM) in Cuffdiff version 1.05 in the DNAnexus analysis pipleline. We filtered for statistically significant ($P < 0.01$) genes with a false discovery rate (FDR) threshold of 0.05 and a biologically relevant change (log fold change >1; logFC). Samples were analyzed in the RNAsequencing pipeline of Seqmonk for mRNAs for opposing strand specific and paired end libraries with merged transcriptome isoforms, correction for DNA contamination and log transformed resulting expression values in log2FPM. Ansamitocin-P3 induced mRNAs that were differentially regulated more that 2-fold (FDR threshold of 0.05) in the Cuffdiff analysis of WT DCs were imported into Seqmonk for per-probe normalized hierarchical clustering of mRNA transcription in control and ansamitocin-P3 stimulated WT and GEFH1 deficient DCs.

To generate a ranked gene list for GSEA analyses stranded reads were aligned and counted using STAR (2.5.2a) (Dobin et al., 2013) in stranded union mode using Illumina's ENSEMBL iGenomes GRCm38 build and GRCm38.90 known gene annotations. Count level data was then analyzed using the edgeR Bioconductor package in R (Robinson et al., 2010). Filtered genes, expressed at >1 count per million (cpm) in at least two samples, were analyzed using the QLF functions comparing WT and GEFH1$^{-/-}$ BMDCs untreated and ansamitocin-P3-treated samples. All genes were ranked according to their –log10 transformed corrected p-value for differential up/down-regulation by ansamitocin-P3 in WT versus GEFH1$^{-/-}$ BMDCs. Mouse genes were mapped to their human orthologs using HCOP (http://www.genenames.org/cgi-

bin/hcop at 8.9.17). The pre-ranked list was used to perform weighted GSEA using the GSEA java application (http://www.broad.mit.edu/gsea/) that uses the Molecular Signature Database (MSigDB).

Co-expression Enrichment Analysis

Co-expression analysis interrogates mouse co-expression maps generated by collecting 3571 microarray datasets irrespective of treatment conditions and tissues (van Dam et al., 2012). The co-expression map highlights the co-expression patterns without enrichment for particular tissue or condition among the datasets. The genes that are dependent on both the treatment, and GEFH1 were used for the co-expression enrichment analysis (clusters I and III from Fig. 3c; 831 genes). This gene signature was used as the input to the online tool (http://www.genefriend.org) that produced a ranked list of genes co-expressed with the signature. This tool restitutes the full list of mouse genes (22,766 genes) ordered by the connectivity score to our GEFH1-dependent gene list. From the full list (22,766 genes) we extracted our 831 genes that were then ordered by their interconnectivity within the gene list itself. From this list we took the top 80 co-expressed genes that also belonged within our gene signature. This procedure allowed us to select in an unbiased manner the genes that have a central role within the gene signature matrix. Among the co-expressed genes, we reported the top 15 transcription factors, which are then very likely to be the main drivers of the expression of our GEFH1-related signature. The analysis was repeated using the human orthologs and interrogating the human co-expression network (Monaco et al., 2015). The R package ComplexHeatmap was used to generate the heatmap of the gene expression of the selected 80 genes.

Integrated System for Motif Activity Response Analysis (ISMARA)

Unprocessed read data in fastq format was submitted for ISMARA analysis through the "https://ismara.unibas.ch/" online platform for RNASeq using the mm10 assembly settings as described (Balwierz et al., 2014). Conditions were averaged and the most significantly changed motif activities were extracted (z-score).

Analysis of TCGA Datasets

From the differential expression analysis described in the previous section, we selected the genes that were upregulated upon ansamitocin-P3 treatment and dependent to GEFH1 (FDR < 0.05 and Fold Change >2). Immune specific genes were extracted using the LM22 matrix (Newman et al., 2015) to deconvolute immune signals from tumor samples. RNA-seq datasets of all solid tumors of the TCGA database were downloaded with the R package TCGAbiolinks (Colaprico et al., 2016). For all patients the FPKM value of each gene within the GEFH1 immune signature was log2 transformed and the median expression of the gene signature was used as a surrogate marker of GEFH1 activity. We used univariable Cox regression analyses to investigate the association between the median expression of the gene signature (continuous independent variable) and survival (dependent variable). To account for possible non-linear associations and to circumvent choosing arbitrary cut-points, we used the multivariable fractional polynomial approach (Sauerbrei et al., 2007) for the Cox model. By qualitative assessment of the resulting regression plots, we identified a cut-off at 14 as clinically important and created Kaplan-Meier plots to visualize the difference in survival. To investigate the association between the gene signature and survival across several tumor types, we used techniques of random and fixed effects meta-analysis. Hazard ratios from each Cox regression model (by each tumour type) were pooled; results from this prognostic meta-analysis are

visualized by a forest plot. Associations are expressed with hazard ratios accompanied by 95% confidence intervals.

Quantification and statistical analysis

All samples or animals from each experiment were included for analysis. GraphPad Prism was used for all statistical analysis. Statistical analysis was carried out by two-way analysis of variance (ANOVA) followed by Tukey's post-hoc test for grouped analyses or by one way ANOVA followed by Tukey's test in case of non-grouped analyses. $P < 0.05$ was considered statistically significant. All graph bars included mean and standard deviation to depict the error.

Data and software availability

The RNAseq data supporting the findings of this study are available within the paper and its supplementary information files. The raw FASTQ files are available from the corresponding authors upon reasonable request.

3.1.6. Acknowledgements

We are grateful to Prof. Karl-Heinz Altmann for providing CW190. This work was supported by grants from the NIH (AI113333, DK068181, and DK043351 to H.-C.R.); the Cancer League Switzerland (KFS-3394-02-2014 to A.Z.); the Huggenberger Foundation and Swiss National Science Foundation (IZK0Z3_170718 to A.S.K.); and the Swiss National Science Foundation (31003A_166608 to M.O.S.). Further financial support was received from BeyondSpring Inc. (to M.O.S. and A.Z.).

3.1.7. Author contributions

A.S.K., H.-C.R., and A.Z. designed the study and wrote the manuscript with contributions from all authors. A.S.K. led and performed most experiments with advice from H.-C.R. and A.Z. Y.Z., K.M., and S.W. helped with coimmunoprecipitation, western immunoblotting, and cell imaging and culture. L.F.-R., N.Y., K.M., P.S., and H.L. helped with flow cytometry and animal studies. A.S. and N.O. performed in vitro microtubule-binding experiments. M.O.S. provided reagents and guidance for experiments with the various microtubule-targeting agents and in vitro microtubule-binding assays. N.K. and M.S. helped with generation of GEF-H1$^{-/-}$ cells and functional validation. G.M., M.P.T., S.-M.P., and H.-C.R. performed RNA-seq and its analyses. B.K. and G.M. performed TCGA survival analyses and B.K. performed meta-analysis. R.Z. performed mice tumor experiments with guidance from A.S.K., H.-C.R., and A.Z. All authors read and reviewed the manuscript

3.1.8. Declaration of Interests

The authors declare no competing interests.

3.1.9. Supplementary Materials

Supplementary Figures S1 to S6, each related to corresponding figures of the main manuscript

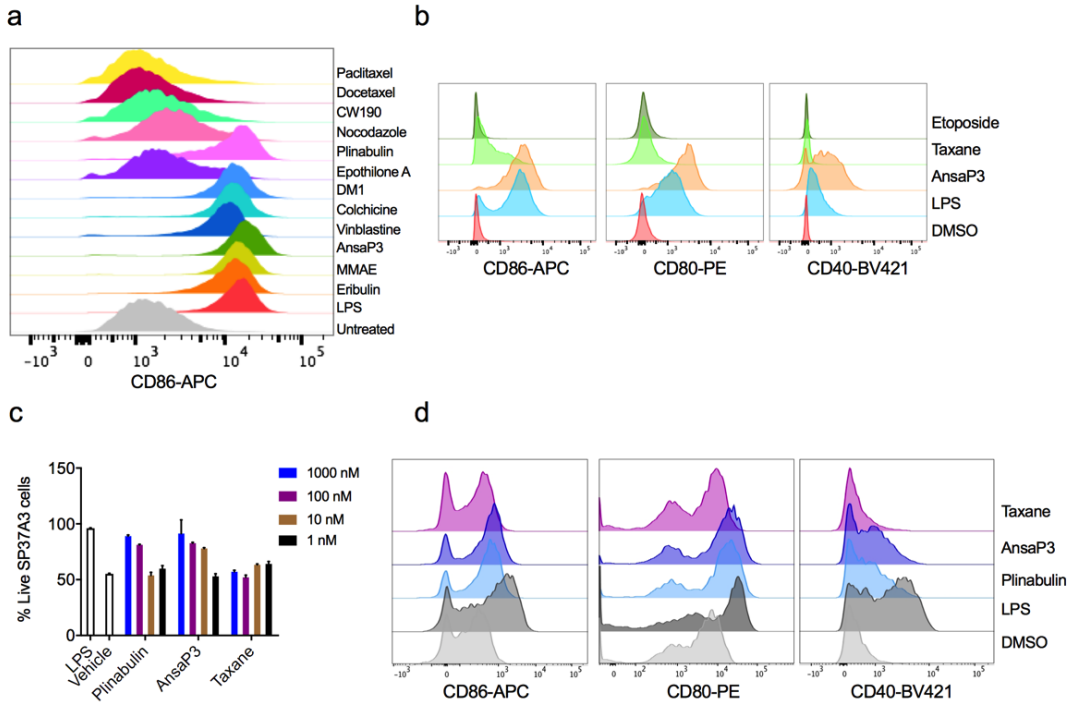

Supplementary Figure S1 (Related to Figure 1) (a, b) Supplementary data for Figure 1a and 1c of main manuscript, respectively. Overlay of representative histograms for indicated proteins assessed by flow cytometry in SP37A3 cells treated for 20 hours with the corresponding drugs at 100 nM or LPS (500 ng/mL). **(c)** SP37A3 cells were treated with plinabulin, ansamitocin-P3 or taxane at the indicated doses for 20 hours after which cell viability was measured using the live/dead Zombie UV dye. LPS (500 ng/mL) and vehicle (0.1% DMSO) were the controls. Data is expressed as percentage of live SP37A3 cells. Experiment was repeated three times with similar results. **(d)** Supplementary data for Figure 1d and 1e of main manuscript. Overlay of representative histograms for indicated proteins assessed by flow cytometry in splenic DCs treated with taxane (100 nM), MDAs ansamitocin-P3 (100 nM) or plinabulin (1000 nM) or LPS at 200 ng/mL. Error bars represent SD.

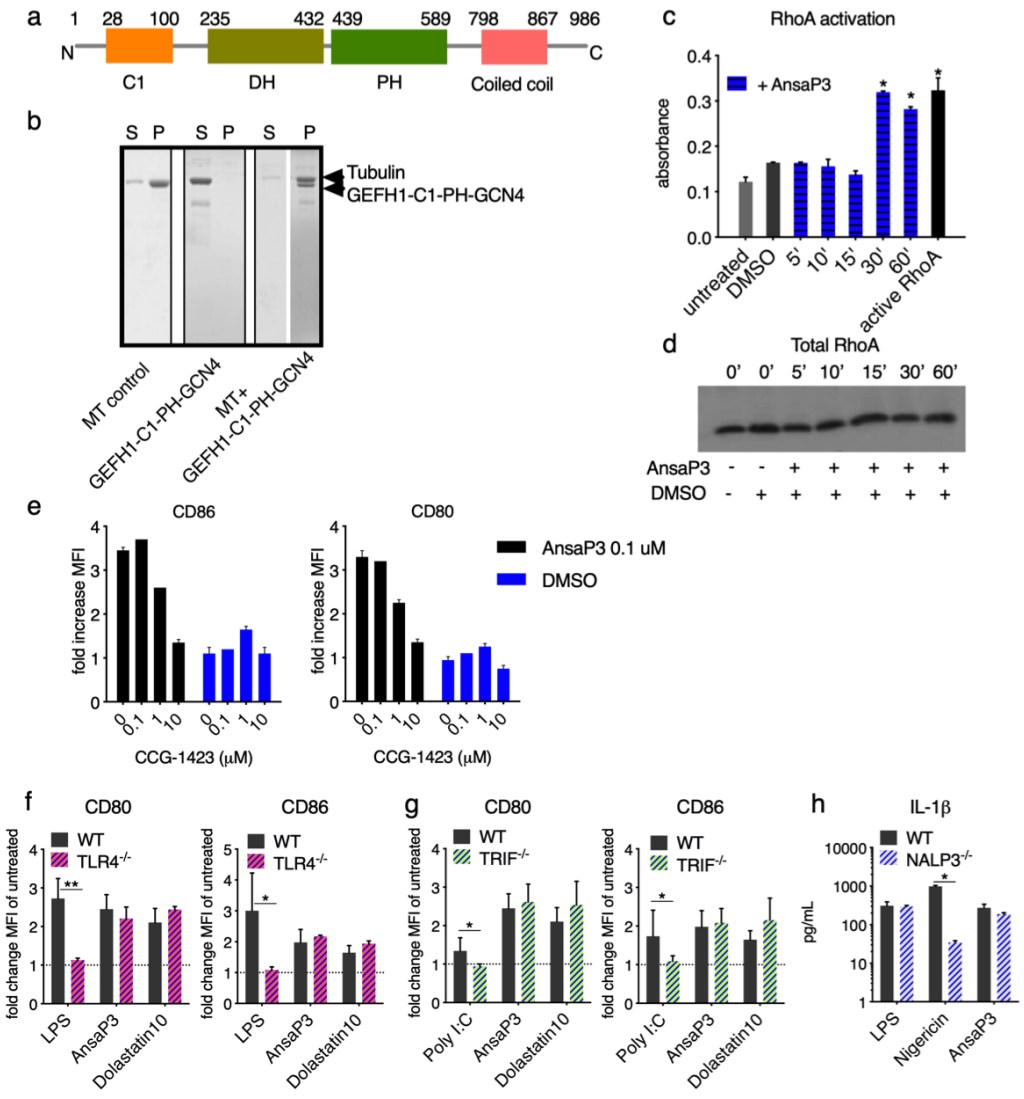

Supplementary Figure S2 (Related to Figure 2) (a) Schematic representation of the domain organization of human GEFH1. Numbers above the schematic correspond to the amino-acids (DH: DbI Homology; PH: Pleckstrin Homology). **(b)** Microtubule pelleting assays with microtubules alone (left panel), GEFH1-C1-PH-GCN4 alone (middle panel) and an equimolar mixture of microtubules and GEFH1-C1-PH-GCN4 (right panel). Shown are Coomasie stained 12% SDS-PAGE gels. S: supernatant; P: pellet; MT: microtubules. **(c)** SP37A3 DCs were incubated with ansamitocin-P3 (100 nM) for indicated time-points (in minutes) before collection of whole cell lysates. Rho-GTP in the lysate was measured using G-LISA. **(d)** Total cell lysate from **c** was probed for RhoA using western blot to determine equal loading. Data is pooled from two independent experiments. **(e)** Serum-starved SP37A3 DCs were pretreated with the RhoA-inhibitor CCG-1423 at indicated concentrations (μM) for two hours before addition of ansamitocin P3 (0.1 μM) or DMSO control (0.1%) for another 18 h. MFI od CD80 and CD86 was assessed by flow cytometry; graphs show fold change of MFI compared with untreated cells, which were set as 1. **(f-h)** BMDCs from WT and the indicated KO mice were treated with MDAs ansamitocin-P3 or dolastatin 10 (100 nM) or controls for 24h. CD80 and CD86 expression was assessed by flow cytometry (fold change MFI compared to mock-treated cells) and IL-1β was measured by ELISA. LPS was the control for TLR4$^{-/-}$ **f**, Poly I:C for TRIF$^{-/-}$ **g**, and Nigericin for NALP3$^{-/-}$ **h**. Data is pooled from two independent experiments. Error bars represent SD.

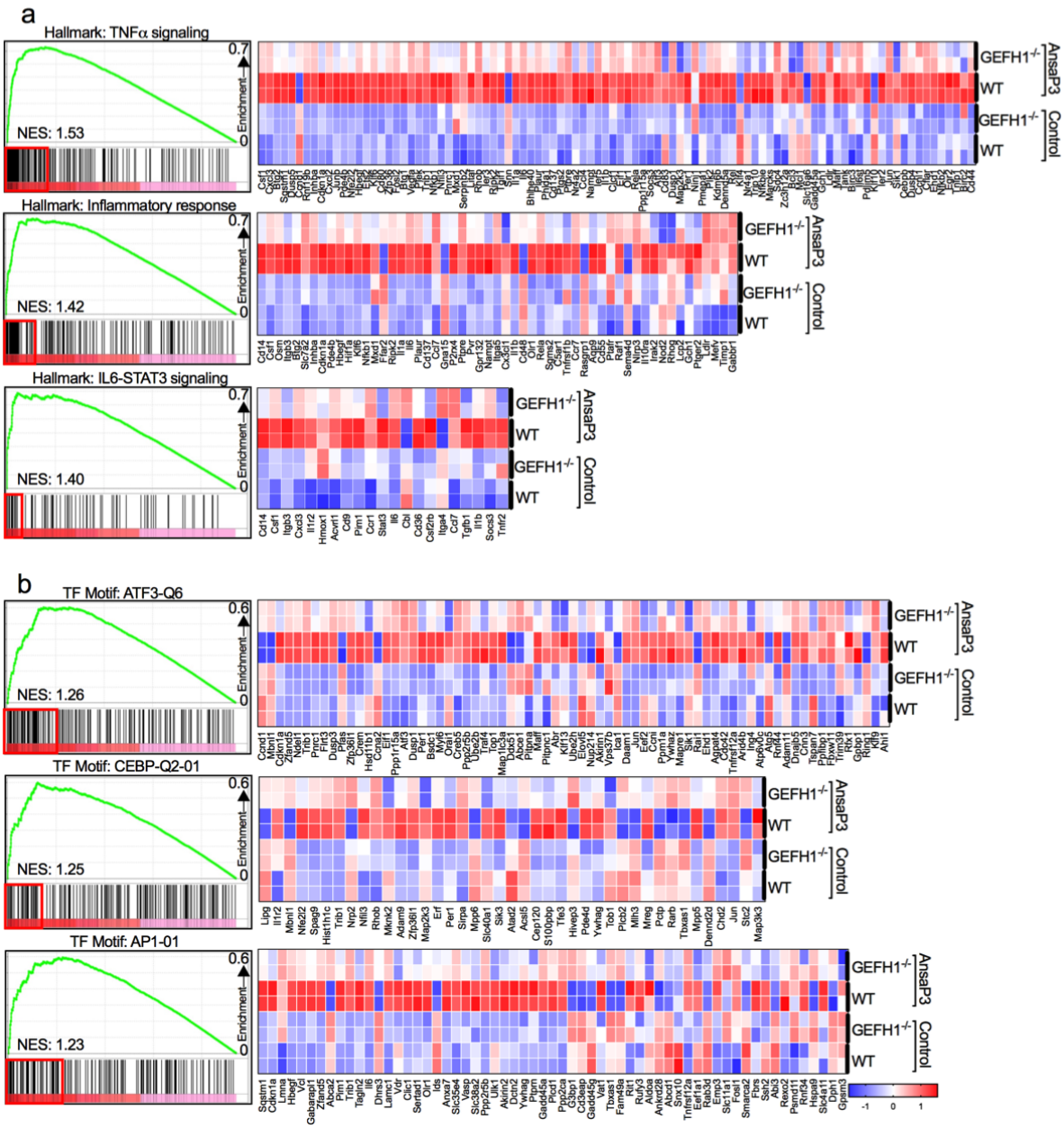

Supplementary Figure S3 (Related to Figure 3) GSEA for differential up/down-regulation by ansamitocin-P3 in WT versus GEFH1$^{-/-}$ BMDCs was performed using ranked list of genes, generated according to the –log10 transformed corrected p-value for differential up/down-regulation by ansamitocin-P3 in WT versus GEFH1$^{-/-}$ BMDCs. Enrichment plots for three selected gene sets are shown for the Hallmark **a** and transcription factor motif **b** collection of MSigDB. NES is indicated within the plot. Leading edge genes are shown as a heat map of scaled, centered logFPKM values across all samples.

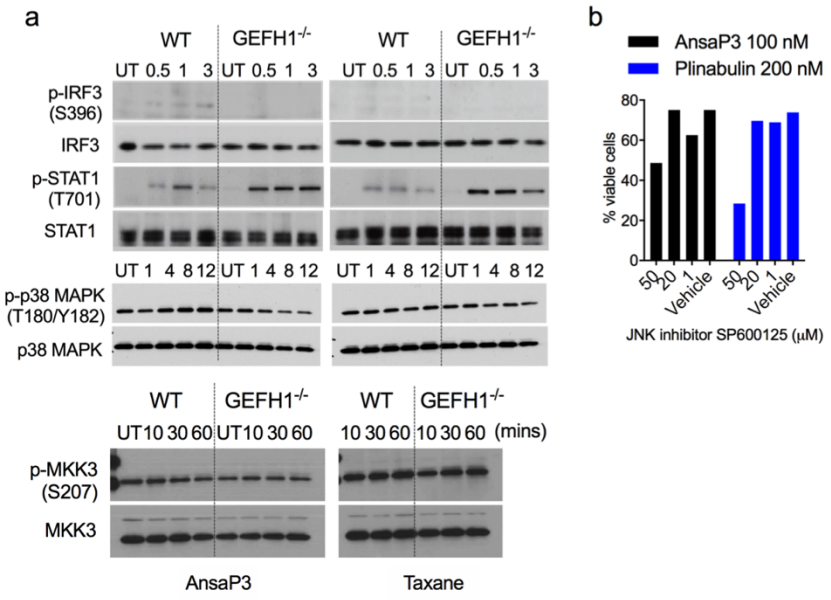

Supplementary Figure S4 (Related to Figure 4) (a) Lysates from WT or GEFH1$^{-/-}$ BMDCs treated for specified time points (indicated in minutes) with ansamitocin-P3 (left) or taxane (right) at 100 nM were probed for phosphorylated IRF3, STAT1, p38 MAPK and MKK3. Blots were stripped and re-probed for the respective total proteins. (b) **(d)** DCs were pre-incubated with the indicated concentrations of the JNK inhibitor SP600125 or Vehicle (0.5% DMSO) for two hours after which they were exposed to MDAs ansamitocin-P3 (100 nM) or plinabulin (200 nM) for 20 hours. Cell viability was then assessed with Live/Dead Zombie UV dye.

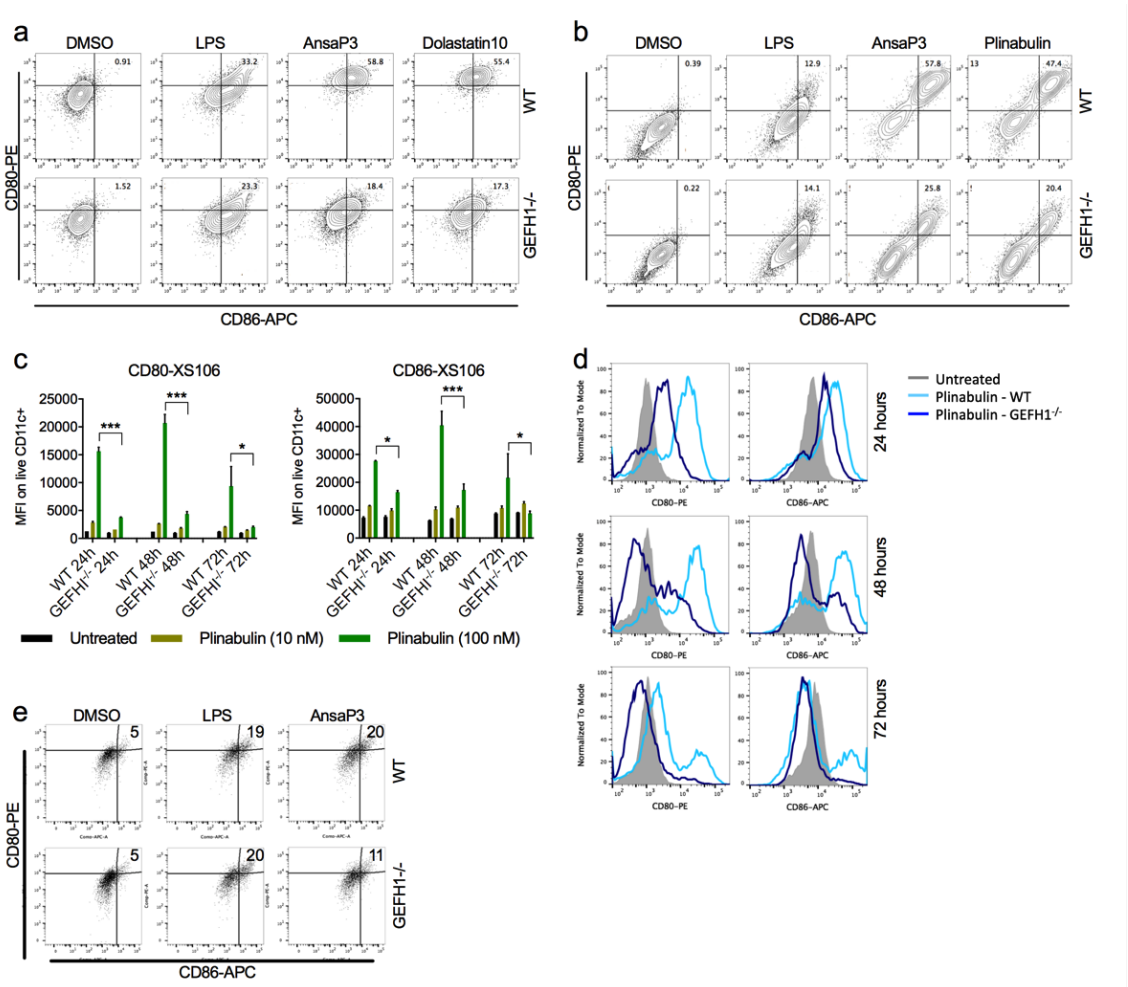

Supplementary Figure S5 (Related to Figure 5) (a) Supplementary data for Figure 5c of main manuscript. BMDCs of WT or GEFH1$^{-/-}$ mice were stimulated with LPS (500 ng/mL), taxane, or MDAs ansamitocin-P3 and dolastatin 10 (all 100 nM) prior to assessment by flow cytometry (20 hours post stimulation). Percentages of gated populations of live CD11c+MHC-II+ BMDCs are indicated. **(b)** Supplementary data for Figure 5d of main manuscript. GEFH1$^{-/-}$ XS106 cells were stimulated with vehicle (0.1% DMSO), LPS (500 ng/mL), or MDAs ansamitocin-P3 and plinabulin (both 100 nM) prior to assessment by flow cytometry (20 hours post stimulation). Percentages of gated populations of live cells are indicated. **(c)** WT or GEFH1$^{-/-}$ XS106 cells were treated at indicated time points with plinabulin (10 nM and 100 nM). At endpoint, MFI for CD80 and CD86 was assessed by flow cytometry. **(d)** Overlapping histograms from **c** are indicated for the 100 nM dose of plinabulin. **(e)** Supplementary data for Figure 5e of main manuscript. Ansamitocin-P3 (4 µg), LPS (8 µg) or vehicle alone (1.5% DMSO) was injected intradermal in the earflaps of WT and GEFH1$^{-/-}$ mice. CD80 and CD86 expression on intradermal CD11c^{+}MHC-II^{+} DCs was analyzed by flow cytometry. Error bars represent SD.

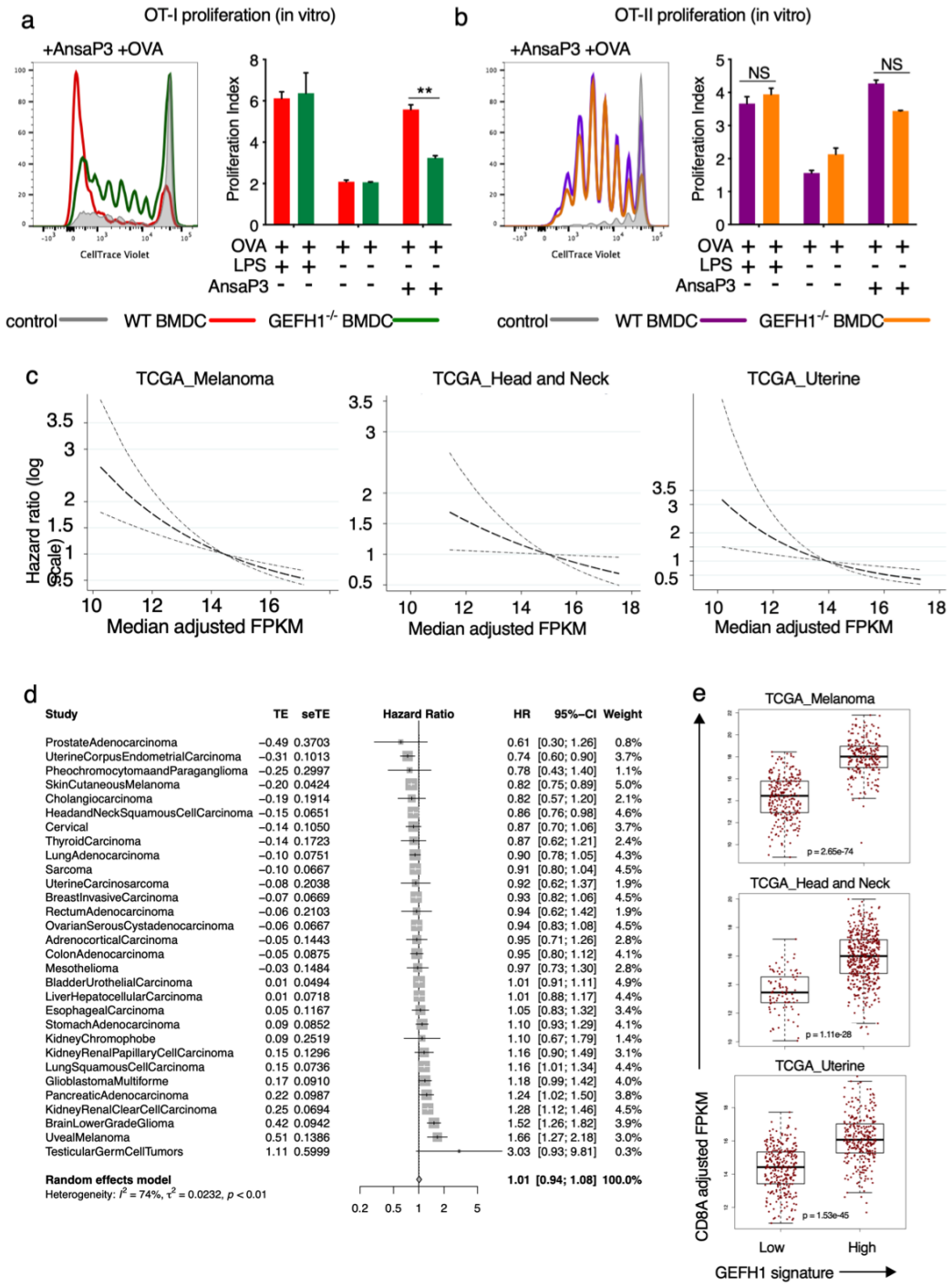

Supplementary Figure S6 (Related to Figure 6) WT or GEFH1$^{-/-}$ BMDCs pre-treated with ansamitocin-P3 (100 nM), LPS (100 ng/mL) or vehicle alone (0.1% DMSO) and pulsed with OVA were co-cultured for 72 hours (without the drugs) with OT-I CD8+ **a** or OT-II CD4+ **b** cells pre-stained with CellTrace Violet. Dye dilution was used to track up to 7 divisions from which the proliferation index was calculated. Bars indicate mean and SD pooled from two independent experiments. Representative histograms indicate overlap of dye dilution in ansamitocin-P3-treated DC:T cell co-culture using WT and GEFH1$^{-/-}$ BMDCs. Control (grey) histograms indicate OVA pulsed but untreated WT BMDCs co-cultured with OT-I/OT-II cells. Error bars represent SD. **(c)** Regression plots (effect with 95% confidence interval) depicting the association of increased expression levels of the GEFH1 Immune Signature with decreased risk of death. Graphs are depicted as hazard ratios versus median adjusted log2 FPKM of the GEFH1 Immune Signature. The upper confidence interval limit has a hazard ratio < 1 after logFPKM of 14. **(d)** Prognostic meta-analysis summarizing the prognostic effect of the GEFH1 immune signature in all solid tumors deposited in TCGA. A hazard ratio smaller than 1 implies a relative risk reduction of

death. **(e)** CD8A expression in patient tumors stratified according to the median expression of GEFH1 Immune Signature (High: median log2 FPKM >=14; Low: median log2 FPKM <14).

Upon request or referred to publication: DOI: https://doi.org/10.1016/j.celrep.2019.08.057

Supplementary Video (Related to Figure 2): GEFH1 release upon microtubule destabilization

Time lapse confocal microscopy was performed to study the localization of GEFH1-GFP in live cells COS7 fibroblasts immediately after treatment with 1 μM ansamitocin-P3. Cells were maintained at 37°C in 5% CO2, and confocal images were acquired using the Nikon A1R-A1 confocal microscope every three minutes for up to 45 minutes after treatment.

Supplementary Table S1 (Related to Figure 3): Expression dataset (gene identifiers and Z scores) of genes differentially expressed in WT BMDCs treated with ansamitocin-P3.

Supplementary Table S2 (Related to Figure 3): Expression dataset (gene identifiers and Z scores) of GEFH1 dependent downregulated genes upon ansamitocin-P3 treatment of BMDCs (Cluster I of Figure 3c of main manuscript).

Supplementary Table S3 (Related to Figure 3): Expression dataset (gene identifiers and Z scores) of GEFH1 independent downregulated genes upon ansamitocin-P3 treatment of BMDCs (Cluster II of Figure 3c of main manuscript).

Supplementary Table S4 (Related to Figure 3): Expression dataset (gene identifiers and Z scores) of GEFH1 dependent upregulated genes upon ansamitocin-P3 treatment of BMDCs (Cluster III of Figure 3c of main manuscript).

Supplementary Table S5 (Related to Figure 3): Expression dataset (gene identifiers and Z scores) of GEFH1 independent upregulated genes upon ansamitocin-P3 treatment of BMDCs (Cluster IV of Figure 3c of main manuscript).

Supplementary Table S6 (Related to Figure 3): Co-expression analyses performed using GeneFriends of RNAseq data from WT and GEFH1-/- BMDCs untreated or treated with ansamitocin-P3 (Figure 3e and f of main manuscript).

Supplementary Table S7 (Related to Figure 3): Integrated System for Motif Activity Response Analysis (ISMARA) of RNAseq data from WT and GEFH1-/- BMDCs untreated or treated with ansamitocin-P3 (Figure 3g of main manuscript).

Supplementary Table S8 (Related to Figure 6): GEFH1-dependent immune genes used for the TCGA analyses.

3.2. Dual TLR9 and PD-L1 targeting unleashes dendritic cells to induce durable antitumor immunity in mice

Laura Fernandez-Rodriguez[1,†], Chiara Cianciaruso[3,4,7,†], Ruben Bill[3,4,7], Marcel P Trefny[1], Richard Klar[5], Nicole Kirchhammer[1], Melanie Buchi[1], Julia Festag[5], Sven Michel[5], Rainer H Kohler[7], Elham Pishali Bejestani[1], Andre Maaske[5], Abhishek S Kashyap[1], Frank Jaschinski[5], Karen O Dixon[1], Mikael J Pittet[3,4,6,7,‡*], and Alfred Zippelius[1,2,‡*]

[1]Department of Biomedicine, University Hospital Basel and University of Basel; Basel, Switzerland

[2]Medical Oncology, University Hospital Basel; Basel, Switzerland

[3]Department of Pathology and Immunology, University of Geneva; Geneva, Switzerland

[4]AGORA Cancer Center, Lausanne, Switzerland

[5]Secarna Pharmaceuticals GmbH & Co. KG; Planegg/Martinsried, Germany

[6]Ludwig Institute for Cancer Research, Lausanne, Switzerland

[7]Center for Systems Biology, Massachusetts General Hospital Research Institute and Harvard Medical School; Boston, MA, USA

[†]These authors contributed equally to this work

[‡]These authors contributed equally to this work

*Corresponding author. Email: Mikael.Pittet@unige.ch and Alfred.Zippelius@usb.ch

Manuscript submitted to a peer-reviewed scientific journal.

3.2.1. Abstract

Although immune checkpoint inhibitors (ICIs) have been a breakthrough in clinical oncology, these agents fail to produce durable responses in the majority of patients. The ineffectiveness of treatment may be due to a poor network linking innate and adaptive immunity. Here, we present an antisense oligonucleotide (ASO)-based strategy that dually targets TLR9 and PD-L1 in mice. Unlike PD-L1 antibody therapy, the immunomodulatory IM-T9P1-ASO elicits durable antitumor responses in multiple mouse models of cancer. Mechanistically, IM-T9P1-ASO acts doubly on intratumoral dendritic cells called DC3s by stimulating them via TLR9 engagement and by downregulating their expression of PD-L1. This unleashes the effector functions of DC3s that can efficiently activate antitumor T cells. In particular, we show that IL-12, an immunostimulatory cytokine produced by DC3s, and *Batf3*, a transcription factor required for DC development, are critical for the antitumor efficacy of IM-T9P1-ASO. As in mice, human intratumoral DC3s are the cells with the highest PD-L1 expression, and also express TLRs. Overall, this study provides mechanistic insights for the design of future therapies aimed at stimulating intratumoral DCs through TLRs while controlling their PD-L1 expression, leading to durable control of solid tumors.

3.2.2. Introduction

Blocking immune checkpoints has transformed cancer treatment, demonstrating unprecedented responses in patients with several types of metastatic tumors that were otherwise refractory to available treatment options (Ribas & Wolchok, 2018; Xin Yu et al., 2020; Zhao, Lee, et al., 2019). Monoclonal antibodies that target programmed cell death 1 (PD-1) and its ligand, programmed cell death ligand 1 (PD-L1), are the most widely used immune checkpoint inhibitors (ICIs). These drugs have been demonstrated to inhibit immune-suppressive signals and reinstate cancer immunosurveillance. However, despite the early clinical success, progress has been thwarted by both intrinsic and acquired resistance to treatment, with only a minority of patients showing durable responses (Haslam et al., 2020).

While a complete understanding of the mechanisms that contribute to efficacy and resistance is still lacking, one limitation of using blocking antibodies targeting the PD-1/PD-L1 axis is the internalization of antibody-receptor complexes from the cell surface and the Fc receptor-mediated antibody uptake by intratumoral host cells, such as macrophages (Arlauckas et al., 2017; H. Jin et al., 2021), thereby reducing antibody bioavailability and consequently overall efficacy. Thus, multiple approaches are being explored to overcome these challenges and develop more efficient therapeutic modalities targeting the PD-1/PD-L1 axis.

The clinical success of blocking the PD-1/PD-L1 axis likely relies on activating a network of cellular and molecular processes, which eventually lead to full-fledged activating of antitumor T cells. For instance, PD-L1 can be expressed by different immune cells, including intratumoral macrophages, dendritic cells (DCs) subsets, and tumor cells (Sun et al., 2018), which may all influence the functions of PD-1^+ T cells. Furthermore, while the blockade of the PD-1/PD-L1 axis is associated with $CD8^+$ T cell reinvigoration (Tang et al., 2016), recent evidence suggests

that activated DCs are critically required for treatment-induced antitumor T cell responses (Garris et al., 2018; Mayoux et al., 2020).

Despite being highly conserved between mice and humans (Gerhard et al., 2021), tumor-infiltrating DCs are a sparse and heterogeneous population, which can be divided into plasmacytoid DC (pDC), known to produce type I interferons (IFNs), and conventional DCs (cDC). The latter can be further categorized into three transcriptionally distinct states: cDC1, which can cross-present antigens to $CD8^+$ T cells, cDC2, which are able to activate $CD4^+$ helper T cells and, to some extent, $CD8^+$ T cells, and DC3s, which express high levels of pro-inflammatory genes, including CD80, CD86, MHC-II and IL-12.

Tumor-associated DC3s were initially identified in lung adenocarcinoma (Zilionis et al., 2019) and have been subsequently found in many cancer types. They have also been attributed different names, including $LAMP3^+$ DC (Zhang et al., 2019), mregDC (Maier et al., 2020) and $CCR7^+$ DC (Qian et al., 2020); however, all describe the same cellular state (Gerhard et al., 2021). The chemokine receptor CCR7 can guide DCs to lymph nodes via lymphatic vessels to traffic tumor antigens and prime tumor-specific $CD8^+$ T cells (Roberts et al., 2016), and is expressed by DC3s. However, at least some of these cells remain within tumors, where they can promote antitumor immunity by supporting incoming T cells with survival signals (Di Pilato et al., 2021) and enabling them to perform their effector functions (Garris et al., 2018). Interestingly, DC3s also express immunomodulatory factors, such as the immune checkpoint molecule PD-L1, which may limit their antitumor activity (Cheng et al., 2021; Leader et al., 2021; Maier et al., 2020).

In light of the advances in understanding the mechanisms of resistance to anti-PD-1/PD-L1 therapies, we hypothesized that developing drugs that overcome the barriers to the successful inhibition of the PD-1/PD-L1 axis while concurrently licensing potent DC responses could be a powerful mechanism for the induction of durable antitumor immunity. In this context, we considered Gapmer locked nucleic acid (LNA) antisense oligonucleotides (ASOs) for several reasons. First, their high-affinity ASOs recruit the cellular enzyme RNase H upon binding to the target pre-mRNA, allowing for efficient degradation of the latter (Gagliardi & Ashizawa, 2021). Second, due to their mechanism of action, ASOs achieve specific target knockdown of all types of proteins (e.g., intracellular, secreted, surface) (Jaschinski et al., 2015), making them possibly relevant to treat a wide range of diseases. For example, the combination of a CD39-targeting ASO with an anti-PD-1 monoclonal antibody (mAb) improves antitumor responses in preclinical models (Kashyap et al., 2019). Third, due to their DNA-based chemical structure, extracellular oligonucleotides such as ASOs can mimic microbial infections and elicit immune stimulation by activating pattern recognition receptors (PRRs). For instance, Toll-like receptor 9 (TLR9) is a PRR expressed by different types of immune cells including DCs and is activated by extracellular DNA, especially DNA-containing unmethylated CpG motifs frequently present in bacterial DNA (Hemmi et al., 2000).

In this study, we sought to overcome the limited therapeutic efficacy of anti-PD-1/PD-L1 mAb by using an ASO-based therapeutic strategy with the dual capacity to trigger DC activation via TLR9 engagement and control of PD-L1 expression by these cells.

3.2.3. Results

PD-L1 antibody treatment triggers insufficient DC and T cell antitumor immunity in the MC38 tumor model

Durable responses to ICIs are observed only in a minority of patients (Shen & Zhao, 2018). To mirror this clinical situation, we treated mice bearing established subcutaneous colorectal MC38 tumors or orthotopic breast EMT-6 tumors with anti-PD-L1 mAb. We observed a delay in MC38 tumor growth in anti-PD-L1–treated mice; however, none (0/8) of the mice showed durable tumor control (Fig. 1A, fig. S1A), making this experimental setup a poor responder model to anti-PD-L1-mAb treatment. In parallel, the same treatment triggered long-term survival in 28% (5/18) of EMT6 tumor-bearing mice (fig. S1B), indicating that durable responses could be seen in this model, but only in a minority of mice.

Due to the critical role of intratumoral PD-L1–expressing DCs in regulating responses to ICIs (Oh et al., 2020), we investigated tumor immune infiltrates in MC38 tumor bearing mice by multiparameter flow cytometry four days after start of treatment (fig. S1C). We found comparable frequencies of total intratumoral $CD11c^+$ $MHC\text{-}II^+$ DCs in control and anti-PD-L1–treated mice (Fig. 1B). However, the proportion of $CCR7^+$ DCs (hereafter DC3s) was higher in anti-PD-L1–treated tumors compared with controls, while $XCR1^+$ DCs (hereafter DC1s, also defined by CD103 expression) and $CD11b^+$ DCs (hereafter cDC2s, also defined by Sirpa expression) were not affected (Fig. 1C). Examining the maturation status of intratumoral DCs in anti-PD-L1–treated mice, we detected a decrease in IL-12 and CD80 expression in DC3s, but not in cDC1s and cDC2s (Fig. 1D). Like in the tumor, we also found increased $CCR7^+$ DCs (fig. S1D) in the tumor-draining lymph nodes (dLN), as well as CD80 downregulation on $CCR7^+$ DCs and macrophages in response to anti-PD-L1 (fig. S1E).

In line with previous data (Zhao, Lee, et al., 2019), these findings may indicate a reduced capacity of APCs to activate T cells through co-stimulatory molecules and cytokine secretion after anti-PD-L1 mAb therapy, reflected in the absence of intratumoral $CD8^+$ T cell expansion and activation, assessed by CD25 expression (fig. S1F). While insufficient activation may dampen tumor-specific T cell responses and prevent durable antitumor immunity, we hypothesized that the therapeutic efficacy of targeting PD-1/PD-L1 might be amplified by strategies that simultaneously promote DC activation.

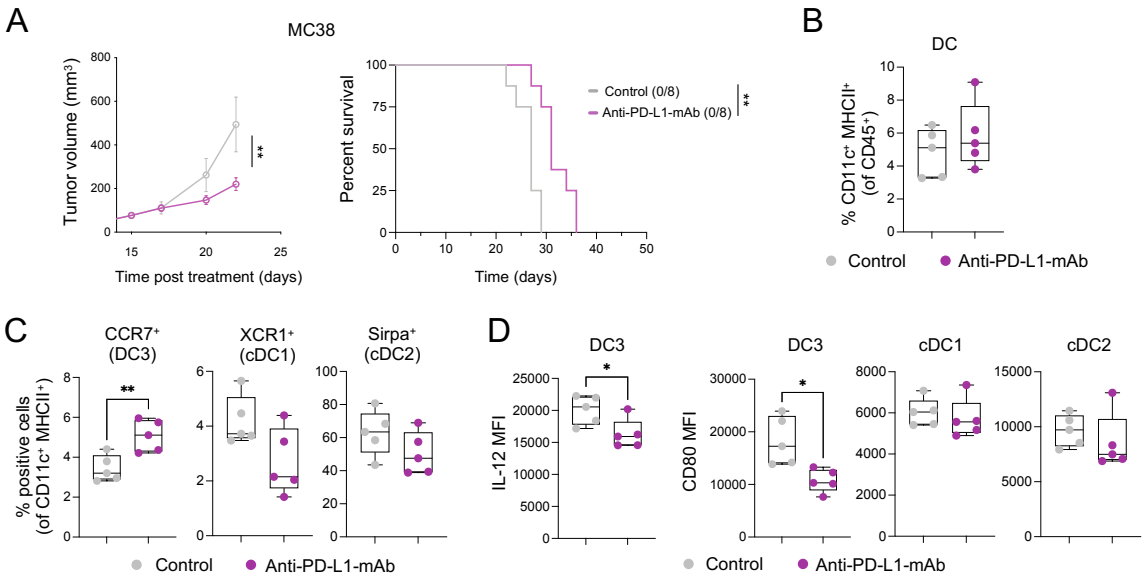

Fig. 1. Anti-PD-L1-mAb does not stimulate sufficient DC3 and T cell activation in MC38 tumors. (A) Average tumor growth (left) and Kaplan-Meier survival curve (right) of MC38 tumor-bearing mice treated with anti-PD-L1-mAb or control (n=8 mice/condition). The number of tumor-free mice is indicated in brackets. **(B and C)** Flow cytometry analysis of MC38 tumors after four days of treatment showing proportions of total DCs **(B)** and DC subsets **(C)** (n = 5 mice/condition). **(D)** Flow cytometry analysis of IL-12 and CD80 expression (mean fluorescence intensity, MFI) in DC subsets in MC38 tumors four days after treatment (n=5 mice/condition).
Data are presented as mean ± SEM. For comparisons between multiple groups and variables, two-way ANOVA was used. For survival analysis, the Mantel-Cox log-rank was used. For comparisons between two groups, Student's two-tailed t test was used. *p < 0.05, **p < 0.01, ***p < 0.001, ****p < 0.0001.

IM-T9P1-ASO downregulates PD-L1 and stimulates DC maturation in vitro

In this endeavor, we aimed to target TLR9, which is known to induce innate and adaptive immune responses (Y. Jin et al., 2021) and is expressed by myeloid cells in MC38 tumors, particularly by cDC1s and DC3s (fig. S2A). To this end, we designed an immuno-modulatory immunomodulatory IM-TLR9:PD-L1-ASO antisense oligonucleotide (hereafter, IM-T9P1-ASO) able to trigger TLR9 stimulation and downregulate *Cd274*, encoding the mouse PD-L1, in the same target cell.

To evaluate the inherent ability of IM-T9P1-ASO to activate cells via TLR9, we exposed established NF-kB reporter cells expressing different TLRs to IM-T9P1-ASO. By measuring NF-kB activity, we confirmed the capacity of IM-T9P1-ASO to specifically induce TLR9 activation while being inactive on TLR3, TLR7 and TLR8 (fig. S2B). Importantly, a non-targeting control oligonucleotide (later Ctr-ASO) demonstrated no activity in these assays (fig. S2B).

We next tested the ability of IM-T9P1-ASO to downregulate PD-L1 expression using two PD-L1^{+} cell lines and found a reduction of PD-L1 in IM-T9P1-ASO–treated cells compared to Ctr-ASO (fig. S2C,D). A similar reduction in PD-L1 expression by IM-T9P1-ASO was observed on IL-4 and IFNγ-matured monocyte-derived dendritic cells (moDCs) (Fig. 2A,B). Finally, considering the blunted activation of intratumoral DC3s after anti-PD-L1 mAb treatment (Fig. 1D), we used immature Flt-3L-cultured conventional DC (FL-cDC) to test whether IM-T9P1-ASO treatment could stimulate a DC3 program *in vitro*. Using this approach, we found that immature FL-cDCs treated with IM-T9P1-ASO upregulated the expression of CD80, MHC-II and CCR7, which was in stark contrast to both Ctr-ASO and anti-PD-L1 mAb (Fig. 2C).

Loss of activity in TLR9$^{-/-}$ DCs demonstrated that the differentiation into a DC3-like program depended on TLR9 (Fig. 2D). Furthermore, treatment of immature FL-cDCs with a TLR9 stimulation oligonucleotide (CpG) showed similar effects as IM-T9P1-ASO. We also confirmed that the *in vitro* generation of DC3-like cells was independent of PD-L1, as immature FL-cDCs from PD-L1$^{-/-}$ mice produced CCR7^{+} IL-12^{+} DC3-like cells upon IM-T9P1-ASO treatment (Fig. 2D).

DCs play a critical role in priming and regulating tumor-specific T cell responses (Böttcher et al., 2018; Roberts et al., 2016; Spranger et al., 2017). To investigate whether DCs exposed to IM-T9P1-ASO could more efficiently present antigens and activate CD8^{+} T cells *in vitro*, SIINFEKL-specific CD8^{+} T cells from OT-I mice were co-cultured with Ctr-ASO or IM-T9P1-ASO–treated moDCs loaded with OVA protein. In co-culture with IM-T9P1-ASO–treated DCs, CD8^{+} T cells showed increased expansion and functionality, as assessed by proliferation (Fig. 2E,F) and production of granzyme B (Fig. 2G).

Altogether, these *in vitro* data show that ASOs can be designed to simultaneously mediate the downregulation of PD-L1 expression and induce maturation of DCs through TLR9, leading to robust T cell activation.

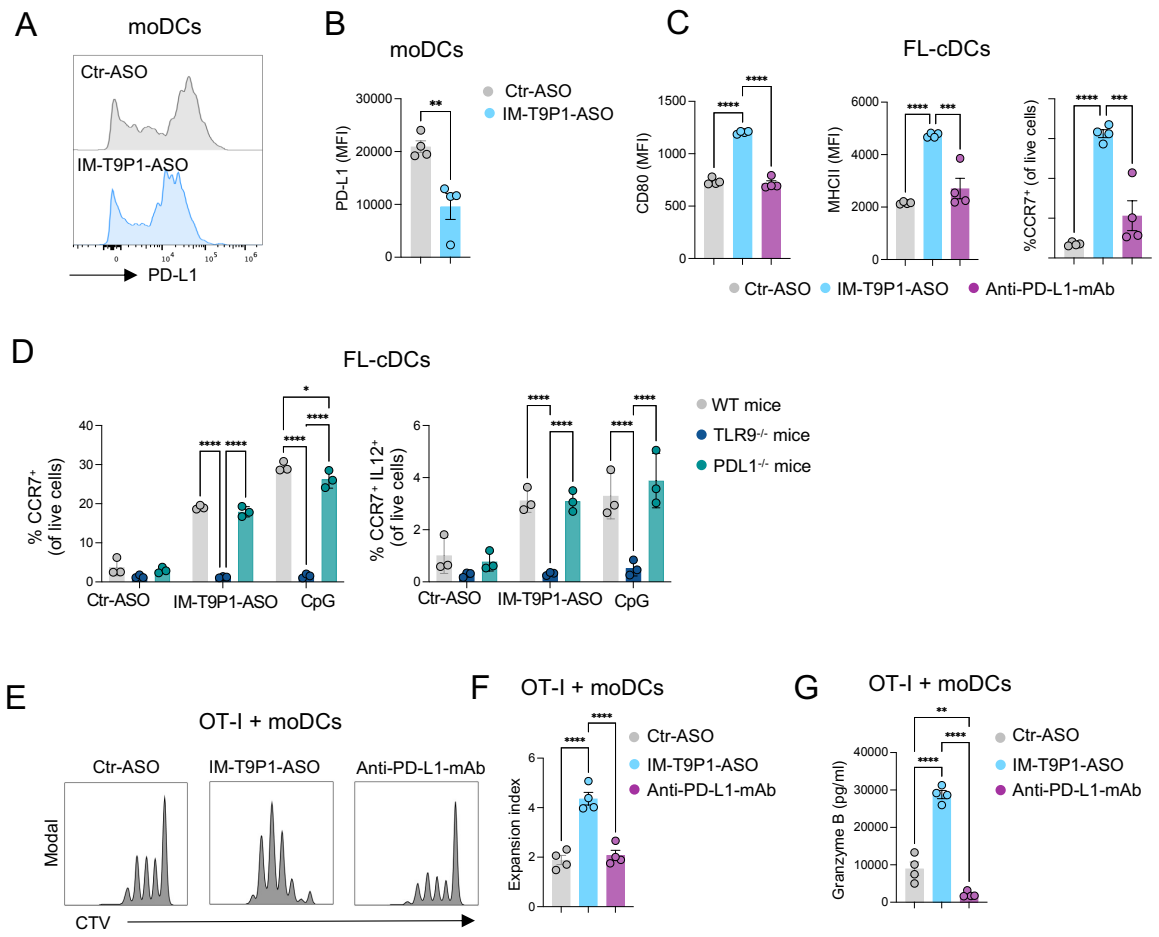

Fig. 2. IM-T9P1-ASO stimulates *in vitro* DC activation and IL-12 secretion while decreasing PD-L1 expression. (A-B) Flow cytometry analysis of PD-L1 expression in *in vitro*-cultured moDCs exposed to Ctr-ASO or IM-T9P1-ASO (n=4 cell cultures/condition). Representative histogram plots **(A)** and cumulative analysis of PD-L1 MFI **(B). (C-D)** Flow cytometry analysis of activation markers in *in vitro*-cultured FL-cDCs derived from wild-type mice **(C and D)**, or transgenic TLR9$^{-/-}$ and PD-L1$^{-/-}$ mice **(D)**, and exposed to Ctr-ASO or IM-T9P1-ASO (n=3-4 cell cultures/condition). **(E-F)** Flow cytometry analysis of CD8^{+} OT-I cell proliferation after three days of culture with OVA-loaded moDCs previously exposed to the indicated agents. **(E)** Representative histograms showing CellTrace Violet (CTV) dilution. **(F)** Quantification of the data (n=4 cell cultures/condition). **(G)** ELISA-based quantification of Granzyme B in medium conditioned by CD8^{+} OT-I cells treated as in **(E-F)**. Data are presented as mean ± SEM. For comparisons between two groups, Student's two-tailed t test was used. For comparisons between multiple groups or variables, one-way (C, F, G) or two-way (D) ANOVA was used. *p < 0.05, **p < 0.01, ***p < 0.001, ****p < 0.0001.

IM-T9P1-ASO shows superior antitumor efficacy compared to PD-L1 mAb treatment

We initially assessed IM-T9P1-ASO's pharmacokinetics *in vivo* in tumor-bearing mice. Using intravital imaging (fig. S3A), we observed a rapid and homogenous diffusion of a fluorescently-labeled IM-T9P1-ASO (AF647-IM-T9P1-ASO) from the tumor vasculature into the tumor parenchyma (fig. S3B-D), indicating the drug's ability to distribute within the tumor and potentially reach its intended target cells.

We next evaluated the therapeutic efficacy of IM-T9P1-ASO. While we did not observe changes in body weight suggesting a lack of overt toxicity (fig. S3E), treatment with IM-T9P1-ASO exhibited potent inhibition of tumor growth in different syngeneic tumor models (Fig. 3A-C, S3F,G and S4A), leading to increased survival and complete tumor regressions (Fig. 3A,B). Notably, IM-T9P1-ASO triggered durable responses in 39% (7/18) of MC38 tumor-bearing mice (compared to the 0% response rate following PD-L1 mAb treatment), and in 77% (30/39) of EMT6 tumor-bearing mice (compared to the 28% response rate following PD-L1 mAb treatment). Additionally, we observed a significant antitumor effect of IM-T9P1-ASO in the D4M.3A melanoma model (Fig. 3C), which is considered poorly immunogenic and unresponsive to anti-PD-1 mAb therapy (Di Pilato et al., 2021). Treatment with Ctr-ASO, anti-PD-L1 mAb or TLR9 agonist CpG-ODN 1826 had no or minimal impact on MC38 tumor growth compared with untreated mice (fig. S4B,C). In addition, IM-T9P1-ASO induced the formation of protective antitumor memory, as mice that survived the initial treatment remained tumor-free after a later rechallenge with the same cell line (Fig. 3D).

We found increased frequencies of $CD8^+$ T cells and an increased CD8/Treg ratio in MC38-tumor bearing mice treated with IM-T9P1-ASO (Fig. 3E), reflecting the induction of an efficient antitumor immune response (Saleh & Elkord, 2020b). In addition, while $FoxP3^+$ Tregs

showed decreased CTLA-4 expression (Fig. 3E), we noted an increase in PD-1 and CTLA-4 expression on $CD8^+$ T cells (Fig. 3F). To test whether targeting all these immune checkpoints in a combined approach may further improve antitumor responses, we treated large MC38 tumors (approx. 150 mm^3) with a combination of IM-T9P1-ASO with either anti-PD-1 or anti-CLTA-4 mAb. Though the tumors at this size are usually treatment refractory even to IM-T9P1-ASO, we observed profound, improved tumor control (Fig. 3G).

Collectively, these data show that IM-T9P1-ASO leads to long-lasting, adaptive antitumor immunity that can be further improved when combined with T cell-targeting ICIs and can have efficacy against large, established tumors in mice.

IM-T9P1-ASO efficacy depends on both TLR9 stimulation and PD-L1 downregulation

PD-L1 is expressed in both cancer and immune cells, and its expression has been reported to positively correlate with the efficacy of anti-PD-1/PD-L1 therapy in some tumor types (Tang & Zheng, 2018). To investigate whether PD-L1 blockade on tumor or host cells contributed to IM-T9P1-ASO–mediated tumor control, we generated *Cd274*$^{-/-}$ (encoding PD-L1) MC38 cells, which we then implanted into wild-type (WT) mice (fig. S4D). Tumor growth of *Cd274*$^{-/-}$ MC38 cells in the presence or absence of IM-T9P1-ASO treatment was similar to MC38-WT, suggesting that PD-L1 knockdown in cancer cells is not sufficient for tumor control and that IM-T9P1-ASO may act predominantly through modulation of host cellular responses (fig. S4E). Accordingly, in situ hybridization combined with flow cytometry revealed broad *Cd274* mRNA downregulation in intratumoral DC3s, cDC2s, and macrophages, already after two doses of IM-T9P1-ASO, while PD-L1 protein levels were still preserved at this stage (Fig. 3H).

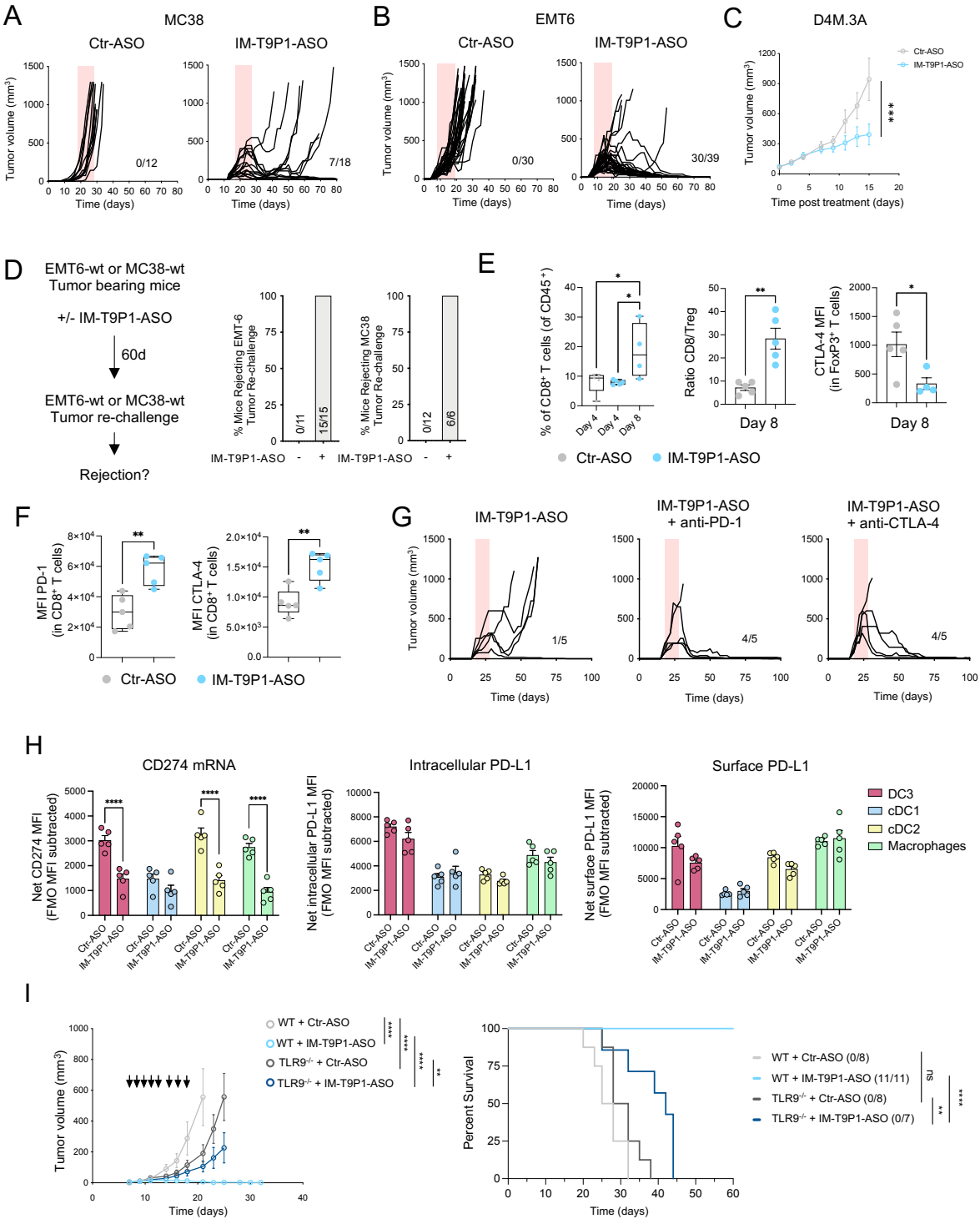

Fig. 3. IM-T9P1-ASO therapeutic *in vivo* efficacy depends on both TLR9 stimulation and PD-L1 downregulation. (A) Tumor growth of MC38 tumor-bearing mice treated with Ctr-ASO or IM-T9P1-ASO (n=12-18 mice/group). The number of tumor-free mice is shown. **(B)** Tumor growth of EMT6 tumor-bearing mice treated with Ctr-ASO or IM-T9P1-ASO (n=30-39 mice/group). The number of tumor-free mice is indicated. **(C)** Average tumor growth of D4M.3A tumor-bearing mice receiving Ctr-ASO or IM-T9P1-ASO (n=7-8 mice/group). **(D)** Mice cured with IM-T9P1-ASO were re-challenged with the same tumor entity in the contralateral flank. The

percentage of mice rejecting the tumor engraftment is shown. Naïve mice were used as controls for tumor growth (n=6-15 mice/group). **(E)** Flow cytometry quantification of $CD8^+$ T cells (left), $CD8^+$ to $FoxP3^+$ $CD4^+$ T cell ratio (middle) and CTLA-4 expression in $FoxP3^+$ $CD4^+$ T cells (right) in MC38 tumors at the indicated time points during Ctr-ASO or IM-T9P1-ASO therapy (n=4-5 mice/group). **(F)** Flow cytometry analysis of PD-1 and CTLA-4 expression in $CD8^+$ T cells in MC38 tumors eight days after Ctr-ASO or IM-T9P1-ASO treatment (n=5 mice/group). **(G)** Tumor growth of MC38 tumors with treatment initiation at large tumor size (~150 mm3) with IM-T9P1-ASO either as a single agent or in combination with anti-PD-1 mAb or anti-CTLA-4 mAb (n=5 mice/group). The number of tumor-free mice is shown. **(H)** Combined in situ hybridization and flow cytometry analysis of MC38 tumors two days after Ctr-ASO or IM-T9P1-ASO treatment, showing PD-L1 mRNA (left), intracellular protein (middle) and surface protein (right) expression in the indicated cell types (n=5 mice/group). **(I)** Average tumor growth (left) and overall survival (right) of MC38 tumor-bearing WT and $TLR9^{-/-}$ mice treated with Ctr-ASO or IM-T9P1-ASO (n=7-11/group). The number of tumor-free mice is indicated in brackets.
Data are presented as mean ± SEM. For comparisons between two groups, Student's two-tailed t test was used. For comparisons between multiple groups and variables, two-way ANOVA was used. For survival analyses, the Mantel-Cox log-rank test was used. *$p < 0.05$, **$p < 0.01$, ***$p < 0.001$, ****$p < 0.0001$.

To understand the contribution of TLR9 in mediating antitumor efficacy, we treated tumor-bearing mice lacking *Tlr9* with IM-T9P1-ASO and observed less efficient clearance of MC38 tumor cells compared to wildtype (WT) mice (Fig. 3I). We concluded that tumor control mediated by IM-T9P1-ASO is partially but not completely dependent on TLR9. Altogether, these data suggest that both TLR9 triggering and reduction of PD-L1 expression contribute to the therapeutic efficacy of IM-T9P1-ASO.

Increased frequency of migratory DCs in tumor-draining lymph nodes after IM-T9P1-ASO therapy

$CCR7^+$ DCs that migrate to tumor-draining lymph nodes (dLNs) contribute to antigen presentation and priming of T cell immunity (Roberts et al., 2016). Therefore, we also investigated the potential effects of IM-T9P1-ASO on different DC subsets in dLNs and considered non-draining LN (ndLNs) as controls. Interestingly, the number of $CD11c^{int}$ MHC-II^{hi} DCs, often referred to as migratory DCs or migDCs (Kedl et al., 2017), but not $CD11c^{hi}$ MHC-II^{int} DCs, often referred to resident DCs or rDCs, increased in dLNs during IM-T9P1-ASO therapy (Fig. 4A). In contrast, the number of $F4/80^+$ macrophages and $CD19^+$ B cells increased in both dLNs and ndLNs, suggesting a tumor-independent effect of IM-T9P1-ASO therapy on these populations (Fig. 4A). Comparing the activation status of migDCs and rDCs in the dLN of IM-T9P1-ASO–treated mice, we detected PD-L1 downregulation and increased CD80:PD-L1 ratio in migDCs only eight days after treatment start (Fig. 4B,C), suggesting activation of these cells during IM-T9P1-ASO therapy.

Notably, these changes were accompanied by increased PD-1^+Tim3^- effector $CD8^+$ T cells after IM-T9P1-ASO treatment (Fig. 4D, fig. S4F). Several studies have demonstrated that this heterogenous TIL population contains both stem-like and effector-like $CD8^+$ T cells (Kurtulus et al., 2019) and positively correlates with response to checkpoint immunotherapy in patients and pre-clinical models (Kurtulus et al., 2019; Miller et al., 2019; Siddiqui et al., 2019). To address the contribution of self-renewing intratumoral T cells and dLN-resident cells to IM-T9P1-ASO–mediated antitumor immunity, we blocked lymphocyte recirculation with the trafficking inhibitor FTY720 (Morris et al., 2005). IM-T9P1-ASO treatment in the presence of FTY720 allowed initial tumor control but failed to mediate complete tumor regression and

long-term survival (Fig. 4E), suggesting that efficient IM-T9P1-ASO requires both, pre-existing and actively recruited lymphocytes from the dLN to the tumor site.

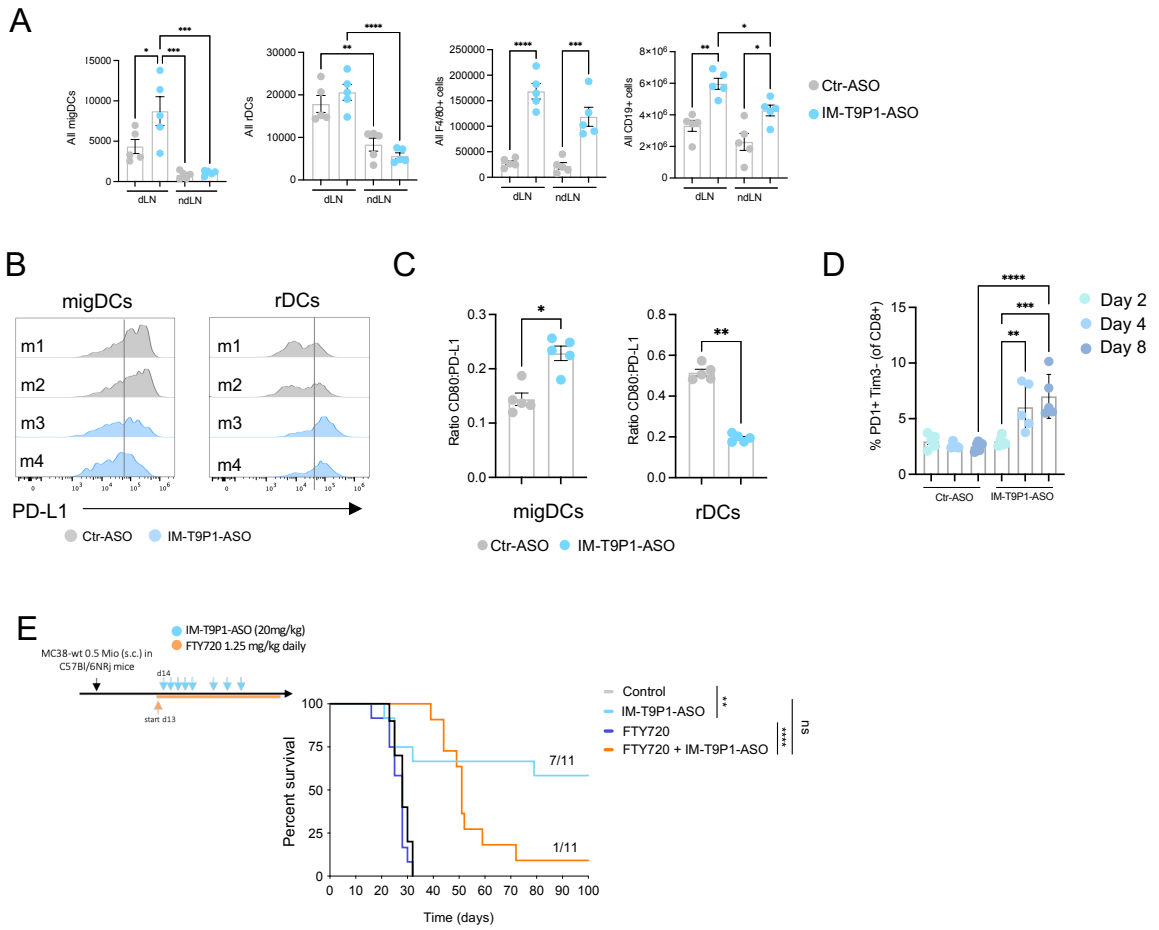

Fig. 4. Increased frequency of migDCs in tumor-draining lymph nodes after IM-T9P1-ASO therapy. (A) Total number of migratory DCs (migDCs - CD11c^{int} MHC-II^{hi} cells), resident DCs (rDCs - CD11c^{hi} MHC-II^{int}), macrophages (F4/80^{+} cells), and B cells (CD19^{+} cells) in MC38 dLN and ndLN, counted by flow cytometry two days after IM-T9P1-ASO or Ctr-ASO treatment (n=5 mice/group). **(B)** Representative flow cytometry histograms of PD-L1 surface expression in migDCs and rDCs eight days after Ctr-ASO or IM-T9P1-ASO treatment. **(C)** Flow cytometry analysis showing the CD80:PD-L1 expression ratio on migDCs and rDCs eight days after Ctr-ASO or IM-T9P1-ASO therapy (n=5 mice/group). **(D)** Proportion of PD-1^{+} Tim3^{-} CD8^{+} T cells after Ctr-ASO or IM-T9P1-ASO therapy at the indicated time points (n=5 mice/group). **(E)** Lymphocyte trafficking was inhibited in MC38 tumor-bearing mice using FTY720 during IM-T9P1-ASO therapy as illustrated (n=11 mice/group). Kaplan-Meier survival curves with the respective number of tumor-free surviving mice are shown.

Data are presented as mean ± SEM. For comparisons between two groups, Student's two-tailed t test was used. For comparisons between multiple groups, one-way ANOVA was used. For survival analyses, the Mantel-Cox log-rank test was used. *p < 0.05, **p < 0.01, ***p < 0.001, ****p < 0.0001.

IM-T9P1-ASO increases intratumoral IL-12$^+$ DC3s

To further understand the contribution of DCs to the therapeutic efficacy of IM-T9P1-ASO, we used *Batf3*$^{-/-}$ mice that show a reduced percentage of cDC1s (Hildner et al., 2008), DC3s and IL-12$^+$ DC3s (fig. S5A,B). Notably, the beneficial therapeutic activity of IM-T9P1-ASO was lost in MC38 tumor-bearing *Batf3*$^{-/-}$ mice (Fig. 5A). Therefore, our data strongly support that the response to IM-T9P1-ASO therapy is driven through the modulation of DCs, leading to better T cell licensing.

To capture early functional and phenotypical changes in tumor-infiltrating DCs, we performed *ex vivo* analysis of MC38 tumors after only two doses of IM-T9P1-ASO. We found that the proportion of intratumoral CD11c$^+$ MHC-II$^+$ DCs, specifically XCR1$^+$ cDC1s and CD11b$^+$ cDC2s, were similar between Ctr-ASO and IM-T9P1-ASO–treated mice (Fig. 5B). However, the frequency of DC3s and SiglecH$^+$ DCs (pDCs) was increased after treatment with IM-T9P1-ASO (Fig. 5B). Because pDC depletion (fig. S5C) had no effect on IM-T9P1-ASO–mediated antitumor immune response (Fig. 5C), we focused our attention on DC3s in further experiments.

We found that the increase in intratumoral DC3s was driven by IFNγ, as demonstrated by the lack of expansion of these cells in IFNgR$^{-/-}$ mice treated with IM-T9P1-ASO (fig. S5D). Furthermore, intratumoral DC3s also failed to expand in TLR9$^{-/-}$ mice treated with IM-T9P1-ASO (fig. S5D), in agreement with our *in vitro* data (Fig. 2D). These data not only support previous studies showing that the presence of a pro-inflammatory milieu is a prerequisite for

DC3 expansion (Garris et al., 2018), but also suggest that conventional DCs, particularly DC3s, and not pDCs, mediate IM-T9P1-ASO therapeutic efficacy.

The production of IL-12 by DCs is critical for successful responses to anti-PD-1 treatment (Garris et al., 2018). Using intravital imaging, we observed that the treatment of IL-12p40-eYFP reporter mice with AF647- IM-T9P1-ASO (fig. S3A) led to an increase in IL-12p40-eYFP^{+} cells (Fig. 5D). Also, about 50% of IL-12p40-eYFP^{+} cells contained AF647-IM-T9P1-ASO four days after treatment, even after a single-dose administration of the drug (fig. S5E). We confirmed the expansion of IL-12^{+} DCs in MC38 tumors by flow cytometry three days after IM-T9P1-ASO treatment (Fig. 5E) and identified DC3s as the dominant IL-12-producing population in this tumor (Fig. 5E). Thus, IM-T9P1-ASO therapy induced IL-12 production primarily by DC3s.

To understand how IM-T9P1-ASO treatment affects the kinetics of PD-L1 expression, we analyzed intratumoral DCs collected at different time points after treatment initiation. We observed that the reduction in PD-L1 expression was particularly evident, at the intracellular and surface level, in DC3s and IL-12-producing DCs on day 3 after the start of treatment (Fig. 5F,G). Furthermore, IM-T9P1-ASO–mediated IL-12 induction was strictly limited to the fraction of TLR9-expressing DC3s (fig. S5F). Overall, these data confirm that induction of the DC3 state is dependent on TLR9 stimulation. In contrast, IM-T9P1-ASO treatment left PD-L1 expression unchanged in other cell types or even increased it in macrophages, cDC1s and cDC2s (Fig. 5G). Thus, IM-T9P1-ASO suppressed PD-L1 expression specifically in DC3s, including those producing IL-12, first at mRNA level and then at the intracellular and surface protein expression level.

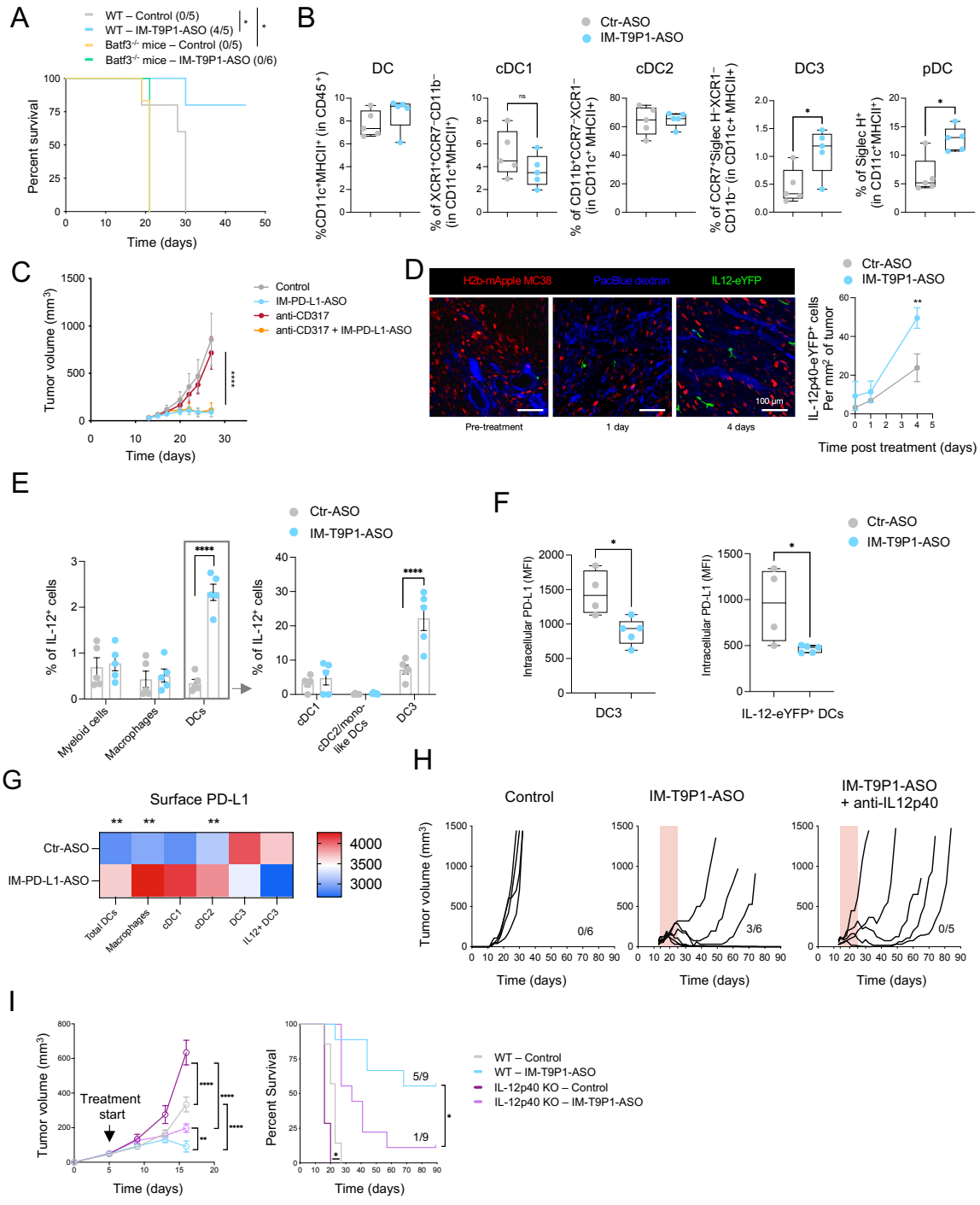

Fig. 5. IM-T9P1-ASO increases intratumoral IL-12$^+$ DC3s. (A) Kaplan-Meier survival curve of MC38 tumor-bearing WT or Batf3$^{-/-}$ mice treated with Ctr-ASO or IM-T9P1-ASO (n=5-6 mice/group). The number of tumor-free mice is indicated in brackets. **(B)** Flow cytometry analysis of the indicated DC subsets in MC38 tumors two days after Ctr-ASO or IM-T9P1-ASO treatment (n=5 mice/group). **(C)** Average tumor growth of MC38 tumor-bearing mice treated with IM-T9P1-ASO both in the presence and absence of pDC depletion antibody CD317

(n=3-6 mice/group). **(D)** Intravital analysis of MC38-mApple tumors in IL-12p40-eYFP reporter mice treated with Ctr-ASO or IM-T9P1-ASO (n=3 mice/group). Left: representative microscopy images (green, IL-12p40-eYFP-expressing cells; red, tumor cells; blue, Pacific Blue-labeled vasculature). Right: quantification of IL-12p40-eYFP^{+} cells up to four days after treatment. **(E)** Flow cytometry analysis of IL-12^{+} cells in the indicated cell subsets in MC38 tumors of WT mice three days after Ctr-ASO or IM-T9P1-ASO treatment (n=5 mice/group). **(F)** Flow cytometry analysis of PD-L1 expression in DC3s (left) and IL-12p40-eYFP^{+} DCs (right) in MC38 tumors of IL-12p40-eYFP reporter mice three days after Ctr-ASO or IM-T9P1-ASO treatment (n=4-5 mice/group). **(G)** Flow cytometry-based heatmap showing the average PD-L1 expression on the surface of the indicated cell types in MC38 tumors three days after IM-T9P1-ASO therapy (n=5 mice/group) (*$p < 0.05$). **(H)** Tumor growth of MC38 tumors during IL-12 neutralization in presence of IM-T9P1-ASO therapy using anti-IL-12p40 neutralizing mAb (n=5 mice/group). The number of tumor-free mice is indicated in brackets. **(I)** Average tumor growth (left) and overall survival (right) of D4M.3A tumor-bearing WT and IL-12p40$^{-/-}$ mice treated with Ctr-ASO or IM-T9P1-ASO (n=7-9 mice/group). The number of tumor-free mice is indicated.

Data are presented as mean ± SEM. For comparisons between two groups, Student's two-tailed t test was used. For comparisons between multiple groups and variables, two-way ANOVA was used. For survival analyses, the Mantel-Cox log-rank test was used. *$p < 0.05$, **$p < 0.01$, ***$p < 0.001$, ****$p < 0.0001$.

To evaluate the role of IL-12 during IM-T9P1-ASO therapy, we treated MC38 tumor-bearing mice with IM-T9P1-ASO in the presence or absence of neutralizing IL-12 mAb (fig. S5G). IM-T9P1-ASO therapy resulted in tumor rejection in 50% of the mice in the absence of neutralizing IL-12 mAb. In contrast, it failed to completely reject tumors in the presence of the neutralizing mAb (Fig. 5H). Similarly, D4M.3A tumor-bearing mice lacking IL-12p40 showed reduced tumor control when treated with IM-T9P1-ASO (Fig. 5I and fig. S5H). Together, these results indicate that IL-12 secretion is necessary to mount an efficient, long-lasting antitumor response in mice during IM-T9P1-ASO therapy.

IL-12, DC3 and pDC signatures are enriched in melanoma patients responding to ICI

Although the clinical efficacy of IM-T9P1-ASO remains uninvestigated so far, we sought to understand the implications our findings may have for anticancer therapies in humans. To this end, we analyzed the mRNA expression of *CD274*, encoding for PD-L1, in tumors of different cancer patients. Like in mice and in agreement with previous data (Cheng et al., 2021; Maier et al., 2020), DC3s expressed the highest level of *CD274* in all tumor entities compared to other DCs and myeloid cells (Fig.6A). Using published works and datasets (Gerhard et al., 2021; Jiang et al., 2021), we generated an IL-12 signature, as well as different DC signatures to distinguish human DC3, cDC1, cDC2 and pDC (Table 1). First, we confirmed the enrichment of the DC3 signature in DC3s compared to all other myeloid cells across tumors in a publicly available human pan-cancer scRNA-seq dataset (Cheng et al., 2021) (fig. S6A). Next, we tested the value of all these signatures in predicting response to the anti-PD-1 mAb nivolumab in melanoma patients (Riaz et al., 2017). Importantly, we identified an enrichment of IL-12, DC3 and pDC signatures in responders compared to non-responders (Fig. 6B), which agrees with the important role of DC3s in the induction of IL-12 stimulated antitumor T cell responses (Garris et al., 2018). Overall, these data suggest that enrichment of DC3s in human melanoma before treatment may predict a better response to anti-PD-1 therapy.

Besides PD-L1 suppression, TLR9 targeting was also critical to IM-T9P1-ASO efficacy in the mouse cancer models used above. Considering that various TLRs may regulate DC functions (Hartmann, 2017; Kawasaki & Kawai, 2014), and that DCs may express distinct TLRs in different cancer indications and/or species, we sought to examine TLR expression in human tumor-infiltrating DCs (Hartmann, 2017). We found that pDCs had the highest *TLR9* mRNA levels among myeloid cells in lung tumors (Fig. 6C), breast tumors (fig. S6B) and melanomas

(fig.S6C), which confirmed previous knowledge (Hartmann, 2017), and indicated that differences exist in TLR9 expression between human and murine DCs. By specifically analyzing human intratumoral DC3s, we found that they could express different TLRs depending on tumor entities. For example, they predominantly expressed *TLR3* in lung tumors (Fig. 6C), but *TLR7* in breast tumors (fig. S6B), and they did not detectably express TLRs, at least at the transcript level, in melanomas (fig. S6C). However, cDC1s and cDC2s, both of which are putative DC3 precursors (Gerhard et al., 2021; Maier et al., 2020; Zhang et al., 2019), expressed several TLRs including *TLR3*, *TLR6* and *TLR10* in the different tumor types analyzed. Therefore, our data suggest that *TLR9* expression in human tumors is likely limited to pDCs; however, several other TLRs, including *TLR3*, are consistently expressed by DC3s and/or their cDC1/cDC2 precursors.

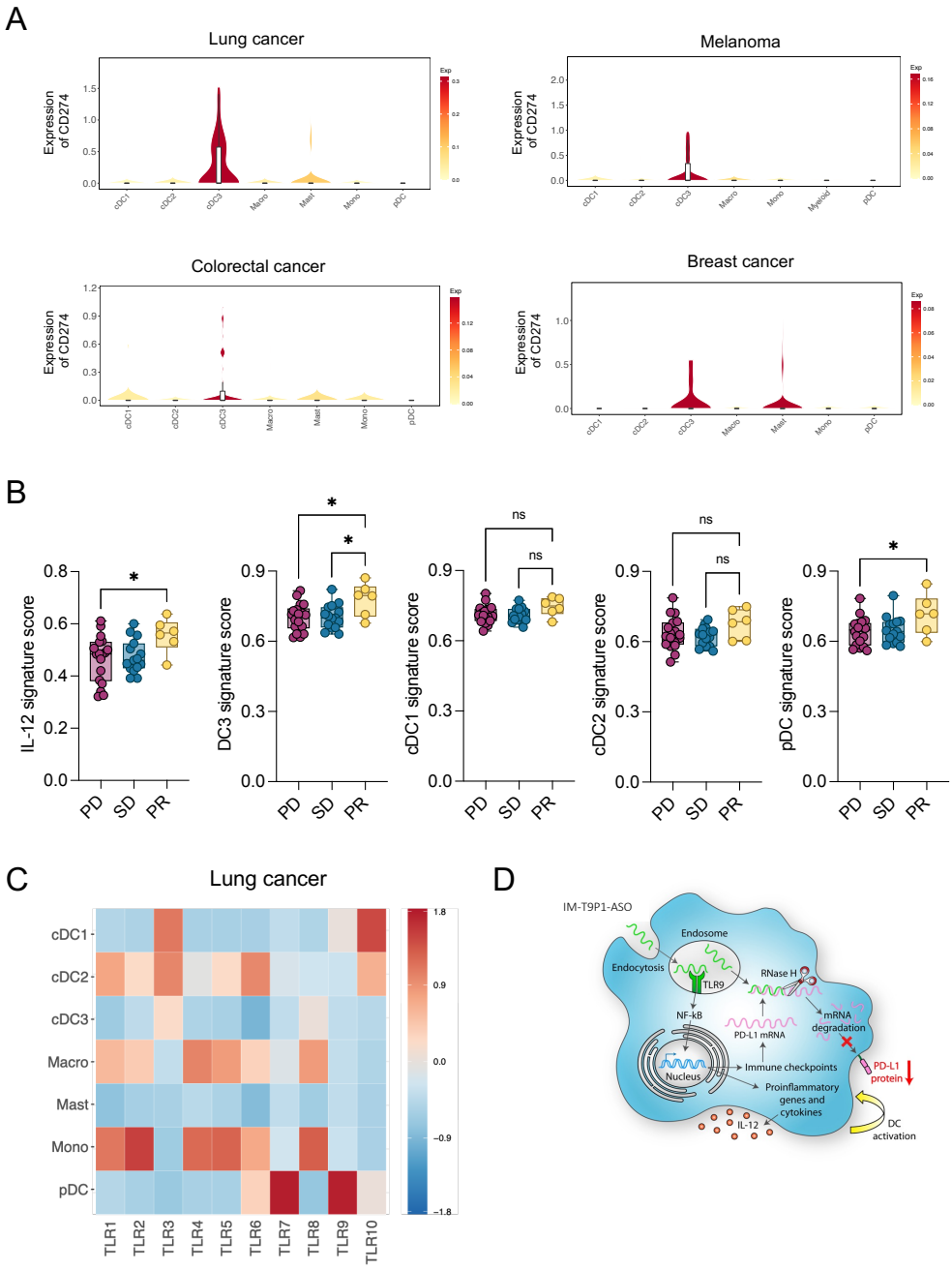

Fig. 6. *CD274* and TLR expression across human myeloid population and enrichment of IL-12 and DC signatures in melanoma patients responding to ICI (A) Violin plots showing mRNA expression of *CD274* across indicated myeloid populations in different tumor entities (*18*). Top-left: lung cancer; Top-right: melanoma; Bottom-left: colorectal cancer; Bottom-right: Breast cancer. **(B)** Enrichment analysis of IL-12, DC3, cDC1, cDC2 and pDC gene signatures (derived from (*37*) and (*11*)) in tumor biopsies of melanoma patients (n = 42) before nivolumab treatment (*38*). Patients are classified according to their response to nivolumab therapy as progressive disease (PD), stable disease (SD) and partial response (PR). **(C)** Heatmap showing mRNA expression of TLRs across indicated myeloid populations in lung cancer patients (*18*). **(D)** Schematic of IM-T9P1-ASO mode of

action. Once internalized, binding of IM-T9P1-ASO to TLR9 and *Cd274* mRNA leads to DC activation and PD-L1 downregulation, respectively.

Data are presented as mean ± SEM. For comparisons between multiple groups, one-way ANOVA was used. *p < 0.05, **p < 0.01, ***p < 0.001, ****p < 0.0001.

3.2.4. Discussion

In this study, we used mouse tumor models poorly responsive to ICIs to uncover key immune cells and pathways required for successful antitumor responses. Following treatment of tumor-bearing mice with anti-PD-L1 mAbs, we detected insufficient capacity of APCs to activate T cells through co-stimulatory molecules and cytokine secretion. Therefore, to improve anti-PD-L1 therapy, we sought to develop a tool that simultaneously activates APC and targets the immune checkpoint PD-L1.

To do so, we took advantage of the ASO technology, which has been used to silence specific target genes (e.g., oncogenes, immune checkpoints), showing encouraging results in preclinical and clinical oncology (Kashyap et al., 2019; H. Xiong et al., 2021). Using bioinformatics algorithms, we generated an immune-modulatory antisense oligonucleotide (IM-T9P1-ASO) with specificity for mouse *Cd274* that contains an unmethylated CpG motif allowing simultaneous stimulation of TLR9 and downregulation of both intracellular and surface expression of PD-L1 (Fig. 6D). Notably, TLR9 agonists typically need to be administered directly in the tumor to be efficacious (Nierkens et al., 2009; Ribas et al., 2021; Sato-Kaneko et al., 2017). Here, we showed that systemic administration of IM-T9P1-ASO had a remarkable capacity to induce effective and long-lasting antitumor responses in multiple mouse tumor models. We then confirmed IM-T9P1-ASO efficacy in mice depends on both TLR9 stimulation and PD-L1 modulation. Specifically, we observed a TLR9-dependent expansion of intratumoral DC3s, the primary IL-12-producers, shortly after IM-T9P1-ASO treatment. While

dissecting the mechanisms responsible for IM-T9P1-ASO efficacy, we found *Batf3*$^{+}$ cells, namely cDC1 and potentially DC3s, and IL-12 to be crucial in linking the innate and adaptive immunity induced by IM-T9P1-ASO. Of note, both recirculating and intratumoral lymphocytes were essential for IM-T9P1-ASO–mediated tumor rejection. In our model, pDC depletion did not abrogate the efficacy of IM-T9P1-ASO therapy, demonstrating the lack of contribution of pDCs in IM-T9P1-ASO–mediated tumor control.

Surprisingly, despite the strong potential of the IM-T9P1-ASO to knock down PD-L1 expression *in vitro*, PD-L1 downregulation was overall rare *in vivo*, probably because counteracted by IFNγ and the pro-inflammatory environment induced by IM-T9P1-ASO treatment. Nevertheless, we detected decreased surface and intracellular PD-L1 protein levels in tumor-infiltrating DC3s starting from three days after IM-T9P1-ASO treatment, but not earlier.

Due to the high co-expression of immunoregulatory genes (*Cd274*, *Pdcd1lg2* and *Cd200*) and maturation genes (*Cd40*, *Ccr7* and *Il12b*), DC3s have also been called ‘mature DCs enriched in immunoregulatory molecules’ (mregDC). This designation highlights a DC3 immunomodulatory program that may limit antitumor immune responses (Maier et al., 2020). Here, we showed that a combined strategy boosting intratumoral DC3s while controlling their PD-L1 expression reinvigorates rather than limits antitumor immunity, leading to durable antitumor responses.

DC subsets are widely conserved across patients and cancer types (Gerhard et al., 2021), as well as between humans and mice (Zilionis et al., 2019), suggesting that studying cancer mouse models to understand human disease might be relevant. Consequently, different DC states can

be identified based on a set of genes that they dominantly express (Gerhard et al., 2021). Here, we showed that IL-12 and DC3 signatures were enriched in biopsies of anti-PD-1 responders, indicating that the presence of DC3s prior to the treatment may predict a better outcome in patients with melanoma treated with ICIs. This is consistent with previous findings in human breast tumors (Bassez et al., 2021). Along the same line, DC3-associated genes at diagnosis are associated with better overall clinical outcomes in patients with lung adenocarcinoma (Zilionis et al., 2019).

Of note, DC3s likely derive from both cDC1s and cDC2s in humans (Gerhard et al., 2021; Zhang et al., 2019). However, it remains unclear what drives the acquisition of the DC3 program, but our data suggest that DC3s may be a mature and activated DC state originating from other DCs, including cDC1s. Specifically, we observed that: i) *Batf3*$^{-/-}$ mice lack both cDC1s and a DC3 subset, ii) IM-T9P1-ASO-mediated DC3 expansion is accompanied by a cDC1 contraction in the tumor, and iii) cDC1s display the highest TLR9 expression in our mouse model. Therefore, it is tempting to speculate that TLR9 engagement may contribute to the conversion of cDC1 into DC3s. However, lineage-tracing studies will be required to fully comprehend the origin of DC3s and confirm or refute this hypothesis.

Compared to mice, TLR9 has a more restricted expression pattern in humans, where it is mainly expressed in pDCs among the different DC states (Hartmann, 2017). This difference in TLR expression between murine and human DCs indicates the need to consider additional ASO variants to optimize cDC activation. For instance, PD-L1 ASOs carrying TLR3 (instead of TLR9) agonistic activities, might prove superior in therapy. Yet, TLR9 targeting in humans may also trigger desired antitumor activities; for instance, treatment with the TLR9 agonist vidutolimod showed therapeutic benefit in metastatic melanoma patients resistant to anti-PD-

1 antibodies (Ribas et al., 2021), indicating that combining TLR9 agonists with ICIs can be a valid strategy for clinical development.

We also show that in humans, the expression of TLRs in DC3s varies between tumor types. Only TLR3 is expressed in DC3s in certain tumor entities and is consistently expressed by cDC1s and cDC2s, which are both likely DC3 precursors (Gerhard et al., 2021; Zhang et al., 2019). Of note, clinical trials using TLR3 agonists in combination with ICIs showed promising results in some solid tumor types (Le Naour et al., 2020). Future studies should examine whether ASOs can be further tailored to activate human DC3s, or other antitumoral DCs, by targeting alternative TLRs while downregulating PD-L1. Altogether, our findings provide a mechanistic groundwork for future therapy design of combinatorial agonistic TLR stimulation and checkpoint blockade for the treatment of solid tumors.

3.2.5. Materials and Methods

Study design

This study was designed to identify combinatorial treatment strategies that lead to durable antitumor responses and reveal critical elements driving long-term immunity. To this aim, we treated tumor-bearing WT or transgenic mice with IM-T9P1-ASO and typically measured tumor growth up to three months post-tumor inoculation. To validate IM-T9P1-ASO activity, we performed *in vitro* studies with cell lines and bone marrow-derived DCs and assessed PD-L1 downregulation and DC activation by flow cytometry. To understand the mechanisms behind IM-T9P1-ASO–mediated antitumor immunity, we analyzed tumors and dLNs shortly after treatment (between days 2 and 8) by flow cytometry. We also performed intravital imaging to examine IM-T9P1-ASO biodistribution and activity in the tumor.

Antisense oligonucleotides

Using the mouse *Cd274* mRNA as basis (NM_021893.3), we identified a *Cd274*-specific antisense oligonucleotide with a length of 15 nucleotides. The basic sequence CTTACGTCTCCTCGA contains two CpG motifs which have been described to have the potential to activate TLR9 when Cs are not methylated. In order to generate a high affinity ASO, we modified the flanks with locked nucleic acids resulting in the sequence +mC+T+TACGTCTCCT+mC+G+A (IM-T9P1-ASO, mC = 5-methyl C), still containing one CpG motif without a methylated C. The following control oligonucleotide was used in all experiments +mC+G+TTTAGGCTATGTA+mC+T+T (Ctr-ASO). All internucleotide linkages in IM-T9P1-ASO and Ctr-ASO are phosphorothioates.

Cell lines

MC38, MC38-H2B-mApple (Garris et al., 2018) and D4M3.A (kindly provided by David E. Fisher and T. Mempel from MGH, Boston, USA) were cultured in DMEM (GIBCO) with 10% of heat-inactivated fetal bovine serum (FBS, GIBCO) + 1% Penicillin/Streptomycin (P/S, GIBCO). EMT6 murine breast cancer cells were cultured in DMEM with 10% FBS + 1% P/S + 0.5% Ciproxin + 0.1% β-Mercaptoethanol. MOC22 (purchased from Kerafast, Boston, USA) were cultured in IMDM/F12 (2:1) + 5% FBS + 1% P/S + hEGF (Millipore, 5 ng/mL) + hydrocortisone (Sigma, 40 ng/ml) + insulin (Sigma, 5µg/mL). Cells were routinely tested and resulted negative for Mycoplasma.

Bone marrow-derived dendritic cells (BMDCs)

Bone-marrow cells from mice were isolated by flushing femurs and tibiae of 8-11-week-old wild-type C57BL/6 or transgenic mice. Cells were strained through a 70-μm filter and centrifuged before resuspension in 1× RBC lysis buffer (Bioscience) for 1 min at RT. Cells were washed with PBS supplemented with FBS and plated in non-treated tissue culture dishes in RPMI 1640 with Glutamax (GIBCO) + 10% FBS + 1% P/S + 50 μM 2-mercaptoethanol. To generate mature monocyte-derived dendritic cells (moDCs), BMDCs were cultured with murine GM-CSF (Peprotech, 100 ng/ml). IL-4 (Peprotech, 20 ng/ml) and IFNγ (Peprotech, 100 ng/ml) were added to moDCs on day 3 and 7, respectively, to boost moDC activation. To generate immature conventional dendritic cells (FL-cDCs), BMDCs were cultured in presence of Flt-3L (Peprotech, 100 ng/ml). Both moDCs and convDCs were analyzed or used in T cell co-culture assay at day 9 post-isolation as described below.

T cells

OT-I $CD8^+$ T cells were purified from the spleen of 7-week-old female C57BL/6-Tg(TcraTcrb)1100Mjb/J (OT-I) mice using the EasySep™ $CD8^+$ T cell isolation kits (STEMCELL), according to manufacturer's instructions. T cells were cultured in RPMI 1640 medium supplemented with 10% FBS, L-glutamine, penicillin/streptomycin, beta-mercaptoethanol (55 μM, GIBCO), non-essential amino acids (0.1 mM, Sigma) and sodium pyruvate (1 mM, GIBCO) and IL-2 (50 ng/ml, Peprotech).

***In vitro* stimulation of BMDCs with IM-T9P1-ASO**

BMDCs (moDCs and FL-cDCs) generated as described above were seeded ($2.5x10^5$ and $5x10^5$ cells/ml, respectively) in a flat bottom 96-well plate on day 6 after isolation. Control or IM-T9P1-ASO (20 μM) was added on days 6 and 8 after isolation. To assess intracellular IL-12

levels, Brefeldin (Biolegend, 1 µg/ml) was added on day 8, 12h before flow cytometry staining and analyses.

Co-culture of BMDCs with OVA-specific OTI

For *in vitro* T cell activation assay, moDCs were prepared and treated with control or IM-T9P1-ASO (20 µM) on days 6 and 8 after isolation as described above. EndoFit OVA (Invivogen, 100 µg/ml) was added to each well on day 8. OT-I T cells were then stained with CellTrace Violet (Thermo Fisher) according to manufacturer's protocols; $1x10^5$ cells were added to each well containing mature moDCs (day 9 post-isolation) and cultured for 3 days. T cell proliferation was assessed by flow cytometry analysis, and the expansion index was calculated using the dedicated tool provided by FlowJo. GranzymeB secretion in the conditioned media was measured with the respective mouse ELISA kit (Thermo Fisher).

TLR reporter assay

The TLR activation profile was assessed by InvivoGen using their PRR Ligand Screening platform service (https://www.invivogen.com/custom-tlr-screening) and blind-coded antisense oligonucleotide samples (20 µM). A recombinant HEK-293 cell line not expressing any PRR gene but only the reporter gene (i.e., the inducible NF-kB reporter gene SEAP) was used as a negative control. Poly I:C, R848, TL8-506 and ODN 1826 were used (all at 1 µg/ml) as a positive control to stimulate the TLR3, TLR7, TLR8 and TLR9 reporter cell lines, respectively. TLR9 activation was further confirmed and evaluated in-house using the HEK-Blue mTLR9 cells and HEK-Blue detection system (InvivoGen) following manufacturer's protocols. Specifically, antisense oligos were incubated with the reporter cells for 15h, followed by measurement of SEAP production with a spectrophotometer (read at 650 nm).

MC38 PD-L1 KO generation

Generation of PD-L1-KO MC38 cells was done using Alt-R CRISPR-Cas9 System (Integrated DNA Technologies, IDT), which consists of the cationic lipid delivery of CRISPR ribonucleoprotein complexes into mammalian cells. Preparation of rRNPs was done by mixing and incubating equal moles (800 pmol) of tracrRNA (IDT) and *Cd274* crRNA (Item # Mm.Cas9.CD274 crRNA (Item # Mm.Cas9.CD274.AA, IDT) or control sgINTERGENIC_27270 (IDT) for 5 min at 95°C. A total of 320 pmol of recombinant Cas9 (Cas9-NLS, Berkeley) was added to each reaction and incubated for 20 min at RT. The SF Cell Line 4D-Nucleofector™ kit (Lonza) was used to deliver tracrRNA:crRNA:Cas9 complexes into $1x10^6$ MC38 cells according to the manufacturer's protocols. Specifically, each reaction consisted of 16 µl rRNPs prepared as described above, mixed with 70 µl SF Cell line solution and 18 µl Supplement (provided by the Lonza kit). After transferring the cell suspension into a Lonza 4D-Nucleofector cuvette, the EN-138 program was used for electroporation. Lack of PD-L1 expression was verified two days later by flow cytometry after staining the cells with two clones (MIH5 and 10F.9G2) of PD-L1 antibodies. To ensure the generation of stable PD-L1-KO cells, MC38 cells were stained with a Pe-Cy7-conjugated PD-L1 antibody (clone MIH5, Thermo Fisher) five days after electroporation, and PD-L1-negative MC38 cells were FACS-sorted using a FACSMelody™ Cell Sorter (BD Biosciences).

Mice

C57BL/6N, C57BL/6J, Balb/c, IL-12p40-IRES-eYFP (B6.129-Il12btm1.1Lky /J, JAX 006412), IL-12p40-KO (B6.129S1-Il12btm1Jm/J, JAX 002693). C57BL/6-Tg(TcraTcrb)1100Mjb/J OT-I TCR transgenic mice were bred in-house either at the University Hospital of Basel (Switzerland), Agora Cancer Research Center (Lausanne, Switzerland) or Massachusetts General Hospital (Boston, USA). In case of unavailability, mice were also

obtained from Janvier Labs (France) or Charles River (France) and Jackson Laboratories (USA). PD-L1 KO (B6/JCD274<em(ex3HindIII)JZvB>) were kindly provided by Johannes vom Berg, University of Zürich (Switzerland). Batf3 KO ((B6.129S(C)-Batf3<tm1Kmm>/J) were obtained from the Jackson Laboratory, USA. IFNgR KO (B6.129S7-Ifngr1<tm1Agt>/J) was kindly provided by Daniel D. Pinschewer, University of Basel, Switzerland. TLR9-KO mice (C57BL/6-Tlr9tm1Aki) were kindly provided by Maries van den Broek, University of Zürich (Switzerland), and Michel Gilliet, University of Lausanne (Switzerland). Each experiment included age and sex-matched littermates from 8 to 13 weeks of age and animals were housed under specific pathogen-free conditions. All animal experiments were performed following the Swiss federal regulations and with the MGH Institutional Animal Care and Use Committee (IACUC).

Tumor models

Wild-type or transgenic mice in the C57BL/6 background were implanted subcutaneously into the right flank with 0.5-2x10^6 MC38 colorectal carcinoma or 1x10^6 D4M.3A melanoma cells. EMT6 murine breast cancer cells (0.25x10^6) were injected into the right mammary gland of female Balb/c mice. All cells were suspended in PBS or phenol red-free DMEM without additives. MOC22 squamous cell carcinoma (1x10^6) were resuspended in PBS and injected by tail vein injection. Cells were routinely tested for mycoplasma contamination before treatment. All tumor models were allowed to grow at least for one week before therapy and, right before treatment initiation, mice were stratified into experimental groups with comparable average tumor size. Tumor volume was calculated according to the formula: D/2*d*d, with “D” being the longest tumor diameter and “d” the shorter tumor diameter in mm. In tumor growth and survival experiments, mice were sacrificed when reaching the humane endpoints described in the authorized animal protocol of the respective laboratory, which were the following: tumor

size exceeding 1000 (Agora), 1500 (University of Basel) or 2000 (MGH) mm3 or the longest diameter exceeding 1.5 (Agora and University of Basel) or 2 cm (MGH). In survival experiments, surviving mice were either tumor-free or tumor-bearing mice that did not reach the termination criteria described above.

Therapy treatments, cytokine, and cell modulation

Mice harboring tumors that reached between around 50-100 mm^3 were treated intraperitoneally (i.p.) with eight doses of 200µl of PBS suspended solutions of IM-T9P1-ASO at 20 mg/kg, non-targeting ASO (Ctr-ASO) at 20 mg/kg (both daily from days 14-18, and days 21, 23, and 25 for MC38 tumor-bearing mice; and daily from days 7-11, and days 14, 16 and 18 for EMT6 tumor-bearing mice), or left untreated. For anti-PD-L1 monoclonal antibody treatment, mice were injected intraperitoneally with 10 mg/kg of anti-PD-L1 10F-9G2 antibody (BioXCell) on days 14, 16, 18, 21, 23 and, 25 in the MC38 colorectal model and days 7, 9, 11, 14, 16 and 18 in the EMT6 breast cancer model. For CpG-ODN 1826, mice were treated intraperitoneally with 0.4 mg/kg of GpG-ODN 1826 at the indicated schedule (from day 14 to 18, day 21, day 23 and day 25). IL-12p40 neutralization was performed intraperitoneally using 500 µg of anti-IL-12p40 depletion antibody (clone 17.8, BioXCell) daily during the first week of IM-T9P1-ASO treatment (day 14 to 18) and twice during the second week of treatment (day 21 and day 24). pDC depletion was performed by administering intraperitoneally 500 µg of anti-CD317 (PDCA-1, clone 927) the day before IM-T9P1-ASO treatment (day 13) followed by 250 µg of anti-CD317 on days 16, 18, 21, 23 and, 25. For combination therapy of IM-T9P1-ASO with blocking antibodies, mice received either 12.5 mg/kg of anti-PD-1 (clone RPM1-14) or 10 mg/kg of anti-CTLA4 (clone 9D9) alone or in combination with 20 mg/kg IM-T9P1-ASO when tumor size was approximately 100-200 mm^3.

In vivo tumor re-challenge

Long-term tumor-free survival mice were implanted with the same tumor entity in the contralateral flank, either 500.000 MC38 or 250.000 EMT6 cells, after 60 days after the primary tumor rejection. Naive C57BL/6 or Balb/c mice were inoculated with MC38 or EMT6 cells respectively, alongside the re-challenged mice, and tumor growth was monitored until the terminal endpoint (1500 mm^3).

Phenotypic characterization of tumor-infiltrating and lymph node cells by multiparameter flow cytometry

MC38 tumor-bearing mice were sacrificed at indicated time points. Tumors were collected, weighed and processed using razor blades. Tumor tissue was then digested using collagenase IV (Worthington), accutase (PAA), hyaluronidase (Sigma), DNAse type IV (Sigma), and Brefeldin A (1000X from Biolegend, at 1:1000) for 30 minutes at 37°C, with constant shacking. The tumor suspension was filtered using a cell strainer (100 μM). Draining and non-draining lymph nodes were cut into small pieces using surgical scissors prior to digestion using Collagenase D (1 mg/ml), DNAse I (40 μg/ml), 2% FBS and Brefeldin A (1000X from Biolegend, at 1:1000) during 30 min at 37°C, with constant shaking. Lymph node suspensions were filtered and mashed through a 70 μM strainer using the end of a 1mL syringe. Precision counting beads (Biolegend) were added before the staining to quantify the number of cells per gram of tumor or the total amount of cells within lymph nodes. Single-cell suspensions derived from tumors and lymph nodes were blocked with rat anti-mouse FcγIII/II receptor (CD16/ CD32) blocking antibodies ("Fc-Block"), and stained with live/dead cell-exclusion dye (Zombie UV dye; Biolegend). The cells were then stained with fluorophore-conjugated extracellular antibodies, washed, and resuspended in FACS buffer containing PBS, EDTA, sodium azide and FCS. For intracellular and intranuclear staining, cells were fixed and

permeabilized using FoxP3/transcription factor staining buffer set (eBioscience) before the incubation with antibodies directed against intracellular antigens. Cell populations were analyzed with BD Fortessa and Cytek Aurora.

Tumor-derived cell types were identified using the following combinations of cell markers:

Macrophages: $CD45^+$ $F4/80^+$

Total DCs: $CD45^+$ $F4/80^-$ $MHC\text{-}II^+$ $CD11c^+$

cDC1: $CD45^+$ $F4/80^-$ $MHC\text{-}II^+$ $CD11c^+$ $CCR7^-XCR1^+$ or $CD45^+$ $F4/80^-$ $MHC\text{-}II^+$ $CD11c^+$ $CCR7^-$ $CD103^+$

cDC2: $CD45^+$ $F4/80^-$ $MHC\text{-}II^+$ $CD11c^+$ $CCR7^-$ $XCR1^-$ $CD11b^+$ or $CD45^+$ $F4/80^-$ MHC^+ $CD11c^+$ $CCR7^-$ $XCR1^-$ $Sirpa^+$

DC3: $CD45^+$ $F4/80^-$ $MHC\text{-}II^+$ $CD11c^+$ $CCR7^+$

pDC: $CD45^+$ $F4/80^-$ $MHC\text{-}II^+$ $CD11c^+$ $SiglecH^+$

$CD8^+$ T cells: $CD45^+$ $F4/80^-$ $CD11c^-$ $CD8^+$

$CD4^+$ T cells: $CD45^+$ $F4/80^-$ $CD4^+$

Tregs: $CD45^+$ $F4/80^-$ $CD4^+$ $CD25^+$ $FOXP3^+$

B cells: $CD45^+$ $F4/80^-$ $CD4^-$ $CD8^-$ $CD19^+$

ECs: $CD45^-$ $CD31^+$

***In vivo* mRNA measure by PrimeFlow Analysis**

Tumor-cell suspensions were prepared as described above. Antibody staining and *Cd274* mRNA detection by flow cytometry were done using the PrimeFlow RNA assay (Thermo Fisher) following the manufacturer's protocol (procedure validated for 96-well plates). Cd274 (assay ID: VB1-17218-PF) and AF647 were used as Target Probe and Label Probe, respectively, diluted 1:20 and 1:100 in their respective PrimeFlow RNA diluents.

FTY720 treatment

C57BL/6N mice were implanted in the right flank with 500.000 MC38 tumor cells subcutaneously and randomized into groups of similar tumor volume between 50 and 100 mm^3. Mice were treated daily with 1.25 mg/kg of FTY720 (Cayman Chemical) intraperitoneally (i.p.) throughout the duration of the experiment. FTY720 injections started the day before IM-T9P1-ASO or Ctr-ASO treatment.

Intravital imaging

IL-12p40 reporter (IL-12p40-eYFP) mice were anesthetized and dorsal skin-fold window chambers were installed as previously described (Garris et al., 2018). Forty-eight hours after window implantation, MC38-H2B-mApple cells ($2x10^6$ in 20 µl) were injected into the fascia layer. One week after cell injection and 10 minutes before imaging, mice were injected intravenously with Pacific Blue-dextran (60 µl of a 4 mg/ml solution) for labelling of the vasculature (within 1 hour after injection) and macrophages (which take up the dye and are consequently labelled within 1 day after injection). The PacBlue-dextran solution was generated by mixing 10 mg of 500,000 MW dextran (Thermo Fisher) with a 10-fold molar excess of Pacific Blue™ Succinimidyl Ester (Thermo Fisher) for 2h in slight agitation at RT and overnight at 4 C, followed by removal of unconjugated dye by washing 3 times with PBS and Amicon (Sigma) concentrators. AF647-conjugated IM-T9P1-ASO was delivered at 20 mg/kg via a 30-gauge catheter inserted in the tail vein of the anesthetized mouse (2% isoflurane in oxygen) during imaging. Anesthetized mice were kept on a heating pad kept at 37°C and imaged using an Olympus FluoView FV1000MPE confocal imaging system (Olympus America). A 2x air objective XL Fluor 2x/340 (NA 0.14; Olympus America) was used to select regions near tumor margins and tumor vasculature. Higher magnification Z stack images were acquired using a XLUMPLFL 20x water immersion objective (NA 0.95; Olympus America)

with 1.5x digital zoom. Sequential scanning with 405, 473, 559, and 635 nm lasers was performed using voltage and power settings that were optimized prior to time-lapse acquisition. Samples were excited using 405 nm, 473 nm, 559 nm and/or 633nm diode lasers with a multiband DM405/473/559/635 nm dichroic excitation filter, and emission light separated using SDM473, SDM560, and SDM 640 dichroic mirrors in combination with emission filters (BA430-455, BA490-540, BA575-620, BA655-755) from Olympus America.

Analyses of *CD274* and TLR expression in human cancers from published datasets

Data showing the expression of *CD274* and TLRs across different myeloid cells were obtained using an interactive web-based tool (http://panmyeloid.cancer-pku.cn) for visualization of human pan-cancer single-cell data (Cheng et al., 2021). Specifically, we explored datasets of lung (Lambrechts et al., 2018; Zilionis et al., 2019), melanoma (Li et al., 2019), colorectal (Zhang et al., 2020) and breast (Azizi et al., 2018) cancers. Of note, we focused our analyses on cells of the tumor microenvironment, excluding cells detected in other tissues (e.g., peripheral blood, normal tissue, lymph nodes).

Bioinformatic analysis of published gene expression data

The DC3, cDC1, cDC2 and pDC gene signatures were derived from (Gerhard et al., 2021), and IL-12 signature was generated using CytoSig (https://cytosig.ccr.cancer.gov/). CytoSig is a web platform that predicts response signatures of the selected cytokines based on a sample's gene expression profile under development in NCI (Jiang et al., 2021). The analysis was performed as reported in (Kirchhammer et al., 2022). In detail, we reanalyzed the dataset by (Riaz et al., 2017), consisting of bulk mRNA sequencing data of melanoma tumors treated with Nivolumab (anti-PD-1). The patients were stratified according to their response to the therapy as progressive disease (PD), stable disease (SD), partial response (PR) and complete response

(CR). Complete responders were excluded from the analysis for two reasons: i) the sample size (n=3), and ii) the signature of CD8 T and B cells, which usually correlates with good prognosis, showed no enrichment in CR. We retrieved the data from the Gene Expression Omnibus (GEO) under accession number GSE91061. We analyzed only patients with reported responses to therapy and both pre- and post-treatment samples. EdgeR was used to normalize counts by library size. Immune cell signature score was calculated as described by (Cursons et al., 2019). All transcripts for each sample were ordered by decreasing expression, and the signature score was defined as (1−mean rank of transcripts in signature)/(number of all transcripts). Therefore, high signature scores indicate enrichment of signature gene expression.

Statistical Analysis

All statistical analyses were performed using GraphPad Prism software. Results were shown as mean ± SEM. Student's two-tailed t-test were done to compare two groups. One-way ANOVA was used to compare multiple groups. Two-way ANOVA was used for comparisons between multiple groups and variables (e.g., time). The Mantel-Cox log-rank test was used for survival analyses.

p values > 0.05 were considered not significant (n.s.); p values < 0.05 were considered significant. * p value < 0.05, ** p value < 0.01, *** p value < 0.001, **** p value < 0.0001.

3.2.6. Acknowledgments

We thank the flow cytometry and animal core facilities at the University of Basel and Agora Research Institute. We thank David E. Fisher and T. Mempel from MGH for providing D4M.3A cells. We thank Johannes vom Berg for kindly provide the PD-L1$^{-/-}$ mice, Daniel D. Pinschewer for the IFNgR$^{-/-}$ mice, and Maries van den Broek and Michel Gilliet for providing the TLR9$^{-/-}$ mice.

3.2.7. Funding

Non-commercial research agreement with Secarna Pharmaceuticals GmbH & Co (AZ)

Monique Dornoville de la Cour Foundation (AZ, LF)

Swiss Cancer League grant KLS-5383-08-2021-R (AZ)

Postdoc.Mobility Fellowship SNSF; P400PM_183852 (RB)

Return Grant of the Swiss National Science Foundation P5R5PM_203164 (RB)

3.2.8. Author contributions

Conceived the idea of the study: AZ, ASK, RK, FJ, and MJP

Funding acquisition: AZ and MJP

Planned the experiments: LFR and CC

Performed and analyzed *in vitro* experiments: LFR, CC, RB, JF, AM and EPB

Performed mouse experiments and related analysis: LFR, CC, RB, MB and EPB

Performed and analyzed intravital imaging: CC, RB and RHK

Performed computational analysis: MPT

Performed in silico identification of antisense oligonucleotides: SM

Interpreted the data, prepared the figures, and wrote the original draft: LF and CC

Provided input for research design and edited the manuscript: LF, CC, RB, MPT, RK, NK, AM, ASK, FJ, KOD, MJP, and AZ

Supervised the study: AZ and MJP

3.2.9. Competing interests

AZ received consulting/advisor fees from BMS, MSD, Hoffmann–La Roche, NBE Therapeutics, Secarna, ACM Pharma, and Hookipa, and maintains further non-commercial research agreements with Secarna, Hookipa, and Beyondsprings. MJP has served as consultant

for Aileron Therapeutics, AstraZeneca, Cygnal Therapeutics, Elstar Therapeutics, ImmuneOncia, KSQ Therapeutics, Merck, Siamab Therapeutics, and Third Rock Ventures. The wife of RB is an employee and shareholder of CSL Behring and R.B. received speakers fee from Janssen. RK, JF, AM, and FJ are employed by Secarna. CC is currently employed by Idorsia Pharmaceuticals Ltd.

3.2.10. Data and materials availability

All data needed to evaluate the conclusions in the manuscript are reported in Results or Supplementary Materials. The IM-T9P1-ASO was provided by Secarna under conditions expressed in a sponsored research agreement between Secarna and University of Basel.

3.2.11. Supplementary figures and Tables

Table 1. Human IL-12 and DC signatures. List of genes used to define human IL-12 and DC (DC3, cCD1, cDC2 and pDC) signatures.

IL-12 signature (derived from (Jiang et al., 2021))	*IFNG, GZMB, IL18RAP, ANXA3, IL12RB2, LAG3, GZMH, P2RX5, MAP3K8, FES, CXCL10, CXCL9, GZMK, IL18R1, LIF, FURIN, GTPBP8, METRNL, TBX21, NKG7, MTHFD2, ZBED2, BATF3, SLC7A5, SLC27A2, ATP2B4, BATF, GADD45G, SERPINB1, SATB1, NAMPT, UPP1, RGS16, ICOS, IRF8*
DC3 signature (derived from	*GSTP1, IDO1, ATOX1, BIRC3, CCL19, CCR7, CD40, CD83, CDKN1A, CFLAR, CLIC2, CSF2RA, DAPP1, EEF1A1, EIF1, ERICH1, FNBP1, FSCN1, GPR157, GPX4, GRSF1, ID2, KIF2A, LAD1, LAMP3, LSP1,*

(Gerhard et al., 2021))	*LY75, MARCKS, MARCKSL1, MGLL, MYL6, NFKB1, NUB1, POGLUT1, PTPN1, RAB8B, RAB9A, RASSF4, SYNGR2, TMEM176A, TMSB10, TNFAIP2, TRAF1, TUBB, TXN, VOPP1, ZFAS1*
cDC1 signature (derived from cDC1 signature (derived from (Gerhard et al., 2021))	*ACTG1, FGL2, ACTB, ASAP1, BATF3, C1orf54, C20orf27, CADM1, CCND1, CD74, CLEC9A, CLNK, CPNE3, CPVL, CST3, CYB5R3, ENSA, HLA-DPA1, LGALS2, LSM6, NAAA, PPT1, RAB7B, RGS10, RPL8, S100A10, SNX3, TMEM14A, TMSB4X, VAC14, WDFY4, XCR1, GSTP1, IDO1*
cDC2 signature (derived from (Gerhard et al., 2021))	*ABI3, ACTR3, AIF1, ALDOA, ARHGDIB, ARPC3, ARPC5, C15orf48, CA2, CKLF, CLEC4A, FCGBP, GAPDH, GSN, LST1, LTB, PAK1, PKIB, PPM1N, RUNX3, S100B, SPI1, TPI1, VASP, ANXA5, CLEC10A, FCER1A*
pDC signature (derived from (Gerhard et al., 2021))	*IRF8, ALOX5AP, APP, BCL11A, C12orf75, CCDC50, CLIC3, CXCR3, CYB561A3, DERL3, ERP29, GPR183, GZMB, HERPUD1, HSP90B1, IL3RA, IRF4, IRF7, ITM2C, LILRA4, LILRB4, MAP1A, MPEG1, PARK7, PLAC8, PLD4, PLP2, PPP1R14B, RPS3A, RPS8, SEC61B, SEL1L3, SELL, SERPINF1, SLC15A4, SMPD3, SPCS1, SPIB, SRP14, TCF4, TPM2, TSPAN13, UGCG*

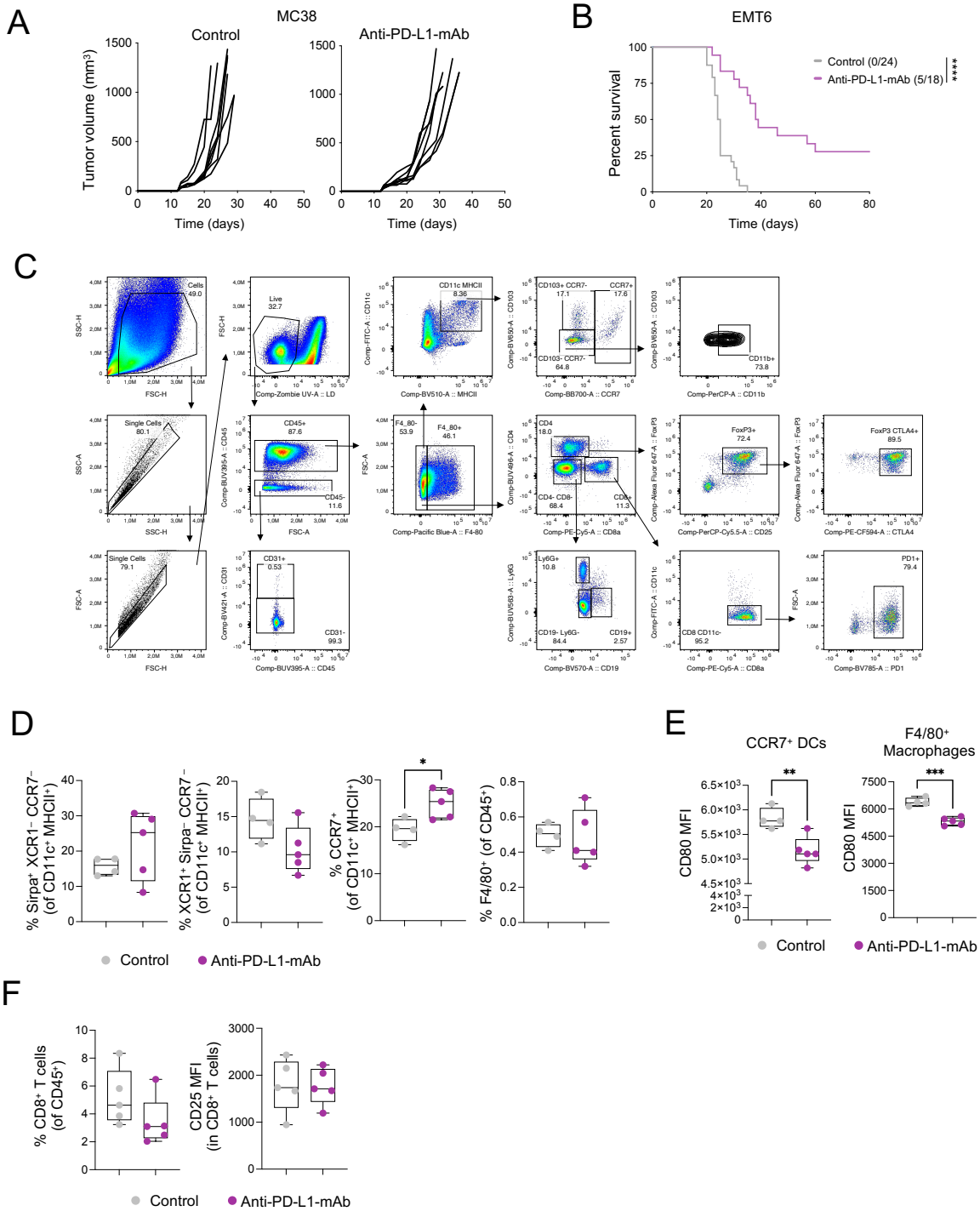

Fig. S1. Flow cytometry gating strategy for immune cell populations and immune cell analysis of LN in anti-PD-L1-mAb treated MC38 tumor bearing mice. (A) Individual mouse tumor growth of MC38 tumor-bearing mice treated with anti-PD-L1-mAb as in Fig. 1A. **(B)** Kaplan-Meier survival of EMT6 tumor-bearing mice treated with anti-PD-L1-mAb or control (n=18-24 mice/group). The number of tumor-free mice is indicated in brackets. **(C)** Flow cytometry gating strategy for myeloid and lymphoid cells in MC38 tumors. **(D-F)** Flow

cytometry analysis of MC38 tumor-bearing mice after two doses of anti-PD-L1-mAb. **(D)** Proportion of Sirpa$^+$ cDC2, XCR1$^+$ cDC1, CCR7$^+$ DCs and F4/80$^+$ macrophages in tumor-draining lymph nodes between the different treatment conditions. **(E)** CD80 expression (mean fluorescence intensity, MFI) in CCR7$^+$ DCs and F4/80$^+$ macrophages in tumor-draining lymph nodes. **(F)** Proportion and activation, assessed by CD25 expression (MFI), of intratumoral CD8$^+$ T cells (n=4-5 mice/group).

Data are presented as mean ± SEM. For comparisons between two groups, Student's two-tailed t-test was used. For survival analysis, the Mantel-Cox log rank was used. *$p < 0.05$, **$p < 0.01$, ***$p < 0.001$, ****$p < 0.0001$.

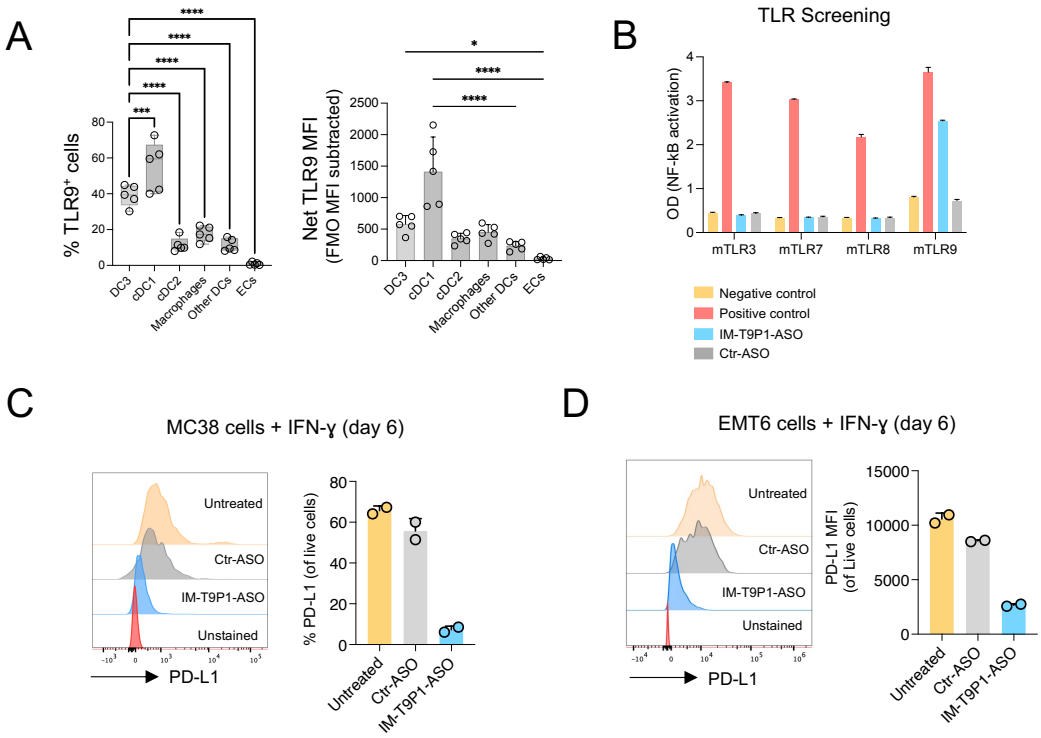

Fig. S2. TLR9 expression in MC38 tumors and *in vitro* validation of IM-T9P1-ASO. (A) Flow cytometry analysis of TLR9-expressing cells in MC38 tumors (n=5 mice). **(B)** Screening of TLR activation by IM-T9P1-ASO or Ctr-ASO using NF-kB reporter cell lines responsive to the indicated TLRs (n=2 cell cultures/condition). PBS and established TLR stimulants (Poly I:C, R848, TL8-506 and ODN 1826) were used as negative and positive controls, respectively. **(C-D)** PD-L1 expression in MC38 **(C)** and EMT6 tumor cell lines **(D)** exposed to Ctr-ASO or IM-T9P1-ASO in presence of IFN-γ (n=2 cell cultures/condition) **(C-D).**

Data are presented as mean ± SEM (A) or mean ± SD (B-D). For comparisons between multiple groups, one-way ANOVA was used. *p < 0.05, **p < 0.01, ***p < 0.001, ****p < 0.0001.

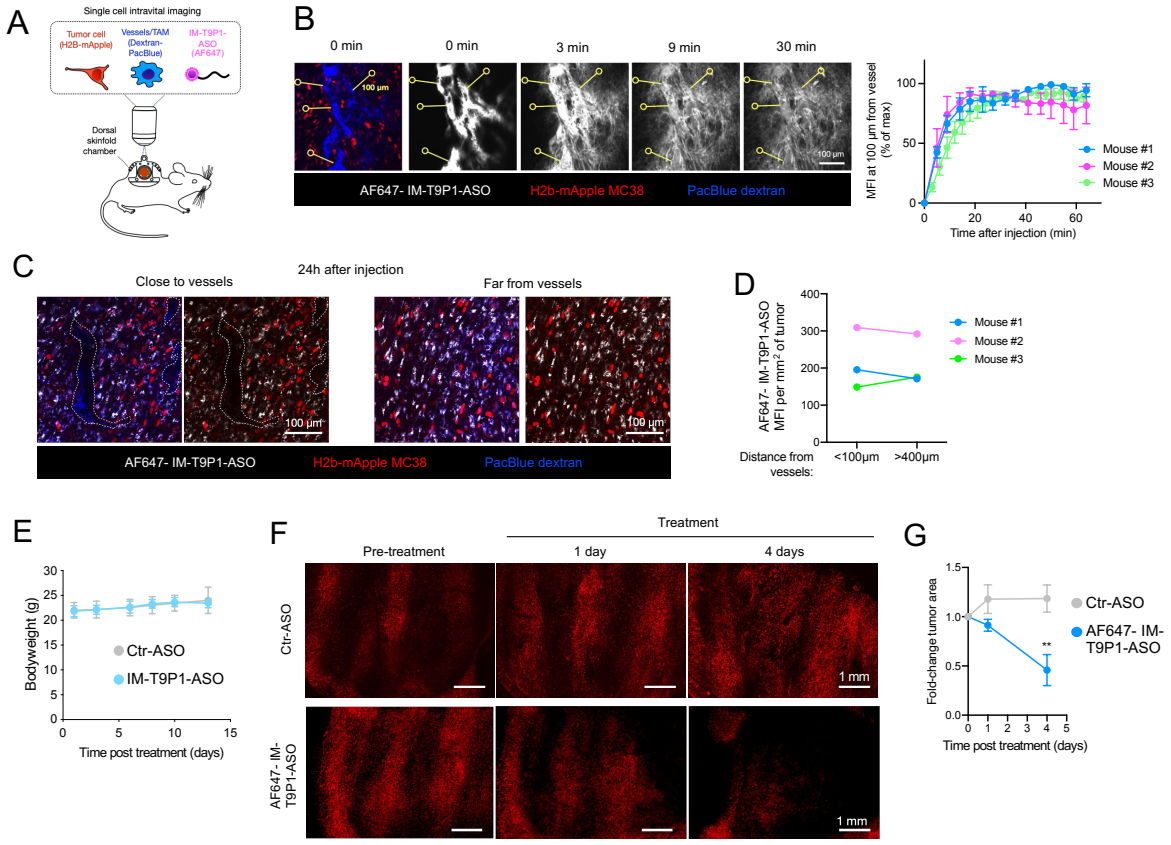

Fig. S3. Biodistribution and tolerability of IM-T9P1-ASO. (A) Diagram describing intravital imaging of MC38-H2B-mApple tumors for tracking pharmacokinetics and pharmacodynamics of AF647-labeled IM-T9P1-ASO. **(B)** Left: representative intravital microscopy images of AF647-IM-T9P1-ASO diffusion shortly after intravenous injection. Right: quantification of the data (n=3 mice). **(C)** Representative intravital microscopy images of AF647-labeled IM-T9P1-ASO accumulation in the tumor close to the vessels (left) and far from the vessels (right) one day after injection. **(D)** Quantification of the data shown in **(C)** (n=3 mice). **(E)** Body weight of MC38 tumor-bearing mice receiving IM-T9P1-ASO or control therapy (n=6-10 mice/group). **(F)** Representative intravital microscopy images of MC38-mApple tumors acquired over 4 days after a single dose of Ctr-ASO or AF647-labeled IM-T9P1-ASO. **(G)** Quantified mApple^{+} tumor area in mice treated with Ctr-ASO or AF647-IM-T9P1-ASO from **(F)** (n=3 mice/group).

Data are presented as mean ± SEM. For comparisons between multiple groups and variables, two-way ANOVA was used. *p < 0.05, **p < 0.01, ***p < 0.001, ****p < 0.0001.

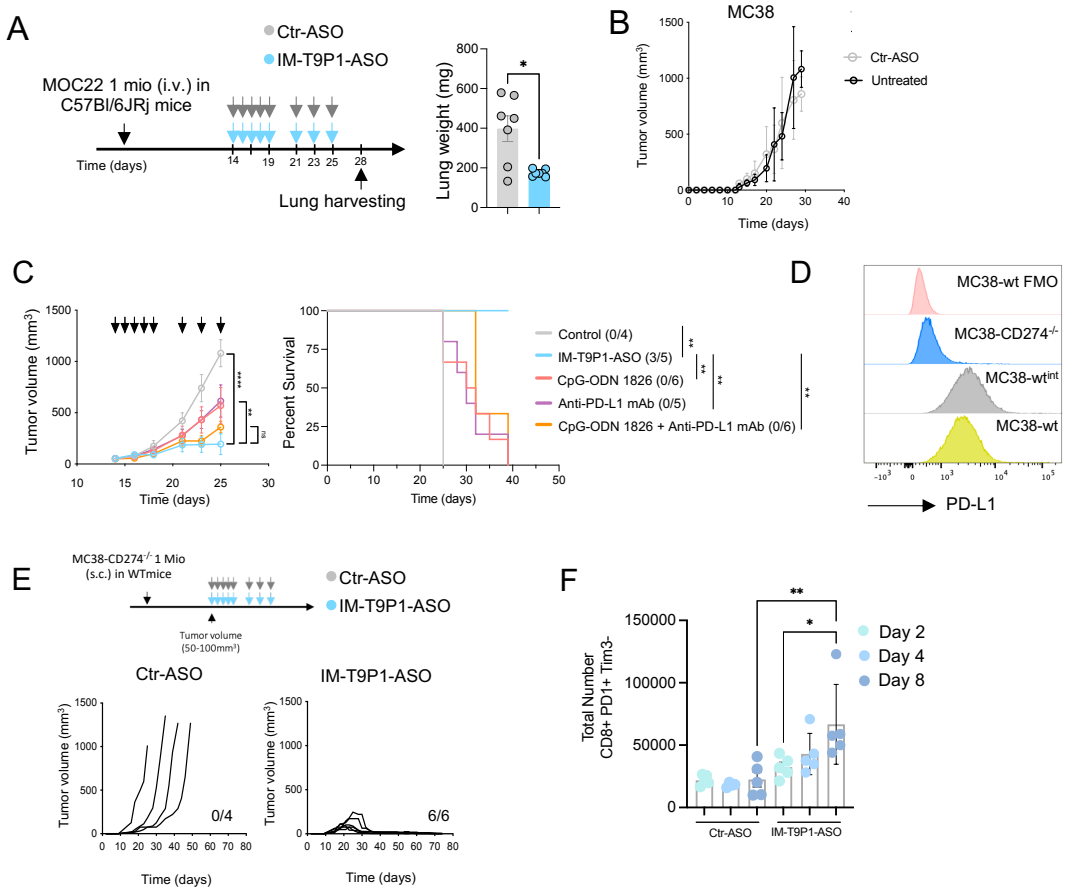

Fig. S4. IM-T9P1-ASO efficacy in different tumor models. (A) Left: Diagram of MOC22 tumor-bearing mice receiving IM-T9P1-ASO or Ctr-ASO. Right: Lung weight as proxy for tumor burden between indicated treatment conditions (n=7 mice/group). **(B)** Average tumor growth of untreated (n=12) and Ctr-ASO–treated (n=6) MC38 tumor-bearing mice. **(C)** Average tumor volume (left) and Kaplan-Meier survival curve (right) of MC38 tumor-bearing mice treated with IM-T9P1-ASO (n=5), CpG-ODN 1826 (n=6), anti-PD-L1 mAb (n=5), combination of CpG-ODN 1826 and anti-PD-L1 mAb (n=6) or controls (n=4). The number of tumor-free mice is indicated in brackets. **(D)** Validation of MC38-PD-L1$^{-/-}$ generation by PD-L1 surface staining and flow cytometry analysis. Representative histograms of fluorescence minus one (FMO) control (pink) and stained MC38-PD-L1$^{-/-}$ (blue), MC38-wt intergenic (grey) or MC38-wt (yellow) are shown. **(E)** Top: Diagram of MC38 PD-L1$^{-/-}$ tumor-bearing mice receiving IM-T9P1-ASO or Ctr-ASO. Bottom: Tumor growth over time (n=4-6

mice/group). The number of tumor-free mice is shown. (F) Total number of PD-1+ Tim3– CD8+ T cells after Ctr-ASO or IM-T9P1-ASO therapy at the indicated time points (n=5 mice/group).

Data are presented as mean ± SEM. For comparisons between two groups, Student's two-tailed t test was used. For comparisons between multiple groups and variables, one-way (F) or two-way (C) ANOVA was used. For survival analyses, the Mantel-Cox log-rank test was used. *$p < 0.05$, **$p < 0.01$, ***$p < 0.001$, ****$p < 0.0001$.

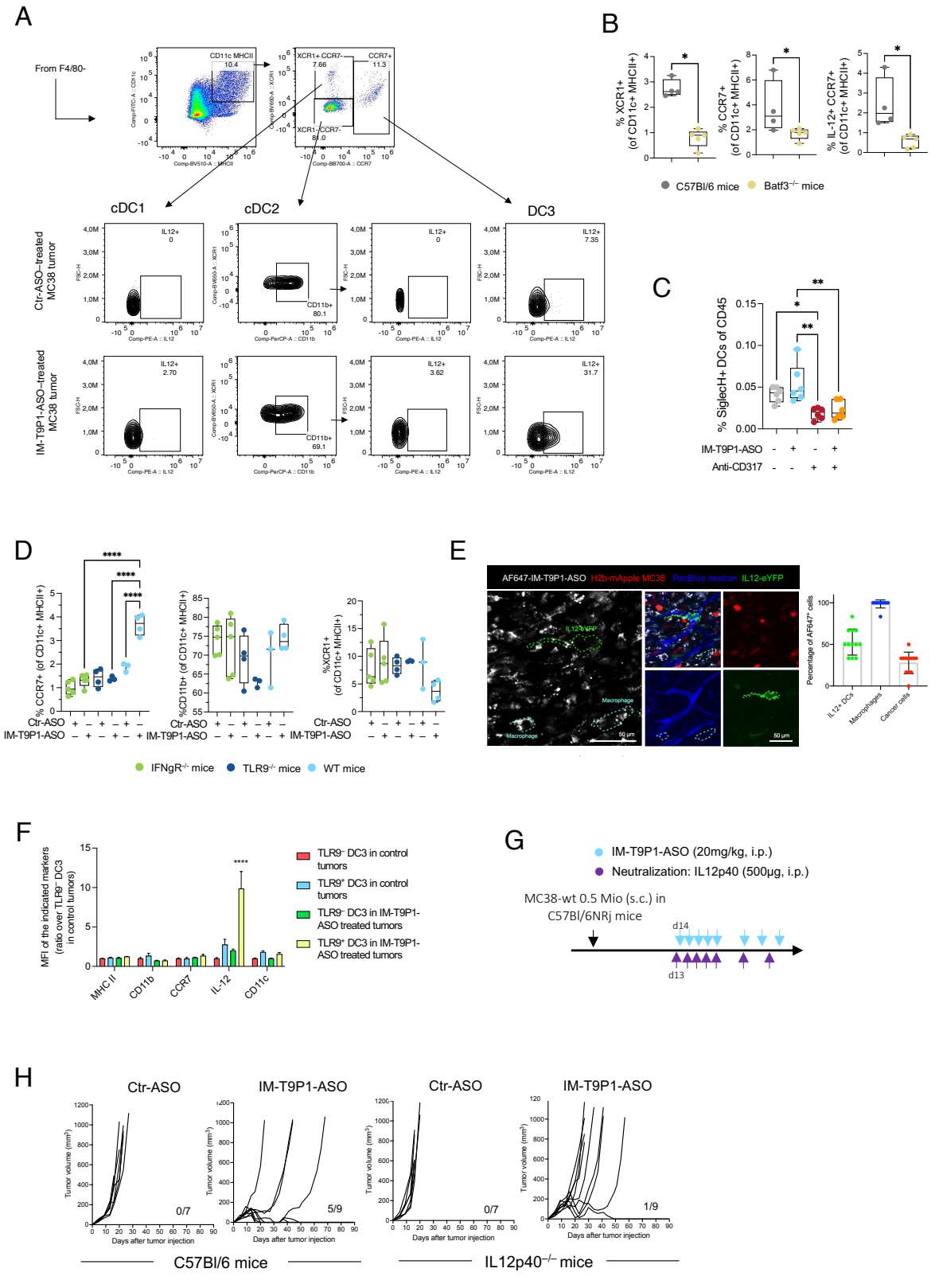

Fig. S5. DC3 gating strategy, pDC depletion and role of IL-12^{+} DC3s during IM-T9P1-ASO treatment. (A) Gating strategy for IL-12^{+} DCs revealed by intracellular cytokine staining. The representative flow cytometry plots illustrate the expansion of IL-12^{+} DC3s in MC38 tumors three days after IM-T9P1-ASO treatment. **(B)**

Frequency of cDC1s, DC3s and IL-12^{+} DC3s assessed by flow cytometry in MC38 tumors of WT and Batf3$^{-/-}$ mice (n=4-5 mice/group). **(C)** Proportion of SiglecH^{+} pDCs in blood of mice receiving IM-T9P1-ASO alone or in combination with anti-CD317 antibody three days after administration of the depletion antibody (n=5-6). **(D)** Proportions of DC3s, cDC2s and cDC1s assessed by flow cytometry in MC38 tumors of IFNgR$^{-/-}$, TLR9$^{-/-}$ or WT mice four days after Ctr-ASO or IM-T9P1-ASO treatment (n=3-5/group). **(E)** Intravital imaging analysis illustrated as in fig. S3A, showing the biodistribution of AF647-IM-T9P1-ASO in selected cells of MC38-mApple tumors. Left: representative microscopy images (white, AF647-IM-T9P1-ASO; green, IL-12p40-eYFP-expressing cells; red, tumor cells; blue, Pacific Blue-labeled vasculature and macrophages). Right: quantification of the data (n=12 images with at least three cells each and pooled from three mice). **(F)** Relative expression of the indicated DC markers in TLR9^{-} and TLR9^{+} DC3s measured by flow cytometry in MC38 tumors two days after Ctr-ASO or IM-T9P1-ASO treatment (n=4-5 mice/group). **(G)** Schematic representation of IL-12p40 neutralization in MC38 tumor-bearing mice during IM-T9P1-ASO treatment. Arrows indicate the days of the treatment. **(H)** Single tumor growth of D4M.3A tumor-bearing WT and IL-12-p40$^{-/-}$ mice treated with Ctr-ASO or IM-T9P1-ASO (n=7-9 mice/group).

Data are presented as mean ± SEM. For comparisons between two groups, Student's two-tailed t test was used. For comparisons between multiple groups and variables, one-way (C and D) or two-way (F) ANOVA was used. *p < 0.05, **p < 0.01, ***p < 0.001, ****p < 0.0001.

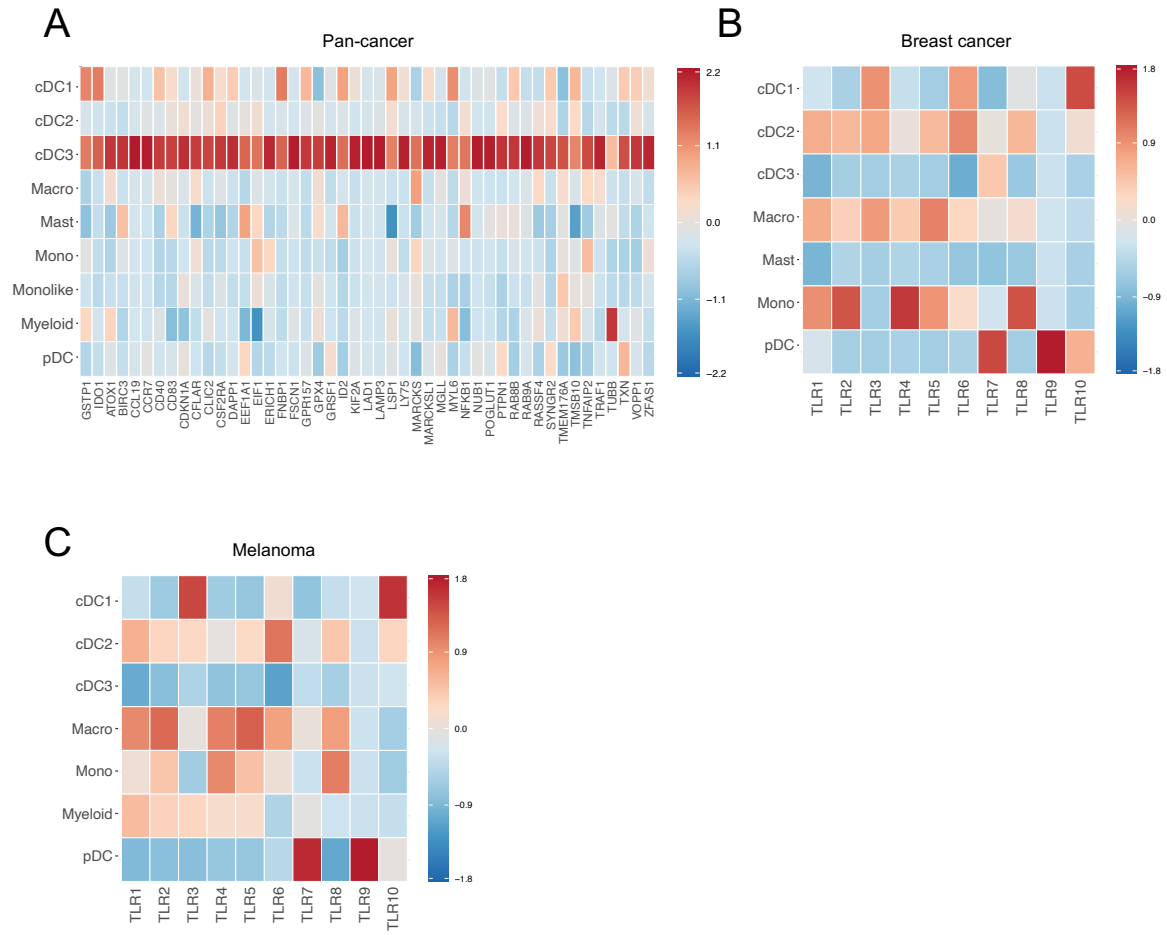

Fig. S6. Enrichment of DC3 genes and TLR screening across different human tumors. (A) Heatmap showing the expression of human DC3 gene signature compared with indicated myeloid cells across patients in a human pan-cancer scRNA-seq dataset including melanoma, lung, and breast cancer, among other cancer entities (Cheng et al., 2021). **(B-C)** Heatmaps showing mRNA expression of TLRs across myeloid cells in breast cancer patients **(B)** and melanoma patients **(C)**, as reported in (Cheng et al., 2021).

Upon request:

Movie S1. Intravital microscopy time-lapse recording of MC38-H2B-mApple tumor-bearing mice (tumor cells are in red) receiving intravenous injection of AF647-IM-T9P1-ASO (white). Tumor vessels were labeled with PacBlue-Dextran (blue). The lower-left corner shows time in hours:minutes:seconds:milliseconds. The scale bar is 100 µm.

4. Summary

Despite the major success and recent advances in therapies treating cancer, including ICI and cancer vaccines, these agents often fail to induce durable responses or complete remissions in the majority of patients. One of the reasons may be the poor network linking innate and adaptive immunity. In this thesis, we focus on targeting the innate immune system, particularly DCs, as recent evidence has highlighted the fundamental role of these cells in orchestrating cancer immunity.

First, I described how chemotherapeutics, particularly microtubule-destabilizing agents, initially designed to target the proliferation or induce cell death of malignant cells, also induce direct DC maturation through GEF-H1. We demonstrate that upon microtubule perturbation induced by MDAs, GEF-H1 is released from the microtubules, inducing upregulation of co-stimulatory molecules and secretion of pro-inflammatory cytokines in DCs, leading to enhanced antitumor responses. This DC activation is distinct from other chemotherapies that cause immunogenic cell death, as GEF-H1-mediated DC maturation is independent of TLR4, TRIF, or NALP3 pathways. These findings suggest an alternate pathway leading to effective DC activation, which may be advantageous to engage in the tumor microenvironment and improve the utility of current immune checkpoint inhibitors and personalized cancer vaccinations.

Second, I present a work where we used an ASO-based technology with the dual capacity of trigger DC activation via TLR9 engagement and control of PD-L1 in mice to overcome the limited therapeutic efficacy of anti-PD-L1 mAb. Notably, we showed that systemic administration of IM-T9P1-ASO had a remarkable capacity to induce effective and long-lasting antitumor response in different mouse models. We observed a TLR9-depedent expansion of intratumoral DC3s, the main producers of IL-12. While we could not specifically deplete DC3s to show their relevance during the treatment, as there is not method available yet to do so, we

found that the therapeutic efficacy of IM-T9P1-ASO in mice depends on the transcription factor Batf3, IL-12 and not on pDCs. Surprisingly, the overall PD-L1 downregulation *in vivo* was rare, probably because it was counteracted by IFNγ and the pro-inflammatory environment induced by IM-T9P1-ASO. However, we detected a downregulation in PD-L1 in DC3s at the mRNA and protein level starting from day 2 after the treatment. Of note, a full downregulation of PD-L1 was not necessary for a remarkable antitumor response. It would be interesting to further study these observations, as it has been shown that the loss of PD-L1 was linked to reduced DC migration towards the dLN during inflammation (Lucas et al., 2020) and that PD-L1 repress the immune checkpoint CLTA-4 by binding to CD80 *in cis*, selectively weaken the CD80-CTLA-4 interaction and not the CD80-CD28 interaction(Zhao, Lee, et al., 2019). We also propose a similar approach to target DC3 and cDC1 and cDC2, both putative precursors of DC3s, in humans. Unlike in mice, in humans TLR9 expression is mainly restricted to pDCs. Nevertheless, other TLRs are expressed in intratumoral DC3s across tumor entities. In particular, TLR3 is expressed in DC3s in lung tumors, as well as in cDC1 and cDC2. It would be interesting to study if ASOs can be further tailored to activate human DC3s, or other antitumoral DCs, by targeting alternative TLRs while downregulating PD-L1.

This work provides a mechanistic groundwork for future therapy design and show how activating intratumoral DCs with chemotherapy or immunomodulatory ASOs improve antitumor immunity, having even greater efficacy when combining with other ICIs for the treatment of solid tumors.

5. Acknowledgments

First, I would like to thank Alfred Zippelius for giving me the opportunity of doing my PhD in his lab, and for the guidance, encouragement, and freedom to develop the research projects. Thank you for all the constant support and trust you put in my work and me during the last years.

I am very grateful to the members of my advisory PhD committee Jean Pieters, Daniel Speiser, and Abhishek Kashyap, for taking the time to discuss my projects constructively and for the helpful discussions and guidance throughout the years.

I especially thank Abhishek Kashyap, who, apart from being a member of my committee during my first years of PhD, was also my direct supervisor and mentor. Thank you for sharing your knowledge, for the very long discussions about science, and for giving me the confidence to trust in myself and grow each year.

Special thanks also to Chiara Cianciaruso. It has been a pleasure to work with you. Thank you for your constant support, for sharing your knowledge, and for working countless hours during days, evenings, weekends, and nights. Thank you for always being supportive and positive and believing in me.

I want to thank all the former and present members of the cancer immunology and cancer immunotherapy labs. Thank you for the discussions, your input, the support, the lunch breaks, and the time we spent outside the lab. Thanks to all my fellow former and present PhD and Master students in the lab: Nicole Kirchhammer, Marcel Trefny, Dominic Schmid, Sofia Tundo, Irene Fusi, Nicole Oelgarth, Clara Serger, Ronja Wieboldt, Jonas Fürst, Michael Sandholzer, Andreas Zingg, Victoria Koch, Franziska Werner, Michal Stanczak, Jinyu Wang and Nicolai Rohner, and especially to Caterina Mariani. And also to the postdocs and scientist: Marina Natoli, Maryam Akramisomeabozorg, Markus Germann, Yang Liu, Elham Pishali, Gianni Monaco, Michela Manni, Anne Bärenwaldt, Natalia Rodrigues Mantuano, Julia Manzetti and especially to Marta Trüb. Thank you all for your help, support, and all the good times in the lab!

A very special thanks to Nicole Kirchhammer, Marcel Trefny, and Dominic Schmid for all your support, always being there for me in the bad and good moments, and for cheering me up when I needed it. For the endless coffees and conversations and for being good friends.

I would also like to thank Mélanie Buchi, Béatrice Dolder, Petra Herzig, and Reto Ritschard for always being willing to help and for your hard work.

Another special thank goes to all my collaboration partners, especially Mikael Pittet and Ruben Bill, and the members of Secarna Pharmaceuticals, Richard Klar, Frank Jaschinski, Julia Festag, and Andre Maaske. Thank you for always working in a very collaborative and excellent environment. And for all your input, ideas, compounds, and hard work.

I want to thank the current and former members of the FACS facility Telma Lopes, Lorenzo Raeli, Emmanuel Traunecker, Stella Stefanova, and Jelena Markovic-Djuric, for all the trainings in the different instruments for being always available to solve the problems and their support during the long hours and critical experiments.

I thank my mother, Maria, my sister Tamara and my father, Juan Manuel. Thank you for encouraging me to pursue my goals and always supporting me. And finally, the biggest thank you to my husband, Pablo. Amor, you are my biggest cheerleader and support. Without you, I would not be now standing here. And thanks to our little Danielle, who makes even the worse days shine.

6. References

Ansell, S. M., Radford, J., Connors, J. M., Długosz-Danecka, M., Kim, W. S., Gallamini, A., Ramchandren, R., Friedberg, J. W., Advani, R., Hutchings, M., Evens, A. M., Smolewski, P., Savage, K. J., Bartlett, N. L., Eom, H. S., Abramson, J. S., Dong, C., Campana, F., Fenton, K., . . . Straus, D. J. (2022). Overall Survival with Brentuximab Vedotin in Stage III or IV Hodgkin's Lymphoma. *N Engl J Med*, *387*(4), 310-320. https://doi.org/10.1056/NEJMoa2206125

Arce Vargas, F., Furness, A. J. S., Litchfield, K., Joshi, K., Rosenthal, R., Ghorani, E., Solomon, I., Lesko, M. H., Ruef, N., Roddie, C., Henry, J. Y., Spain, L., Ben Aissa, A., Georgiou, A., Wong, Y. N. S., Smith, M., Strauss, D., Hayes, A., Nicol, D., . . . Quezada, S. A. (2018). Fc Effector Function Contributes to the Activity of Human Anti-CTLA-4 Antibodies. *Cancer Cell*, *33*(4), 649-663.e644. https://doi.org/10.1016/j.ccell.2018.02.010

Arlauckas, S. P., Garris, C. S., Kohler, R. H., Kitaoka, M., Cuccarese, M. F., Yang, K. S., Miller, M. A., Carlson, J. C., Freeman, G. J., Anthony, R. M., Weissleder, R., & Pittet, M. J. (2017). In vivo imaging reveals a tumor-associated macrophage-mediated resistance pathway in anti-PD-1 therapy. *Sci Transl Med*, *9*(389). https://doi.org/10.1126/scitranslmed.aal3604

Arnette, C., Frye, K., & Kaverina, I. (2016). Microtubule and Actin Interplay Drive Intracellular c-Src Trafficking. *PLoS One*, *11*(2), e0148996. https://doi.org/10.1371/journal.pone.0148996

Azizi, E., Carr, A. J., Plitas, G., Cornish, A. E., Konopacki, C., Prabhakaran, S., Nainys, J., Wu, K., Kiseliovas, V., Setty, M., Choi, K., Fromme, R. M., Dao, P., McKenney, P. T., Wasti, R. C., Kadaveru, K., Mazutis, L., Rudensky, A. Y., & Pe'er, D. (2018). Single-Cell Map of Diverse Immune Phenotypes in the Breast Tumor Microenvironment. *Cell*, *174*(5), 1293-1308 e1236. https://doi.org/10.1016/j.cell.2018.05.060

Baghban, R., Roshangar, L., Jahanban-Esfahlan, R., Seidi, K., Ebrahimi-Kalan, A., Jaymand, M., Kolahian, S., Javaheri, T., & Zare, P. (2020). Tumor microenvironment complexity and therapeutic implications at a glance. *Cell Commun Signal*, *18*(1), 59. https://doi.org/10.1186/s12964-020-0530-4

Balwierz, P. J., Pachkov, M., Arnold, P., Gruber, A. J., Zavolan, M., & van Nimwegen, E. (2014). ISMARA: automated modeling of genomic signals as a democracy of regulatory motifs. *Genome Res*, *24*(5), 869-884. https://doi.org/10.1101/gr.169508.113

Barry, K. C., Hsu, J., Broz, M. L., Cueto, F. J., Binnewies, M., Combes, A. J., Nelson, A. E., Loo, K., Kumar, R., Rosenblum, M. D., Alvarado, M. D., Wolf, D. M., Bogunovic, D., Bhardwaj, N., Daud, A. I., Ha, P. K., Ryan, W. R., Pollack, J. L., Samad, B., . . . Krummel, M. F. (2018). A natural killer-dendritic cell axis defines checkpoint therapy-responsive tumor microenvironments. *Nat Med*, *24*(8), 1178-1191. https://doi.org/10.1038/s41591-018-0085-8

Bashraheel, S. S., Domling, A., & Goda, S. K. (2020). Update on targeted cancer therapies, single or in combination, and their fine tuning for precision medicine. *Biomed Pharmacother*, *125*, 110009. https://doi.org/10.1016/j.biopha.2020.110009

Bassez, A., Vos, H., Van Dyck, L., Floris, G., Arijs, I., Desmedt, C., Boeckx, B., Vanden Bempt, M., Nevelsteen, I., Lambein, K., Punie, K., Neven, P., Garg, A. D., Wildiers, H., Qian, J., Smeets, A., & Lambrechts, D. (2021). A single-cell map of intratumoral changes during anti-PD1 treatment of patients with breast cancer. *Nat Med*, *27*(5), 820-832. https://doi.org/10.1038/s41591-021-01323-8

Beck, A., Goetsch, L., Dumontet, C., & Corvaia, N. (2017). Strategies and challenges for the next generation of antibody-drug conjugates. *Nat Rev Drug Discov*, *16*(5), 315-337. https://doi.org/10.1038/nrd.2016.268

Binnewies, M., Mujal, A. M., Pollack, J. L., Combes, A. J., Hardison, E. A., Barry, K. C., Tsui, J., Ruhland, M. K., Kersten, K., Abushawish, M. A., Spasic, M., Giurintano, J. P., Chan, V., Daud, A. I., Ha, P., Ye, C. J., Roberts, E. W., & Krummel, M. F. (2019). Unleashing Type-2 Dendritic Cells to Drive Protective Antitumor CD4(+) T Cell Immunity. *Cell*, *177*(3), 556-571.e516. https://doi.org/10.1016/j.cell.2019.02.005

Birkenfeld, J., Nalbant, P., Yoon, S. H., & Bokoch, G. M. (2008). Cellular functions of GEF-H1, a microtubule-regulated Rho-GEF: is altered GEF-H1 activity a crucial determinant of disease pathogenesis? *Trends Cell Biol*, *18*(5), 210-219. https://doi.org/10.1016/j.tcb.2008.02.006

Blank, C. U., Rozeman, E. A., Fanchi, L. F., Sikorska, K., van de Wiel, B., Kvistborg, P., Krijgsman, O., van den Braber, M., Philips, D., Broeks, A., van Thienen, J. V., Mallo, H. A., Adriaansz, S., Ter Meulen, S., Pronk, L. M., Grijpink-Ongering, L. G., Bruining, A., Gittelman, R. M., Warren, S., . . . Schumacher, T. N. (2018). Neoadjuvant versus adjuvant ipilimumab plus nivolumab in macroscopic stage III melanoma. *Nat Med*, *24*(11), 1655-1661. https://doi.org/10.1038/s41591-018-0198-0

Böttcher, J. P., Bonavita, E., Chakravarty, P., Blees, H., Cabeza-Cabrerizo, M., Sammicheli, S., Rogers, N. C., Sahai, E., Zelenay, S., & Reis e Sousa, C. (2018). NK Cells Stimulate Recruitment of cDC1 into the Tumor Microenvironment Promoting Cancer Immune Control. *Cell*, *172*(5), 1022-1037.e1014. https://doi.org/10.1016/j.cell.2018.01.004

Böttcher, J. P., & Reis e Sousa, C. (2018). The Role of Type 1 Conventional Dendritic Cells in Cancer Immunity. *Trends Cancer*, *4*(11), 784-792. https://doi.org/10.1016/j.trecan.2018.09.001

Bourdely, P., Anselmi, G., Vaivode, K., Ramos, R. N., Missolo-Koussou, Y., Hidalgo, S., Tosselo, J., Nuñez, N., Richer, W., Vincent-Salomon, A., Saxena, A., Wood, K., Lladser, A., Piaggio, E., Helft, J., & Guermonprez, P. (2020). Transcriptional and Functional Analysis of CD1c(+) Human Dendritic Cells Identifies a CD163(+) Subset Priming CD8(+)CD103(+) T Cells. *Immunity*, *53*(2), 335-352.e338. https://doi.org/10.1016/j.immuni.2020.06.002

Broz, M. L., Binnewies, M., Boldajipour, B., Nelson, A. E., Pollack, J. L., Erle, D. J., Barczak, A., Rosenblum, M. D., Daud, A., Barber, D. L., Amigorena, S., Van't Veer, L. J., Sperling, A. I., Wolf, D. M., & Krummel, M. F. (2014). Dissecting the tumor myeloid compartment reveals rare activating antigen-presenting cells critical for T cell immunity. *Cancer Cell*, *26*(5), 638-652. https://doi.org/10.1016/j.ccell.2014.09.007

Cabeza-Cabrerizo, M., Cardoso, A., Minutti, C. M., Pereira da Costa, M., & Reis e Sousa, C. (2021). Dendritic Cells Revisited. *Annu Rev Immunol*, *39*, 131-166. https://doi.org/10.1146/annurev-immunol-061020-053707

Chen, D. S., & Mellman, I. (2013). Oncology meets immunology: the cancer-immunity cycle. *Immunity*, *39*(1), 1-10. https://doi.org/10.1016/j.immuni.2013.07.012

Chen, L., Xiong, Y., Li, J., Zheng, X., Zhou, Q., Turner, A., Wu, C., Lu, B., & Jiang, J. (2017). PD-L1 Expression Promotes Epithelial to Mesenchymal Transition in Human Esophageal Cancer. *Cell Physiol Biochem*, *42*(6), 2267-2280. https://doi.org/10.1159/000480000

Cheng, S., Li, Z., Gao, R., Xing, B., Gao, Y., Yang, Y., Qin, S., Zhang, L., Ouyang, H., Du, P., Jiang, L., Zhang, B., Yang, Y., Wang, X., Ren, X., Bei, J. X., Hu, X., Bu, Z., Ji, J., & Zhang, Z. (2021). A pan-cancer single-cell transcriptional atlas of tumor infiltrating myeloid cells. *Cell*, *184*(3), 792-809 e723. https://doi.org/10.1016/j.cell.2021.01.010

Chiang, H. S., Zhao, Y., Song, J. H., Liu, S., Wang, N., Terhorst, C., Sharpe, A. H., Basavappa, M., Jeffrey, K. L., & Reinecker, H. C. (2014). GEF-H1 controls microtubule-dependent sensing of nucleic acids for antiviral host defenses. *Nat Immunol*, *15*(1), 63-71. https://doi.org/10.1038/ni.2766

Chiba, S., Baghdadi, M., Akiba, H., Yoshiyama, H., Kinoshita, I., Dosaka-Akita, H., Fujioka, Y., Ohba, Y., Gorman, J. V., Colgan, J. D., Hirashima, M., Uede, T., Takaoka, A., Yagita, H., & Jinushi, M. (2012). Tumor-infiltrating DCs suppress nucleic acid-mediated innate immune responses through interactions between the receptor TIM-3 and the alarmin HMGB1. *Nat Immunol*, *13*(9), 832-842. https://doi.org/10.1038/ni.2376

Cirillo, L., Gotta, M., & Meraldi, P. (2017). The Elephant in the Room: The Role of Microtubules in Cancer. *Adv Exp Med Biol*, *1002*, 93-124. https://doi.org/10.1007/978-3-319-57127-0_5

Colaprico, A., Silva, T. C., Olsen, C., Garofano, L., Cava, C., Garolini, D., Sabedot, T. S., Malta, T. M., Pagnotta, S. M., Castiglioni, I., Ceccarelli, M., Bontempi, G., & Noushmehr, H. (2016). TCGAbiolinks: an R/Bioconductor package for integrative analysis of TCGA data. *Nucleic Acids Res*, *44*(8), e71. https://doi.org/10.1093/nar/gkv1507

Connors, J. M., Jurczak, W., Straus, D. J., Ansell, S. M., Kim, W. S., Gallamini, A., Younes, A., Alekseev, S., Illés, Á., Picardi, M., Lech-Maranda, E., Oki, Y., Feldman, T., Smolewski, P., Savage, K. J., Bartlett, N. L., Walewski, J., Chen, R., Ramchandren, R., . . . Radford, J. (2018). Brentuximab Vedotin with Chemotherapy for Stage III or IV Hodgkin's Lymphoma. *N Engl J Med*, *378*(4), 331-344. https://doi.org/10.1056/NEJMoa1708984

Corrales, L., Matson, V., Flood, B., Spranger, S., & Gajewski, T. F. (2017). Innate immune signaling and regulation in cancer immunotherapy. *Cell Res*, *27*(1), 96-108. https://doi.org/10.1038/cr.2016.149

Cursons, J., Souza-Fonseca-Guimaraes, F., Foroutan, M., Anderson, A., Hollande, F., Hediyeh-Zadeh, S., Behren, A., Huntington, N. D., & Davis, M. J. (2019). A Gene Signature Predicting Natural Killer Cell Infiltration and Improved Survival in Melanoma Patients. *Cancer Immunol Res*, *7*(7), 1162-1174. https://doi.org/10.1158/2326-6066.CIR-18-0500

Cytlak, U., Resteu, A., Pagan, S., Green, K., Milne, P., Maisuria, S., McDonald, D., Hulme, G., Filby, A., Carpenter, B., Queen, R., Hambleton, S., Hague, R., Lango Allen, H., Thaventhiran, J. E. D., Doody, G., Collin, M., & Bigley, V. (2020). Differential IRF8 Transcription Factor Requirement Defines Two Pathways of Dendritic Cell Development in Humans. *Immunity*, *53*(2), 353-370.e358. https://doi.org/10.1016/j.immuni.2020.07.003

Daniels, M. A., Teixeiro, E., Gill, J., Hausmann, B., Roubaty, D., Holmberg, K., Werlen, G., Hollander, G. A., Gascoigne, N. R., & Palmer, E. (2006). Thymic selection threshold defined by compartmentalization of Ras/MAPK signalling. *Nature*, *444*(7120), 724-729. https://doi.org/10.1038/nature05269

de Mingo Pulido, Á., Hänggi, K., Celias, D. P., Gardner, A., Li, J., Batista-Bittencourt, B., Mohamed, E., Trillo-Tinoco, J., Osunmakinde, O., Peña, R., Onimus, A., Kaisho, T., Kaufmann, J., McEachern, K., Soliman, H., Luca, V. C., Rodriguez, P. C., Yu, X., & Ruffell, B. (2021). The inhibitory receptor TIM-3 limits activation

of the cGAS-STING pathway in intra-tumoral dendritic cells by suppressing extracellular DNA uptake. *Immunity*, *54*(6), 1154-1167.e1157. https://doi.org/10.1016/j.immuni.2021.04.019

Deng, L., Liang, H., Xu, M., Yang, X., Burnette, B., Arina, A., Li, X. D., Mauceri, H., Beckett, M., Darga, T., Huang, X., Gajewski, T. F., Chen, Z. J., Fu, Y. X., & Weichselbaum, R. R. (2014). STING-Dependent Cytosolic DNA Sensing Promotes Radiation-Induced Type I Interferon-Dependent Antitumor Immunity in Immunogenic Tumors. *Immunity*, *41*(5), 843-852. https://doi.org/10.1016/j.immuni.2014.10.019

Derijard, B., Raingeaud, J., Barrett, T., Wu, I. H., Han, J., Ulevitch, R. J., & Davis, R. J. (1995). Independent human MAP-kinase signal transduction pathways defined by MEK and MKK isoforms. *Science*, *267*(5198), 682-685. https://doi.org/10.1126/science.7839144

Desch, A. N., Gibbings, S. L., Clambey, E. T., Janssen, W. J., Slansky, J. E., Kedl, R. M., Henson, P. M., & Jakubzick, C. (2014). Dendritic cell subsets require cis-activation for cytotoxic CD8 T-cell induction. *Nat Commun*, *5*, 4674. https://doi.org/10.1038/ncomms5674

Devred, F., Barbier, P., Lafitte, D., Landrieu, I., Lippens, G., & Peyrot, V. (2010). Microtubule and MAPs: thermodynamics of complex formation by AUC, ITC, fluorescence, and NMR. *Methods Cell Biol*, *95*, 449-480. https://doi.org/10.1016/S0091-679X(10)95023-1

Di Pilato, M., Kfuri-Rubens, R., Pruessmann, J. N., Ozga, A. J., Messemaker, M., Cadilha, B. L., Sivakumar, R., Cianciaruso, C., Warner, R. D., Marangoni, F., Carrizosa, E., Lesch, S., Billingsley, J., Perez-Ramos, D., Zavala, F., Rheinbay, E., Luster, A. D., Gerner, M. Y., Kobold, S., . . . Mempel, T. R. (2021). CXCR6 positions cytotoxic T cells to receive critical survival signals in the tumor microenvironment. *Cell*, *184*(17), 4512-4530 e4522. https://doi.org/10.1016/j.cell.2021.07.015

Di Pucchio, T., Chatterjee, B., Smed-Sörensen, A., Clayton, S., Palazzo, A., Montes, M., Xue, Y., Mellman, I., Banchereau, J., & Connolly, J. E. (2008). Direct proteasome-independent cross-presentation of viral antigen by plasmacytoid dendritic cells on major histocompatibility complex class I. *Nat Immunol*, *9*(5), 551-557. https://doi.org/10.1038/ni.1602

Dixon, K. O., Tabaka, M., Schramm, M. A., Xiao, S., Tang, R., Dionne, D., Anderson, A. C., Rozenblatt-Rosen, O., Regev, A., & Kuchroo, V. K. (2021). TIM-3 restrains anti-tumour immunity by regulating inflammasome activation. *Nature*, *595*(7865), 101-106. https://doi.org/10.1038/s41586-021-03626-9

Dobin, A., Davis, C. A., Schlesinger, F., Drenkow, J., Zaleski, C., Jha, S., Batut, P., Chaisson, M., & Gingeras, T. R. (2013). STAR: ultrafast universal RNA-seq aligner. *Bioinformatics*, *29*(1), 15-21. https://doi.org/10.1093/bioinformatics/bts635

Domogalla, M. P., Rostan, P. V., Raker, V. K., & Steinbrink, K. (2017). Tolerance through Education: How Tolerogenic Dendritic Cells Shape Immunity. *Front Immunol*, *8*, 1764. https://doi.org/10.3389/fimmu.2017.01764

Dress, R. J., Dutertre, C. A., Giladi, A., Schlitzer, A., Low, I., Shadan, N. B., Tay, A., Lum, J., Kairi, M., Hwang, Y. Y., Becht, E., Cheng, Y., Chevrier, M., Larbi, A., Newell, E. W., Amit, I., Chen, J., & Ginhoux, F. (2019). Plasmacytoid dendritic cells develop from Ly6D(+) lymphoid progenitors distinct from the myeloid lineage. *Nat Immunol*, *20*(7), 852-864. https://doi.org/10.1038/s41590-019-0420-3

Dumontet, C., & Jordan, M. A. (2010). Microtubule-binding agents: a dynamic field of cancer therapeutics. *Nat Rev Drug Discov*, *9*(10), 790-803. https://doi.org/10.1038/nrd3253

Dutertre, C. A., Becht, E., Irac, S. E., Khalilnezhad, A., Narang, V., Khalilnezhad, S., Ng, P. Y., van den Hoogen, L. L., Leong, J. Y., Lee, B., Chevrier, M., Zhang, X. M., Yong, P. J. A., Koh, G., Lum, J., Howland, S. W., Mok, E., Chen, J., Larbi, A., . . . Ginhoux, F. (2019). Single-Cell Analysis of Human Mononuclear Phagocytes Reveals Subset-Defining Markers and Identifies Circulating Inflammatory Dendritic Cells. *Immunity*, *51*(3), 573-589.e578. https://doi.org/10.1016/j.immuni.2019.08.008

Emens, L. A., & Middleton, G. (2015). The interplay of immunotherapy and chemotherapy: harnessing potential synergies. *Cancer Immunol Res*, *3*(5), 436-443. https://doi.org/10.1158/2326-6066.Cir-15-0064

Ferlay, J., Colombet, M., Soerjomataram, I., Parkin, D. M., Pineros, M., Znaor, A., & Bray, F. (2021). Cancer statistics for the year 2020: An overview. *Int J Cancer*. https://doi.org/10.1002/ijc.33588

Ferris, S. T., Durai, V., Wu, R., Theisen, D. J., Ward, J. P., Bern, M. D., Davidson, J. T. t., Bagadia, P., Liu, T., Briseño, C. G., Li, L., Gillanders, W. E., Wu, G. F., Yokoyama, W. M., Murphy, T. L., Schreiber, R. D., & Murphy, K. M. (2020). cDC1 prime and are licensed by CD4(+) T cells to induce anti-tumour immunity. *Nature*, *584*(7822), 624-629. https://doi.org/10.1038/s41586-020-2611-3

Filin, I. Y., Kitaeva, K. V., Rutland, C. S., Rizvanov, A. A., & Solovyeva, V. V. (2021). Recent Advances in Experimental Dendritic Cell Vaccines for Cancer. *Front Oncol*, *11*, 730824. https://doi.org/10.3389/fonc.2021.730824

Fine, N., Dimitriou, I. D., Rullo, J., Sandi, M. J., Petri, B., Haitsma, J., Ibrahim, H., La Rose, J., Glogauer, M., Kubes, P., Cybulsky, M., & Rottapel, R. (2016). GEF-H1 is necessary for neutrophil shear stress-induced migration during inflammation. *J Cell Biol*, *215*(1), 107-119. https://doi.org/10.1083/jcb.201603109

Friedman, K. M., Prieto, P. A., Devillier, L. E., Gross, C. A., Yang, J. C., Wunderlich, J. R., Rosenberg, S. A., & Dudley, M. E. (2012). Tumor-specific CD4+ melanoma tumor-infiltrating lymphocytes. *J Immunother*, *35*(5), 400-408. https://doi.org/10.1097/CJI.0b013e31825898c5

Fucikova, J., Kepp, O., Kasikova, L., Petroni, G., Yamazaki, T., Liu, P., Zhao, L., Spisek, R., Kroemer, G., & Galluzzi, L. (2020). Detection of immunogenic cell death and its relevance for cancer therapy. *Cell Death Dis*, *11*(11), 1013. https://doi.org/10.1038/s41419-020-03221-2

Fukazawa, A., Alonso, C., Kurachi, K., Gupta, S., Lesser, C. F., McCormick, B. A., & Reinecker, H. C. (2008). GEF-H1 mediated control of NOD1 dependent NF-kappaB activation by Shigella effectors. *PLoS Pathog*, *4*(11), e1000228. https://doi.org/10.1371/journal.ppat.1000228

Gagliardi, M., & Ashizawa, A. T. (2021). The Challenges and Strategies of Antisense Oligonucleotide Drug Delivery. *Biomedicines*, *9*(4). https://doi.org/10.3390/biomedicines9040433

Gajewski, T. F., Schreiber, H., & Fu, Y. X. (2013). Innate and adaptive immune cells in the tumor microenvironment. *Nat Immunol*, *14*(10), 1014-1022. https://doi.org/10.1038/ni.2703

Gallo, P. M., & Gallucci, S. (2013). The dendritic cell response to classic, emerging, and homeostatic danger signals. Implications for autoimmunity. *Front Immunol*, *4*, 138. https://doi.org/10.3389/fimmu.2013.00138

Galluzzi, L., Vacchelli, E., Bravo-San Pedro, J. M., Buqué, A., Senovilla, L., Baracco, E. E., Bloy, N., Castoldi, F., Abastado, J. P., Agostinis, P., Apte, R. N., Aranda, F., Ayyoub, M., Beckhove, P., Blay, J. Y., Bracci, L., Caignard, A., Castelli, C., Cavallo, F., . . . Kroemer, G. (2014). Classification of current anticancer immunotherapies. *Oncotarget*, *5*(24), 12472-12508. https://doi.org/10.18632/oncotarget.2998

Gan, X., Shan, Q., Li, H., Janssens, R., Shen, Y., He, Y., Chen, F., van Haperen, R., Drabek, D., Li, J., Zhang, Y., Zhao, J., Qin, B., Jheng, M. J., Chen, V., Wang, J., Rong, Y., & Grosveld, F. (2022). An anti-CTLA-4 heavy chain-only antibody with enhanced T(reg) depletion shows excellent preclinical efficacy and safety profile. *Proc Natl Acad Sci U S A*, *119*(32), e2200879119. https://doi.org/10.1073/pnas.2200879119

Gao, Y., Nihira, N. T., Bu, X., Chu, C., Zhang, J., Kolodziejczyk, A., Fan, Y., Chan, N. T., Ma, L., Liu, J., Wang, D., Dai, X., Liu, H., Ono, M., Nakanishi, A., Inuzuka, H., North, B. J., Huang, Y. H., Sharma, S., . . . Wei, W. (2020). Acetylation-dependent regulation of PD-L1 nuclear translocation dictates the efficacy of anti-PD-1 immunotherapy. *Nat Cell Biol*, *22*(9), 1064-1075. https://doi.org/10.1038/s41556-020-0562-4

Garcia-Diaz, A., Shin, D. S., Moreno, B. H., Saco, J., Escuin-Ordinas, H., Rodriguez, G. A., Zaretsky, J. M., Sun, L., Hugo, W., Wang, X., Parisi, G., Saus, C. P., Torrejon, D. Y., Graeber, T. G., Comin-Anduix, B., Hu-Lieskovan, S., Damoiseaux, R., Lo, R. S., & Ribas, A. (2017). Interferon Receptor Signaling Pathways Regulating PD-L1 and PD-L2 Expression. *Cell Rep*, *19*(6), 1189-1201. https://doi.org/10.1016/j.celrep.2017.04.031

Gardner, A., & Ruffell, B. (2016). Dendritic Cells and Cancer Immunity. *Trends Immunol*, *37*(12), 855-865. https://doi.org/10.1016/j.it.2016.09.006

Garris, C. S., Arlauckas, S. P., Kohler, R. H., Trefny, M. P., Garren, S., Piot, C., Engblom, C., Pfirschke, C., Siwicki, M., Gungabeesoon, J., Freeman, G. J., Warren, S. E., Ong, S., Browning, E., Twitty, C. G., Pierce, R. H., Le, M. H., Algazi, A. P., Daud, A. I., . . . Pittet, M. J. (2018). Successful Anti-PD-1 Cancer Immunotherapy Requires T Cell-Dendritic Cell Crosstalk Involving the Cytokines IFN-gamma and IL-12. *Immunity*, *49*(6), 1148-1161 e1147. https://doi.org/10.1016/j.immuni.2018.09.024

Gerhard, G. M., Bill, R., Messemaker, M., Klein, A. M., & Pittet, M. J. (2021). Tumor-infiltrating dendritic cell states are conserved across solid human cancers. *J Exp Med*, *218*(1). https://doi.org/10.1084/jem.20200264

Germain, C., Gnjatic, S., Tamzalit, F., Knockaert, S., Remark, R., Goc, J., Lepelley, A., Becht, E., Katsahian, S., Bizouard, G., Validire, P., Damotte, D., Alifano, M., Magdeleinat, P., Cremer, I., Teillaud, J. L., Fridman, W. H., Sautès-Fridman, C., & Dieu-Nosjean, M. C. (2014). Presence of B cells in tertiary lymphoid structures is associated with a protective immunity in patients with lung cancer. *Am J Respir Crit Care Med*, *189*(7), 832-844. https://doi.org/10.1164/rccm.201309-1611OC

Gerstung, M., Jolly, C., Leshchiner, I., Dentro, S. C., Gonzalez, S., Rosebrock, D., Mitchell, T. J., Rubanova, Y., Anur, P., Yu, K., Tarabichi, M., Deshwar, A., Wintersinger, J., Kleinheinz, K., Vázquez-García, I., Haase, K., Jerman, L., Sengupta, S., Macintyre, G., . . . Van Loo, P. (2020). The evolutionary history of 2,658 cancers. *Nature*, *578*(7793), 122-128. https://doi.org/10.1038/s41586-019-1907-7

Gigant, B., Wang, C., Ravelli, R. B., Roussi, F., Steinmetz, M. O., Curmi, P. A., Sobel, A., & Knossow, M. (2005). Structural basis for the regulation of tubulin by vinblastine. *Nature*, *435*(7041), 519-522. https://doi.org/10.1038/nature03566

Gilliet, M., Cao, W., & Liu, Y. J. (2008). Plasmacytoid dendritic cells: sensing nucleic acids in viral infection and autoimmune diseases. *Nat Rev Immunol*, *8*(8), 594-606. https://doi.org/10.1038/nri2358

Glaven, J. A., Whitehead, I., Bagrodia, S., Kay, R., & Cerione, R. A. (1999). The Dbl-related protein, Lfc, localizes to microtubules and mediates the activation of Rac signaling pathways in cells. *J Biol Chem*, *274*(4), 2279-2285. https://doi.org/10.1074/jbc.274.4.2279

Gu, Y. Z., Zhao, X., & Song, X. R. (2020). Ex vivo pulsed dendritic cell vaccination against cancer. *Acta Pharmacol Sin*, *41*(7), 959-969. https://doi.org/10.1038/s41401-020-0415-5

Guilliams, M., Ginhoux, F., Jakubzick, C., Naik, S. H., Onai, N., Schraml, B. U., Segura, E., Tussiwand, R., & Yona, S. (2014). Dendritic cells, monocytes and macrophages: a unified nomenclature based on ontogeny. *Nat Rev Immunol*, *14*(8), 571-578. https://doi.org/10.1038/nri3712

Halama, N., Zoernig, I., Berthel, A., Kahlert, C., Klupp, F., Suarez-Carmona, M., Suetterlin, T., Brand, K., Krauss, J., Lasitschka, F., Lerchl, T., Luckner-Minden, C., Ulrich, A., Koch, M., Weitz, J., Schneider, M., Buechler, M. W., Zitvogel, L., Herrmann, T., . . . Jaeger, D. (2016). Tumoral Immune Cell Exploitation in Colorectal Cancer Metastases Can Be Targeted Effectively by Anti-CCR5 Therapy in Cancer Patients. *Cancer Cell*, *29*(4), 587-601. https://doi.org/10.1016/j.ccell.2016.03.005

Hanahan, D., & Weinberg, R. A. (2011). Hallmarks of cancer: the next generation. *Cell*, *144*(5), 646-674. https://doi.org/10.1016/j.cell.2011.02.013

Hargadon, K. M., Johnson, C. E., & Williams, C. J. (2018). Immune checkpoint blockade therapy for cancer: An overview of FDA-approved immune checkpoint inhibitors. *Int Immunopharmacol*, *62*, 29-39. https://doi.org/10.1016/j.intimp.2018.06.001

Hartmann, G. (2017). Nucleic Acid Immunity. *Adv Immunol*, *133*, 121-169. https://doi.org/10.1016/bs.ai.2016.11.001

Haslam, A., Gill, J., & Prasad, V. (2020). Estimation of the Percentage of US Patients With Cancer Who Are Eligible for Immune Checkpoint Inhibitor Drugs. *JAMA Netw Open*, *3*(3), e200423. https://doi.org/10.1001/jamanetworkopen.2020.0423

Hellmann, M. D., Ciuleanu, T. E., Pluzanski, A., Lee, J. S., Otterson, G. A., Audigier-Valette, C., Minenza, E., Linardou, H., Burgers, S., Salman, P., Borghaei, H., Ramalingam, S. S., Brahmer, J., Reck, M., O'Byrne, K. J., Geese, W. J., Green, G., Chang, H., Szustakowski, J., . . . Paz-Ares, L. (2018). Nivolumab plus Ipilimumab in Lung Cancer with a High Tumor Mutational Burden. *N Engl J Med*, *378*(22), 2093-2104. https://doi.org/10.1056/NEJMoa1801946

Hemmi, H., Takeuchi, O., Kawai, T., Kaisho, T., Sato, S., Sanjo, H., Matsumoto, M., Hoshino, K., Wagner, H., Takeda, K., & Akira, S. (2000). A Toll-like receptor recognizes bacterial DNA. *Nature*, *408*(6813), 740-745. https://doi.org/10.1038/35047123

Higano, C. S., Schellhammer, P. F., Small, E. J., Burch, P. A., Nemunaitis, J., Yuh, L., Provost, N., & Frohlich, M. W. (2009). Integrated data from 2 randomized, double-blind, placebo-controlled, phase 3 trials of active cellular immunotherapy with sipuleucel-T in advanced prostate cancer. *Cancer*, *115*(16), 3670-3679. https://doi.org/10.1002/cncr.24429

Hildner, K., Edelson, B. T., Purtha, W. E., Diamond, M., Matsushita, H., Kohyama, M., Calderon, B., Schraml, B. U., Unanue, E. R., Diamond, M. S., Schreiber, R. D., Murphy, T. L., & Murphy, K. M. (2008). Batf3 deficiency reveals a critical role for CD8alpha+ dendritic cells in cytotoxic T cell immunity. *Science*, *322*(5904), 1097-1100. https://doi.org/10.1126/science.1164206

Hill, C. S., Wynne, J., & Treisman, R. (1995). The Rho family GTPases RhoA, Rac1, and CDC42Hs regulate transcriptional activation by SRF. *Cell*, *81*(7), 1159-1170. https://doi.org/10.1016/s0092-8674(05)80020-0

Huber, R., Pietsch, D., Panterodt, T., & Brand, K. (2012). Regulation of C/EBPbeta and resulting functions in cells of the monocytic lineage. *Cell Signal*, *24*(6), 1287-1296. https://doi.org/10.1016/j.cellsig.2012.02.007

Humbert, M., Guery, L., Brighouse, D., Lemeille, S., & Hugues, S. (2018). Intratumoral CpG-B Promotes Antitumoral Neutrophil, cDC, and T-cell Cooperation without Reprograming Tolerogenic pDC. *Cancer Res*, *78*(12), 3280-3292. https://doi.org/10.1158/0008-5472.Can-17-2549

Imai, K., & Takaoka, A. (2006). Comparing antibody and small-molecule therapies for cancer. *Nat Rev Cancer*, *6*(9), 714-727. https://doi.org/10.1038/nrc1913

Inaba, K., Turley, S., Iyoda, T., Yamaide, F., Shimoyama, S., Reis e Sousa, C., Germain, R. N., Mellman, I., & Steinman, R. M. (2000). The formation of immunogenic major histocompatibility complex class II-

peptide ligands in lysosomal compartments of dendritic cells is regulated by inflammatory stimuli. *J Exp Med*, *191*(6), 927-936. https://doi.org/10.1084/jem.191.6.927

Jaschinski, F., Korhonen, H., & Janicot, M. (2015). Design and Selection of Antisense Oligonucleotides Targeting Transforming Growth Factor Beta (TGF-beta) Isoform mRNAs for the Treatment of Solid Tumors. *Methods Mol Biol*, *1317*, 137-151. https://doi.org/10.1007/978-1-4939-2727-2_9

Jensen, T. O., Schmidt, H., Møller, H. J., Donskov, F., Høyer, M., Sjoegren, P., Christensen, I. J., & Steiniche, T. (2012). Intratumoral neutrophils and plasmacytoid dendritic cells indicate poor prognosis and are associated with pSTAT3 expression in AJCC stage I/II melanoma. *Cancer*, *118*(9), 2476-2485. https://doi.org/10.1002/cncr.26511

Jiang, P., Zhang, Y., Ru, B., Yang, Y., Vu, T., Paul, R., Mirza, A., Altan-Bonnet, G., Liu, L., Ruppin, E., Wakefield, L., & Wucherpfennig, K. W. (2021). Systematic investigation of cytokine signaling activity at the tissue and single-cell levels. *Nat Methods*, *18*(10), 1181-1191. https://doi.org/10.1038/s41592-021-01274-5

Jin, H., D'Urso, V., Neuteboom, B., McKenna, S. D., Schweickhardt, R., Gross, A. W., Fomekong Nanfack, Y., Paoletti, A., Carter, C., Toleikis, L., Fluck, M., Scheuenpflug, J., & Cai, T. (2021). Avelumab internalization by human circulating immune cells is mediated by both Fc gamma receptor and PD-L1 binding. *Oncoimmunology*, *10*(1), 1958590. https://doi.org/10.1080/2162402X.2021.1958590

Jin, Y., Zhuang, Y., Dong, X., & Liu, M. (2021). Development of CpG oligodeoxynucleotide TLR9 agonists in anti-cancer therapy. *Expert Rev Anticancer Ther*, *21*(8), 841-851. https://doi.org/10.1080/14737140.2021.1915136

Jordan, M. A., & Wilson, L. (2004). Microtubules as a target for anticancer drugs. *Nat Rev Cancer*, *4*(4), 253-265. https://doi.org/10.1038/nrc1317

Kamon, H., Kawabe, T., Kitamura, H., Lee, J., Kamimura, D., Kaisho, T., Akira, S., Iwamatsu, A., Koga, H., Murakami, M., & Hirano, T. (2006). TRIF-GEFH1-RhoB pathway is involved in MHCII expression on dendritic cells that is critical for CD4 T-cell activation. *EMBO J*, *25*(17), 4108-4119. https://doi.org/10.1038/sj.emboj.7601286

Kantoff, P. W., Higano, C. S., Shore, N. D., Berger, E. R., Small, E. J., Penson, D. F., Redfern, C. H., Ferrari, A. C., Dreicer, R., Sims, R. B., Xu, Y., Frohlich, M. W., & Schellhammer, P. F. (2010). Sipuleucel-T immunotherapy for castration-resistant prostate cancer. *N Engl J Med*, *363*(5), 411-422. https://doi.org/10.1056/NEJMoa1001294

Kashyap, A. S., Thelemann, T., Klar, R., Kallert, S. M., Festag, J., Buchi, M., Hinterwimmer, L., Schell, M., Michel, S., Jaschinski, F., & Zippelius, A. (2019). Antisense oligonucleotide targeting CD39 improves anti-tumor T cell immunity. *J Immunother Cancer*, *7*(1), 67. https://doi.org/10.1186/s40425-019-0545-9

Kawai, T., & Akira, S. (2011). Toll-like receptors and their crosstalk with other innate receptors in infection and immunity. *Immunity*, *34*(5), 637-650. https://doi.org/10.1016/j.immuni.2011.05.006

Kawasaki, T., & Kawai, T. (2014). Toll-like receptor signaling pathways. *Front Immunol*, *5*, 461. https://doi.org/10.3389/fimmu.2014.00461

Kedl, R. M., Lindsay, R. S., Finlon, J. M., Lucas, E. D., Friedman, R. S., & Tamburini, B. A. J. (2017). Migratory dendritic cells acquire and present lymphatic endothelial cell-archived antigens during lymph node contraction. *Nat Commun*, *8*(1), 2034. https://doi.org/10.1038/s41467-017-02247-z

Kim, J. G., Islam, R., Cho, J. Y., Jeong, H., Cap, K. C., Park, Y., Hossain, A. J., & Park, J. B. (2018). Regulation of RhoA GTPase and various transcription factors in the RhoA pathway. *J Cell Physiol*, *233*(9), 6381-6392. https://doi.org/10.1002/jcp.26487

Kirchhammer, N., Trefny, M. P., Natoli, M., Brucher, D., Smith, S. N., Werner, F., Koch, V., Schreiner, D., Bartoszek, E., Buchi, M., Schmid, M., Breu, D., Hartmann, K. P., Zaytseva, P., Thommen, D. S., Laubli, H., Bottcher, J. P., Stanczak, M. A., Kashyap, A. S., . . . Zippelius, A. (2022). NK cells with tissue-resident traits shape response to immunotherapy by inducing adaptive antitumor immunity. *Sci Transl Med*, *14*(653), eabm9043. https://doi.org/10.1126/scitranslmed.abm9043

Koucký, V., Bouček, J., & Fialová, A. (2019). Immunology of Plasmacytoid Dendritic Cells in Solid Tumors: A Brief Review. *Cancers (Basel)*, *11*(4). https://doi.org/10.3390/cancers11040470

Krendel, M., Zenke, F. T., & Bokoch, G. M. (2002). Nucleotide exchange factor GEF-H1 mediates cross-talk between microtubules and the actin cytoskeleton. *Nat Cell Biol*, *4*(4), 294-301. https://doi.org/10.1038/ncb773

Kurtulus, S., Madi, A., Escobar, G., Klapholz, M., Nyman, J., Christian, E., Pawlak, M., Dionne, D., Xia, J., Rozenblatt-Rosen, O., Kuchroo, V. K., Regev, A., & Anderson, A. C. (2019). Checkpoint Blockade Immunotherapy Induces Dynamic Changes in PD-1(-)CD8(+) Tumor-Infiltrating T Cells. *Immunity*, *50*(1), 181-194 e186. https://doi.org/10.1016/j.immuni.2018.11.014

Kvedaraite, E., & Ginhoux, F. (2022). Human dendritic cells in cancer. *Sci Immunol*, *7*(70), eabm9409. https://doi.org/10.1126/sciimmunol.abm9409

Labidi-Galy, S. I., Treilleux, I., Goddard-Leon, S., Combes, J. D., Blay, J. Y., Ray-Coquard, I., Caux, C., & Bendriss-Vermare, N. (2012). Plasmacytoid dendritic cells infiltrating ovarian cancer are associated with poor prognosis. *Oncoimmunology*, *1*(3), 380-382. https://doi.org/10.4161/onci.18801

Lambrechts, D., Wauters, E., Boeckx, B., Aibar, S., Nittner, D., Burton, O., Bassez, A., Decaluwe, H., Pircher, A., Van den Eynde, K., Weynand, B., Verbeken, E., De Leyn, P., Liston, A., Vansteenkiste, J., Carmeliet, P., Aerts, S., & Thienpont, B. (2018). Phenotype molding of stromal cells in the lung tumor microenvironment. *Nat Med*, *24*(8), 1277-1289. https://doi.org/10.1038/s41591-018-0096-5

Lasek, W., Zagożdżon, R., & Jakobisiak, M. (2014). Interleukin 12: still a promising candidate for tumor immunotherapy? *Cancer Immunol Immunother*, *63*(5), 419-435. https://doi.org/10.1007/s00262-014-1523-1

Le Naour, J., Galluzzi, L., Zitvogel, L., Kroemer, G., & Vacchelli, E. (2020). Trial watch: TLR3 agonists in cancer therapy. *Oncoimmunology*, *9*(1), 1771143. https://doi.org/10.1080/2162402X.2020.1771143

Leader, A. M., Grout, J. A., Maier, B. B., Nabet, B. Y., Park, M. D., Tabachnikova, A., Chang, C., Walker, L., Lansky, A., Le Berichel, J., Troncoso, L., Malissen, N., Davila, M., Martin, J. C., Magri, G., Tuballes, K., Zhao, Z., Petralia, F., Samstein, R., . . . Merad, M. (2021). Single-cell analysis of human non-small cell lung cancer lesions refines tumor classification and patient stratification. *Cancer Cell*. https://doi.org/10.1016/j.ccell.2021.10.009

Lecis, D., Sangaletti, S., Colombo, M. P., & Chiodoni, C. (2019). Immune Checkpoint Ligand Reverse Signaling: Looking Back to Go Forward in Cancer Therapy. *Cancers (Basel)*, *11*(5). https://doi.org/10.3390/cancers11050624

Li, H., van der Leun, A. M., Yofe, I., Lubling, Y., Gelbard-Solodkin, D., van Akkooi, A. C. J., van den Braber, M., Rozeman, E. A., Haanen, J., Blank, C. U., Horlings, H. M., David, E., Baran, Y., Bercovich, A., Lifshitz, A., Schumacher, T. N., Tanay, A., & Amit, I. (2019). Dysfunctional CD8 T Cells Form a Proliferative, Dynamically Regulated Compartment within Human Melanoma. *Cell*, *176*(4), 775-789 e718. https://doi.org/10.1016/j.cell.2018.11.043

Liu, Y., & Zheng, P. (2020). Preserving the CTLA-4 Checkpoint for Safer and More Effective Cancer Immunotherapy. *Trends Pharmacol Sci*, *41*(1), 4-12. https://doi.org/10.1016/j.tips.2019.11.003

Lu, H. (2014). TLR Agonists for Cancer Immunotherapy: Tipping the Balance between the Immune Stimulatory and Inhibitory Effects. *Front Immunol*, *5*, 83. https://doi.org/10.3389/fimmu.2014.00083

Lucas, E. D., Schafer, J. B., Matsuda, J., Kraus, M., Burchill, M. A., & Tamburini, B. A. J. (2020). PD-L1 Reverse Signaling in Dermal Dendritic Cells Promotes Dendritic Cell Migration Required for Skin Immunity. *Cell Rep*, *33*(2), 108258. https://doi.org/10.1016/j.celrep.2020.108258

Maier, B., Leader, A. M., Chen, S. T., Tung, N., Chang, C., LeBerichel, J., Chudnovskiy, A., Maskey, S., Walker, L., Finnigan, J. P., Kirkling, M. E., Reizis, B., Ghosh, S., D'Amore, N. R., Bhardwaj, N., Rothlin, C. V., Wolf, A., Flores, R., Marron, T., . . . Merad, M. (2020). A conserved dendritic-cell regulatory program limits antitumour immunity. *Nature*, *580*(7802), 257-262. https://doi.org/10.1038/s41586-020-2134-y

Marciscano, A. E., Walker, J. M., McGee, H. M., Kim, M. M., Kunos, C. A., Monjazeb, A. M., Shiao, S. L., Tran, P. T., & Ahmed, M. M. (2018). Incorporating Radiation Oncology into Immunotherapy: proceedings from the ASTRO-SITC-NCI immunotherapy workshop. *J Immunother Cancer*, *6*(1), 6. https://doi.org/10.1186/s40425-018-0317-y

Martin, K., Muller, P., Schreiner, J., Prince, S. S., Lardinois, D., Heinzelmann-Schwarz, V. A., Thommen, D. S., & Zippelius, A. (2014). The microtubule-depolymerizing agent ansamitocin P3 programs dendritic cells toward enhanced anti-tumor immunity. *Cancer Immunol Immunother*, *63*(9), 925-938. https://doi.org/10.1007/s00262-014-1565-4

Matsuzawa, T., Kuwae, A., Yoshida, S., Sasakawa, C., & Abe, A. (2004). Enteropathogenic Escherichia coli activates the RhoA signaling pathway via the stimulation of GEF-H1. *EMBO J*, *23*(17), 3570-3582. https://doi.org/10.1038/sj.emboj.7600359

Mayoux, M., Roller, A., Pulko, V., Sammicheli, S., Chen, S., Sum, E., Jost, C., Fransen, M. F., Buser, R. B., Kowanetz, M., Rommel, K., Matos, I., Colombetti, S., Belousov, A., Karanikas, V., Ossendorp, F., Hegde, P. S., Chen, D. S., Umana, P., . . . Xu, W. (2020). Dendritic cells dictate responses to PD-L1 blockade cancer immunotherapy. *Sci Transl Med*, *12*(534). https://doi.org/10.1126/scitranslmed.aav7431

McShane, L. M., Altman, D. G., Sauerbrei, W., Taube, S. E., Gion, M., Clark, G. M., & Statistics Subcommittee of the, N. C. I. E. W. G. o. C. D. (2005). Reporting recommendations for tumor marker prognostic studies. *J Clin Oncol*, *23*(36), 9067-9072. https://doi.org/10.1200/JCO.2004.01.0454

Meiri, D., Marshall, C. B., Greeve, M. A., Kim, B., Balan, M., Suarez, F., Bakal, C., Wu, C., Larose, J., Fine, N., Ikura, M., & Rottapel, R. (2012). Mechanistic insight into the microtubule and actin cytoskeleton coupling through dynein-dependent RhoGEF inhibition. *Mol Cell*, *45*(5), 642-655. https://doi.org/10.1016/j.molcel.2012.01.027

Melief, C. J. (2008). Cancer immunotherapy by dendritic cells. *Immunity*, *29*(3), 372-383. https://doi.org/10.1016/j.immuni.2008.08.004

Mellman, I., & Steinman, R. M. (2001). Dendritic cells: specialized and regulated antigen processing machines. *Cell*, *106*(3), 255-258. https://doi.org/10.1016/s0092-8674(01)00449-4

Michaud, M., Martins, I., Sukkurwala, A. Q., Adjemian, S., Ma, Y., Pellegatti, P., Shen, S., Kepp, O., Scoazec, M., Mignot, G., Rello-Varona, S., Tailler, M., Menger, L., Vacchelli, E., Galluzzi, L., Ghiringhelli, F., di Virgilio, F., Zitvogel, L., & Kroemer, G. (2011). Autophagy-dependent anticancer immune responses induced by chemotherapeutic agents in mice. *Science*, *334*(6062), 1573-1577. https://doi.org/10.1126/science.1208347

Mikucki, M. E., Fisher, D. T., Matsuzaki, J., Skitzki, J. J., Gaulin, N. B., Muhitch, J. B., Ku, A. W., Frelinger, J. G., Odunsi, K., Gajewski, T. F., Luster, A. D., & Evans, S. S. (2015). Non-redundant requirement for CXCR3 signalling during tumoricidal T-cell trafficking across tumour vascular checkpoints. *Nat Commun*, *6*, 7458. https://doi.org/10.1038/ncomms8458

Mildner, A., & Jung, S. (2014). Development and function of dendritic cell subsets. *Immunity*, *40*(5), 642-656. https://doi.org/10.1016/j.immuni.2014.04.016

Miller, B. C., Sen, D. R., Al Abosy, R., Bi, K., Virkud, Y. V., LaFleur, M. W., Yates, K. B., Lako, A., Felt, K., Naik, G. S., Manos, M., Gjini, E., Kuchroo, J. R., Ishizuka, J. J., Collier, J. L., Griffin, G. K., Maleri, S., Comstock, D. E., Weiss, S. A., . . . Haining, W. N. (2019). Subsets of exhausted CD8(+) T cells differentially mediate tumor control and respond to checkpoint blockade. *Nat Immunol*, *20*(3), 326-336. https://doi.org/10.1038/s41590-019-0312-6

Mita, M. M., Spear, M. A., Yee, L. K., Mita, A. C., Heath, E. I., Papadopoulos, K. P., Federico, K. C., Reich, S. D., Romero, O., Malburg, L., Pilat, M., Lloyd, G. K., Neuteboom, S. T., Cropp, G., Ashton, E., & LoRusso, P. M. (2010). Phase 1 first-in-human trial of the vascular disrupting agent plinabulin(NPI-2358) in patients with solid tumors or lymphomas. *Clin Cancer Res*, *16*(23), 5892-5899. https://doi.org/10.1158/1078-0432.CCR-10-1096

Mittag, D., Proietto, A. I., Loudovaris, T., Mannering, S. I., Vremec, D., Shortman, K., Wu, L., & Harrison, L. C. (2011). Human dendritic cell subsets from spleen and blood are similar in phenotype and function but modified by donor health status. *J Immunol*, *186*(11), 6207-6217. https://doi.org/10.4049/jimmunol.1002632

Mizumoto, N., Gao, J., Matsushima, H., Ogawa, Y., Tanaka, H., & Takashima, A. (2005). Discovery of novel immunostimulants by dendritic-cell-based functional screening. *Blood*, *106*(9), 3082-3089. https://doi.org/10.1182/blood-2005-03-1161

Mizumoto, N., Tanaka, H., Matsushima, H., Vishwanath, M., & Takashima, A. (2007). Colchicine promotes antigen cross-presentation by murine dendritic cells. *J Invest Dermatol*, *127*(6), 1543-1546. https://doi.org/10.1038/sj.jid.5700699

Mohanlal, R., Aren, O. R., Polikoff, J., Reich, S. D., Mikrut, W., Huang, L., & Bazhenova, L. (2016). The plinabulin/docetaxel combination to mitigate the known safety concerns of docetaxel. *Journal of Clinical Oncology*, *34*(15_suppl), e20595-e20595. https://doi.org/10.1200/JCO.2016.34.15_suppl.e20595

Molavi, O., Ma, Z., Hamdy, S., Lai, R., Lavasanifar, A., & Samuel, J. (2008). Synergistic antitumor effects of CpG oligodeoxynucleotide and STAT3 inhibitory agent JSI-124 in a mouse melanoma tumor model. *Immunol Cell Biol*, *86*(6), 506-514. https://doi.org/10.1038/icb.2008.27

Monaco, G., van Dam, S., Casal Novo Ribeiro, J. L., Larbi, A., & de Magalhaes, J. P. (2015). A comparison of human and mouse gene co-expression networks reveals conservation and divergence at the tissue, pathway and disease levels. *BMC Evol Biol*, *15*, 259. https://doi.org/10.1186/s12862-015-0534-7

Morris, M. A., Gibb, D. R., Picard, F., Brinkmann, V., Straume, M., & Ley, K. (2005). Transient T cell accumulation in lymph nodes and sustained lymphopenia in mice treated with FTY720. *Eur J Immunol*, *35*(12), 3570-3580. https://doi.org/10.1002/eji.200526218

Movassagh, M., Spatz, A., Davoust, J., Lebecque, S., Romero, P., Pittet, M., Rimoldi, D., Liénard, D., Gugerli, O., Ferradini, L., Robert, C., Avril, M. F., Zitvogel, L., & Angevin, E. (2004). Selective accumulation of mature DC-Lamp+ dendritic cells in tumor sites is associated with efficient T-cell-mediated antitumor response and control of metastatic dissemination in melanoma. *Cancer Res*, *64*(6), 2192-2198. https://doi.org/10.1158/0008-5472.can-03-2969

Muller, P., Kreuzaler, M., Khan, T., Thommen, D. S., Martin, K., Glatz, K., Savic, S., Harbeck, N., Nitz, U., Gluz, O., von Bergwelt-Baildon, M., Kreipe, H., Reddy, S., Christgen, M., & Zippelius, A. (2015). Trastuzumab emtansine (T-DM1) renders HER2+ breast cancer highly susceptible to CTLA-4/PD-1 blockade. *Sci Transl Med*, *7*(315), 315ra188. https://doi.org/10.1126/scitranslmed.aac4925

Müller, P., Martin, K., Theurich, S., Schreiner, J., Savic, S., Terszowski, G., Lardinois, D., Heinzelmann-Schwarz, V. A., Schlaak, M., Kvasnicka, H. M., Spagnoli, G., Dirnhofer, S., Speiser, D. E., von Bergwelt-Baildon, M., & Zippelius, A. (2014). Microtubule-depolymerizing agents used in antibody-drug conjugates induce antitumor immunity by stimulation of dendritic cells. *Cancer Immunol Res*, *2*(8), 741-755. https://doi.org/10.1158/2326-6066.Cir-13-0198

Muller, P., Martin, K., Theurich, S., von Bergwelt-Baildon, M., & Zippelius, A. (2014). Cancer chemotherapy agents target intratumoral dendritic cells to potentiate antitumor immunity. *Oncoimmunology*, *3*(8), e954460. https://doi.org/10.4161/21624011.2014.954460

Nagarsheth, N., Wicha, M. S., & Zou, W. (2017). Chemokines in the cancer microenvironment and their relevance in cancer immunotherapy. *Nat Rev Immunol*, *17*(9), 559-572. https://doi.org/10.1038/nri.2017.49

Nefedova, Y., Nagaraj, S., Rosenbauer, A., Muro-Cacho, C., Sebti, S. M., & Gabrilovich, D. I. (2005). Regulation of dendritic cell differentiation and antitumor immune response in cancer by pharmacologic-selective inhibition of the janus-activated kinase 2/signal transducers and activators of transcription 3 pathway. *Cancer Res*, *65*(20), 9525-9535. https://doi.org/10.1158/0008-5472.Can-05-0529

Newman, A. M., Liu, C. L., Green, M. R., Gentles, A. J., Feng, W., Xu, Y., Hoang, C. D., Diehn, M., & Alizadeh, A. A. (2015). Robust enumeration of cell subsets from tissue expression profiles. *Nat Methods*, *12*(5), 453-457. https://doi.org/10.1038/nmeth.3337

Ni, L., & Lu, J. (2018). Interferon gamma in cancer immunotherapy. *Cancer Med*, *7*(9), 4509-4516. https://doi.org/10.1002/cam4.1700

Nierkens, S., den Brok, M. H., Roelofsen, T., Wagenaars, J. A., Figdor, C. G., Ruers, T. J., & Adema, G. J. (2009). Route of administration of the TLR9 agonist CpG critically determines the efficacy of cancer immunotherapy in mice. *PLoS One*, *4*(12), e8368. https://doi.org/10.1371/journal.pone.0008368

O'Shea, E. K., Klemm, J. D., Kim, P. S., & Alber, T. (1991). X-ray structure of the GCN4 leucine zipper, a two-stranded, parallel coiled coil. *Science*, *254*(5031), 539-544. https://doi.org/10.1126/science.1948029

Odate, S., Veschi, V., Yan, S., Lam, N., Woessner, R., & Thiele, C. J. (2017). Inhibition of STAT3 with the Generation 2.5 Antisense Oligonucleotide, AZD9150, Decreases Neuroblastoma Tumorigenicity and Increases Chemosensitivity. *Clin Cancer Res*, *23*(7), 1771-1784. https://doi.org/10.1158/1078-0432.Ccr-16-1317

Oh, S. A., Wu, D. C., Cheung, J., Navarro, A., Xiong, H., Cubas, R., Totpal, K., Chiu, H., Wu, Y., Comps-Agrar, L., Leader, A. M., Merad, M., Roose-Germa, M., Warming, S., Yan, M., Kim, J. M., Rutz, S., & Mellman, I. (2020). PD-L1 expression by dendritic cells is a key regulator of T-cell immunity in cancer. *Nat Cancer*, *1*(7), 681-691. https://doi.org/10.1038/s43018-020-0075-x

Olieric, N., Kuchen, M., Wagen, S., Sauter, M., Crone, S., Edmondson, S., Frey, D., Ostermeier, C., Steinmetz, M. O., & Jaussi, R. (2010). Automated seamless DNA co-transformation cloning with direct expression vectors applying positive or negative insert selection. *BMC Biotechnol*, *10*, 56. https://doi.org/10.1186/1472-6750-10-56

Oosterhoff, D., Lougheed, S., van de Ven, R., Lindenberg, J., van Cruijsen, H., Hiddingh, L., Kroon, J., van den Eertwegh, A. J., Hangalapura, B., Scheper, R. J., & de Gruijl, T. D. (2012). Tumor-mediated inhibition of human dendritic cell differentiation and function is consistently counteracted by combined p38 MAPK and STAT3 inhibition. *Oncoimmunology*, *1*(5), 649-658. https://doi.org/10.4161/onci.20365

Palucka, K., & Banchereau, J. (2012). Cancer immunotherapy via dendritic cells. *Nat Rev Cancer*, *12*(4), 265-277. https://doi.org/10.1038/nrc3258

Pan, C., Liu, H., Robins, E., Song, W., Liu, D., Li, Z., & Zheng, L. (2020). Next-generation immuno-oncology agents: current momentum shifts in cancer immunotherapy. *J Hematol Oncol*, *13*(1), 29. https://doi.org/10.1186/s13045-020-00862-w

Pandey, S., Singh, S., Anang, V., Bhatt, A. N., Natarajan, K., & Dwarakanath, B. S. (2015). Pattern Recognition Receptors in Cancer Progression and Metastasis. *Cancer Growth Metastasis*, *8*, 25-34. https://doi.org/10.4137/CGM.S24314

Patente, T. A., Pelgrom, L. R., & Everts, B. (2019). Dendritic cells are what they eat: how their metabolism shapes T helper cell polarization. *Curr Opin Immunol*, *58*, 16-23. https://doi.org/10.1016/j.coi.2019.02.003

Perrot, I., Michaud, H. A., Giraudon-Paoli, M., Augier, S., Docquier, A., Gros, L., Courtois, R., Déjou, C., Jecko, D., Becquart, O., Rispaud-Blanc, H., Gauthier, L., Rossi, B., Chanteux, S., Gourdin, N., Amigues, B., Roussel, A., Bensussan, A., Eliaou, J. F., . . . Bonnefoy, N. (2019). Blocking Antibodies Targeting the CD39/CD73

Immunosuppressive Pathway Unleash Immune Responses in Combination Cancer Therapies. *Cell Rep*, *27*(8), 2411-2425.e2419. https://doi.org/10.1016/j.celrep.2019.04.091

Prota, A. E., Bargsten, K., Diaz, J. F., Marsh, M., Cuevas, C., Liniger, M., Neuhaus, C., Andreu, J. M., Altmann, K. H., & Steinmetz, M. O. (2014). A new tubulin-binding site and pharmacophore for microtubule-destabilizing anticancer drugs. *Proc Natl Acad Sci U S A*, *111*(38), 13817-13821. https://doi.org/10.1073/pnas.1408124111

Qian, J., Olbrecht, S., Boeckx, B., Vos, H., Laoui, D., Etlioglu, E., Wauters, E., Pomella, V., Verbandt, S., Busschaert, P., Bassez, A., Franken, A., Bempt, M. V., Xiong, J., Weynand, B., van Herck, Y., Antoranz, A., Bosisio, F. M., Thienpont, B., . . . Lambrechts, D. (2020). A pan-cancer blueprint of the heterogeneous tumor microenvironment revealed by single-cell profiling. *Cell Res*, *30*(9), 745-762. https://doi.org/10.1038/s41422-020-0355-0

Qin, S., Xu, L., Yi, M., Yu, S., Wu, K., & Luo, S. (2019). Novel immune checkpoint targets: moving beyond PD-1 and CTLA-4. *Mol Cancer*, *18*(1), 155. https://doi.org/10.1186/s12943-019-1091-2

Quezada, S. A., Simpson, T. R., Peggs, K. S., Merghoub, T., Vider, J., Fan, X., Blasberg, R., Yagita, H., Muranski, P., Antony, P. A., Restifo, N. P., & Allison, J. P. (2010). Tumor-reactive CD4(+) T cells develop cytotoxic activity and eradicate large established melanoma after transfer into lymphopenic hosts. *J Exp Med*, *207*(3), 637-650. https://doi.org/10.1084/jem.20091918

Qureshi, O. S., Zheng, Y., Nakamura, K., Attridge, K., Manzotti, C., Schmidt, E. M., Baker, J., Jeffery, L. E., Kaur, S., Briggs, Z., Hou, T. Z., Futter, C. E., Anderson, G., Walker, L. S., & Sansom, D. M. (2011). Trans-endocytosis of CD80 and CD86: a molecular basis for the cell-extrinsic function of CTLA-4. *Science*, *332*(6029), 600-603. https://doi.org/10.1126/science.1202947

Ravelli, R. B., Gigant, B., Curmi, P. A., Jourdain, I., Lachkar, S., Sobel, A., & Knossow, M. (2004). Insight into tubulin regulation from a complex with colchicine and a stathmin-like domain. *Nature*, *428*(6979), 198-202. https://doi.org/10.1038/nature02393

Riaz, N., Havel, J. J., Makarov, V., Desrichard, A., Urba, W. J., Sims, J. S., Hodi, F. S., Martin-Algarra, S., Mandal, R., Sharfman, W. H., Bhatia, S., Hwu, W. J., Gajewski, T. F., Slingluff, C. L., Jr., Chowell, D., Kendall, S. M., Chang, H., Shah, R., Kuo, F., . . . Chan, T. A. (2017). Tumor and Microenvironment Evolution during Immunotherapy with Nivolumab. *Cell*, *171*(4), 934-949 e916. https://doi.org/10.1016/j.cell.2017.09.028

Ribas, A., Medina, T., Kirkwood, J. M., Zakharia, Y., Gonzalez, R., Davar, D., Chmielowski, B., Campbell, K. M., Bao, R., Kelley, H., Morris, A., Mauro, D., Wooldridge, J. E., Luke, J. J., Weiner, G. J., Krieg, A. M., & Milhem, M. M. (2021). Overcoming PD-1 Blockade Resistance with CpG-A Toll-Like Receptor 9 Agonist Vidutolimod in Patients with Metastatic Melanoma. *Cancer Discov*. https://doi.org/10.1158/2159-8290.CD-21-0425

Ribas, A., & Wolchok, J. D. (2018). Cancer immunotherapy using checkpoint blockade. *Science*, *359*(6382), 1350-1355. https://doi.org/10.1126/science.aar4060

Riley, J. L. (2009). PD-1 signaling in primary T cells. *Immunol Rev*, *229*(1), 114-125. https://doi.org/10.1111/j.1600-065X.2009.00767.x

Robbins, P. F., Lu, Y. C., El-Gamil, M., Li, Y. F., Gross, C., Gartner, J., Lin, J. C., Teer, J. K., Cliften, P., Tycksen, E., Samuels, Y., & Rosenberg, S. A. (2013). Mining exomic sequencing data to identify mutated antigens recognized by adoptively transferred tumor-reactive T cells. *Nat Med*, *19*(6), 747-752. https://doi.org/10.1038/nm.3161

Robert, C. (2020). A decade of immune-checkpoint inhibitors in cancer therapy. *Nat Commun*, *11*(1), 3801. https://doi.org/10.1038/s41467-020-17670-y

Roberts, E. W., Broz, M. L., Binnewies, M., Headley, M. B., Nelson, A. E., Wolf, D. M., Kaisho, T., Bogunovic, D., Bhardwaj, N., & Krummel, M. F. (2016). Critical Role for CD103(+)/CD141(+) Dendritic Cells Bearing CCR7 for Tumor Antigen Trafficking and Priming of T Cell Immunity in Melanoma. *Cancer Cell*, *30*(2), 324-336. https://doi.org/10.1016/j.ccell.2016.06.003

Robinson, M. D., McCarthy, D. J., & Smyth, G. K. (2010). edgeR: a Bioconductor package for differential expression analysis of digital gene expression data. *Bioinformatics*, *26*(1), 139-140. https://doi.org/10.1093/bioinformatics/btp616

Rodrigues, P. F., Alberti-Servera, L., Eremin, A., Grajales-Reyes, G. E., Ivanek, R., & Tussiwand, R. (2018). Distinct progenitor lineages contribute to the heterogeneity of plasmacytoid dendritic cells. *Nat Immunol*, *19*(7), 711-722. https://doi.org/10.1038/s41590-018-0136-9

Rowshanravan, B., Halliday, N., & Sansom, D. M. (2018). CTLA-4: a moving target in immunotherapy. *Blood*, *131*(1), 58-67. https://doi.org/10.1182/blood-2017-06-741033

Saleh, R., & Elkord, E. (2020a). Acquired resistance to cancer immunotherapy: Role of tumor-mediated immunosuppression. *Semin Cancer Biol*, *65*, 13-27. https://doi.org/10.1016/j.semcancer.2019.07.017

Saleh, R., & Elkord, E. (2020b). FoxP3(+) T regulatory cells in cancer: Prognostic biomarkers and therapeutic targets. *Cancer Lett*, *490*, 174-185. https://doi.org/10.1016/j.canlet.2020.07.022

Salmon, H., Idoyaga, J., Rahman, A., Leboeuf, M., Remark, R., Jordan, S., Casanova-Acebes, M., Khudoynazarova, M., Agudo, J., Tung, N., Chakarov, S., Rivera, C., Hogstad, B., Bosenberg, M., Hashimoto, D., Gnjatic, S., Bhardwaj, N., Palucka, A. K., Brown, B. D., . . . Merad, M. (2016). Expansion and Activation of CD103(+) Dendritic Cell Progenitors at the Tumor Site Enhances Tumor Responses to Therapeutic PD-L1 and BRAF Inhibition. *Immunity*, *44*(4), 924-938. https://doi.org/10.1016/j.immuni.2016.03.012

Sato-Kaneko, F., Yao, S., Ahmadi, A., Zhang, S. S., Hosoya, T., Kaneda, M. M., Varner, J. A., Pu, M., Messer, K. S., Guiducci, C., Coffman, R. L., Kitaura, K., Matsutani, T., Suzuki, R., Carson, D. A., Hayashi, T., & Cohen, E. E. (2017). Combination immunotherapy with TLR agonists and checkpoint inhibitors suppresses head and neck cancer. *JCI Insight*, *2*(18). https://doi.org/10.1172/jci.insight.93397

Satpathy, A. T., Kc, W., Albring, J. C., Edelson, B. T., Kretzer, N. M., Bhattacharya, D., Murphy, T. L., & Murphy, K. M. (2012). Zbtb46 expression distinguishes classical dendritic cells and their committed progenitors from other immune lineages. *J Exp Med*, *209*(6), 1135-1152. https://doi.org/10.1084/jem.20120030

Sauerbrei, W., Royston, P., & Binder, H. (2007). Selection of important variables and determination of functional form for continuous predictors in multivariable model building. *Stat Med*, *26*(30), 5512-5528. https://doi.org/10.1002/sim.3148

Schachter, J., Ribas, A., Long, G. V., Arance, A., Grob, J. J., Mortier, L., Daud, A., Carlino, M. S., McNeil, C., Lotem, M., Larkin, J., Lorigan, P., Neyns, B., Blank, C., Petrella, T. M., Hamid, O., Zhou, H., Ebbinghaus, S., Ibrahim, N., & Robert, C. (2017). Pembrolizumab versus ipilimumab for advanced melanoma: final overall survival results of a multicentre, randomised, open-label phase 3 study (KEYNOTE-006). *Lancet*, *390*(10105), 1853-1862. https://doi.org/10.1016/s0140-6736(17)31601-x

Schreiber, R. D., Old, L. J., & Smyth, M. J. (2011). Cancer immunoediting: integrating immunity's roles in cancer suppression and promotion. *Science*, *331*(6024), 1565-1570. https://doi.org/10.1126/science.1203486

Schwartz, R. H. (2003). T cell anergy. *Annu Rev Immunol*, *21*, 305-334. https://doi.org/10.1146/annurev.immunol.21.120601.141110

Sckisel, G. D., Bouchlaka, M. N., Monjazeb, A. M., Crittenden, M., Curti, B. D., Wilkins, D. E., Alderson, K. A., Sungur, C. M., Ames, E., Mirsoian, A., Reddy, A., Alexander, W., Soulika, A., Blazar, B. R., Longo, D. L., Wiltrout, R. H., & Murphy, W. J. (2015). Out-of-Sequence Signal 3 Paralyzes Primary CD4(+) T-Cell-Dependent Immunity. *Immunity*, *43*(2), 240-250. https://doi.org/10.1016/j.immuni.2015.06.023

Seeger, P., Musso, T., & Sozzani, S. (2015). The TGF-β superfamily in dendritic cell biology. *Cytokine Growth Factor Rev*, *26*(6), 647-657. https://doi.org/10.1016/j.cytogfr.2015.06.002

Segura, E., Touzot, M., Bohineust, A., Cappuccio, A., Chiocchia, G., Hosmalin, A., Dalod, M., Soumelis, V., & Amigorena, S. (2013). Human inflammatory dendritic cells induce Th17 cell differentiation. *Immunity*, *38*(2), 336-348. https://doi.org/10.1016/j.immuni.2012.10.018

Selby, M. J., Engelhardt, J. J., Quigley, M., Henning, K. A., Chen, T., Srinivasan, M., & Korman, A. J. (2013). Anti-CTLA-4 antibodies of IgG2a isotype enhance antitumor activity through reduction of intratumoral regulatory T cells. *Cancer Immunol Res*, *1*(1), 32-42. https://doi.org/10.1158/2326-6066.Cir-13-0013

Sharma, N., Vacher, J., & Allison, J. P. (2019). TLR1/2 ligand enhances antitumor efficacy of CTLA-4 blockade by increasing intratumoral Treg depletion. *Proc Natl Acad Sci U S A*, *116*(21), 10453-10462. https://doi.org/10.1073/pnas.1819004116

Sharma, P., Hu-Lieskovan, S., Wargo, J. A., & Ribas, A. (2017). Primary, Adaptive, and Acquired Resistance to Cancer Immunotherapy. *Cell*, *168*(4), 707-723. https://doi.org/10.1016/j.cell.2017.01.017

Shastri, A., Choudhary, G., Teixeira, M., Gordon-Mitchell, S., Ramachandra, N., Bernard, L., Bhattacharyya, S., Lopez, R., Pradhan, K., Giricz, O., Ravipati, G., Wong, L. F., Cole, S., Bhagat, T. D., Feld, J., Dhar, Y., Bartenstein, M., Thiruthuvanathan, V. J., Wickrema, A., . . . Verma, A. (2018). Antisense STAT3 inhibitor decreases viability of myelodysplastic and leukemic stem cells. *J Clin Invest*, *128*(12), 5479-5488. https://doi.org/10.1172/jci120156

Shekarian, T., Valsesia-Wittmann, S., Brody, J., Michallet, M. C., Depil, S., Caux, C., & Marabelle, A. (2017). Pattern recognition receptors: immune targets to enhance cancer immunotherapy. *Ann Oncol*, *28*(8), 1756-1766. https://doi.org/10.1093/annonc/mdx179

Shen, X., & Zhao, B. (2018). Efficacy of PD-1 or PD-L1 inhibitors and PD-L1 expression status in cancer: meta-analysis. *BMJ*, *362*, k3529. https://doi.org/10.1136/bmj.k3529

Shi, Y., Yu, P., Zeng, D., Qian, F., Lei, X., Zhao, Y., Tang, B., Hao, Y., Luo, H., Chen, J., & Tan, Y. (2014). Suppression of vascular endothelial growth factor abrogates the immunosuppressive capability of murine gastric

cancer cells and elicits antitumor immunity. *Febs j*, *281*(17), 3882-3893. https://doi.org/10.1111/febs.12923

Siddiqui, I., Schaeuble, K., Chennupati, V., Fuertes Marraco, S. A., Calderon-Copete, S., Pais Ferreira, D., Carmona, S. J., Scarpellino, L., Gfeller, D., Pradervand, S., Luther, S. A., Speiser, D. E., & Held, W. (2019). Intratumoral Tcf1(+)PD-1(+)CD8(+) T Cells with Stem-like Properties Promote Tumor Control in Response to Vaccination and Checkpoint Blockade Immunotherapy. *Immunity*, *50*(1), 195-211 e110. https://doi.org/10.1016/j.immuni.2018.12.021

Simpson, T. R., Li, F., Montalvo-Ortiz, W., Sepulveda, M. A., Bergerhoff, K., Arce, F., Roddie, C., Henry, J. Y., Yagita, H., Wolchok, J. D., Peggs, K. S., Ravetch, J. V., Allison, J. P., & Quezada, S. A. (2013). Fc-dependent depletion of tumor-infiltrating regulatory T cells co-defines the efficacy of anti-CTLA-4 therapy against melanoma. *J Exp Med*, *210*(9), 1695-1710. https://doi.org/10.1084/jem.20130579

Sisirak, V., Faget, J., Gobert, M., Goutagny, N., Vey, N., Treilleux, I., Renaudineau, S., Poyet, G., Labidi-Galy, S. I., Goddard-Leon, S., Durand, I., Le Mercier, I., Bajard, A., Bachelot, T., Puisieux, A., Puisieux, I., Blay, J. Y., Ménétrier-Caux, C., Caux, C., & Bendriss-Vermare, N. (2012). Impaired IFN-α production by plasmacytoid dendritic cells favors regulatory T-cell expansion that may contribute to breast cancer progression. *Cancer Res*, *72*(20), 5188-5197. https://doi.org/10.1158/0008-5472.Can-11-3468

Sosa Cuevas, E., Bendriss-Vermare, N., Mouret, S., De Fraipont, F., Charles, J., Valladeau-Guilemond, J., Chaperot, L., & Aspord, C. (2022). Diversification of circulating and tumor-infiltrating plasmacytoid DCs towards the P3 (CD80(+) PDL1(-))-pDC subset negatively correlated with clinical outcomes in melanoma patients. *Clin Transl Immunology*, *11*(5), e1382. https://doi.org/10.1002/cti2.1382

Spranger, S., Bao, R., & Gajewski, T. F. (2015). Melanoma-intrinsic β-catenin signalling prevents anti-tumour immunity. *Nature*, *523*(7559), 231-235. https://doi.org/10.1038/nature14404

Spranger, S., Dai, D., Horton, B., & Gajewski, T. F. (2017). Tumor-Residing Batf3 Dendritic Cells Are Required for Effector T Cell Trafficking and Adoptive T Cell Therapy. *Cancer Cell*, *31*(5), 711-723 e714. https://doi.org/10.1016/j.ccell.2017.04.003

Steinmetz, M. O., & Prota, A. E. (2018). Microtubule-Targeting Agents: Strategies To Hijack the Cytoskeleton. *Trends Cell Biol*, *28*(10), 776-792. https://doi.org/10.1016/j.tcb.2018.05.001

Sugiura, D., Maruhashi, T., Okazaki, I. M., Shimizu, K., Maeda, T. K., Takemoto, T., & Okazaki, T. (2019). Restriction of PD-1 function by cis-PD-L1/CD80 interactions is required for optimal T cell responses. *Science*, *364*(6440), 558-566. https://doi.org/10.1126/science.aav7062

Sun, C., Mezzadra, R., & Schumacher, T. N. (2018). Regulation and Function of the PD-L1 Checkpoint. *Immunity*, *48*(3), 434-452. https://doi.org/10.1016/j.immuni.2018.03.014

Swiecki, M., & Colonna, M. (2015). The multifaceted biology of plasmacytoid dendritic cells. *Nat Rev Immunol*, *15*(8), 471-485. https://doi.org/10.1038/nri3865

Takeshima, H., & Ushijima, T. (2019). Accumulation of genetic and epigenetic alterations in normal cells and cancer risk. *NPJ Precis Oncol*, *3*, 7. https://doi.org/10.1038/s41698-019-0079-0

Tamburini, B. A. J. (2021). Contributions of PD-L1 reverse signaling to dendritic cell trafficking. *Febs j*. https://doi.org/10.1111/febs.16084

Tan, M. C., Goedegebuure, P. S., Belt, B. A., Flaherty, B., Sankpal, N., Gillanders, W. E., Eberlein, T. J., Hsieh, C. S., & Linehan, D. C. (2009). Disruption of CCR5-dependent homing of regulatory T cells inhibits tumor growth in a murine model of pancreatic cancer. *J Immunol*, *182*(3), 1746-1755. https://doi.org/10.4049/jimmunol.182.3.1746

Tanaka, H., Matsushima, H., Nishibu, A., Clausen, B. E., & Takashima, A. (2009). Dual therapeutic efficacy of vinblastine as a unique chemotherapeutic agent capable of inducing dendritic cell maturation. *Cancer Res*, *69*(17), 6987-6994. https://doi.org/10.1158/0008-5472.CAN-09-1106

Tang, F., & Zheng, P. (2018). Tumor cells versus host immune cells: whose PD-L1 contributes to PD-1/PD-L1 blockade mediated cancer immunotherapy? *Cell Biosci*, *8*, 34. https://doi.org/10.1186/s13578-018-0232-4

Tang, H., Wang, Y., Chlewicki, L. K., Zhang, Y., Guo, J., Liang, W., Wang, J., Wang, X., & Fu, Y. X. (2016). Facilitating T Cell Infiltration in Tumor Microenvironment Overcomes Resistance to PD-L1 Blockade. *Cancer Cell*, *29*(3), 285-296. https://doi.org/10.1016/j.ccell.2016.02.004

Tang, J., Pearce, L., O'Donnell-Tormey, J., & Hubbard-Lucey, V. M. (2018). Trends in the global immuno-oncology landscape. *Nat Rev Drug Discov*, *17*(12), 922. https://doi.org/10.1038/nrd.2018.202

Thompson, M. R., Xu, D., & Williams, B. R. (2009). ATF3 transcription factor and its emerging roles in immunity and cancer. *J Mol Med (Berl)*, *87*(11), 1053-1060. https://doi.org/10.1007/s00109-009-0520-x

Topalian, S. L., Taube, J. M., Anders, R. A., & Pardoll, D. M. (2016). Mechanism-driven biomarkers to guide immune checkpoint blockade in cancer therapy. *Nat Rev Cancer*, *16*(5), 275-287. https://doi.org/10.1038/nrc.2016.36

Turley, S. J., Inaba, K., Garrett, W. S., Ebersold, M., Unternaehrer, J., Steinman, R. M., & Mellman, I. (2000). Transport of peptide-MHC class II complexes in developing dendritic cells. *Science*, *288*(5465), 522-527. https://doi.org/10.1126/science.288.5465.522

Ullrich, O., Reinsch, S., Urbe, S., Zerial, M., & Parton, R. G. (1996). Rab11 regulates recycling through the pericentriolar recycling endosome. *J Cell Biol*, *135*(4), 913-924. https://doi.org/10.1083/jcb.135.4.913

van Dam, S., Cordeiro, R., Craig, T., van Dam, J., Wood, S. H., & de Magalhães, J. P. (2012). GeneFriends: an online co-expression analysis tool to identify novel gene targets for aging and complex diseases. *BMC Genomics*, *13*, 535. https://doi.org/10.1186/1471-2164-13-535

Verma, S., Miles, D., Gianni, L., Krop, I. E., Welslau, M., Baselga, J., Pegram, M., Oh, D. Y., Dieras, V., Guardino, E., Fang, L., Lu, M. W., Olsen, S., Blackwell, K., & Group, E. S. (2012). Trastuzumab emtansine for HER2-positive advanced breast cancer. *N Engl J Med*, *367*(19), 1783-1791. https://doi.org/10.1056/NEJMoa1209124

Vigneron, N. (2015). Human Tumor Antigens and Cancer Immunotherapy. *Biomed Res Int*, *2015*, 948501. https://doi.org/10.1155/2015/948501

Villani, A. C., Satija, R., Reynolds, G., Sarkizova, S., Shekhar, K., Fletcher, J., Griesbeck, M., Butler, A., Zheng, S., Lazo, S., Jardine, L., Dixon, D., Stephenson, E., Nilsson, E., Grundberg, I., McDonald, D., Filby, A., Li, W., De Jager, P. L., . . . Hacohen, N. (2017). Single-cell RNA-seq reveals new types of human blood dendritic cells, monocytes, and progenitors. *Science*, *356*(6335). https://doi.org/10.1126/science.aah4573

von Minckwitz, G., Huang, C. S., Mano, M. S., Loibl, S., Mamounas, E. P., Untch, M., Wolmark, N., Rastogi, P., Schneeweiss, A., Redondo, A., Fischer, H. H., Jacot, W., Conlin, A. K., Arce-Salinas, C., Wapnir, I. L., Jackisch, C., DiGiovanna, M. P., Fasching, P. A., Crown, J. P., . . . Investigators, K. (2019). Trastuzumab Emtansine for Residual Invasive HER2-Positive Breast Cancer. *N Engl J Med*, *380*(7), 617-628. https://doi.org/10.1056/NEJMoa1814017

Wculek, S. K., Cueto, F. J., Mujal, A. M., Melero, I., Krummel, M. F., & Sancho, D. (2020). Dendritic cells in cancer immunology and immunotherapy. *Nat Rev Immunol*, *20*(1), 7-24. https://doi.org/10.1038/s41577-019-0210-z

Wei, S. C., Anang, N. A. S., Sharma, R., Andrews, M. C., Reuben, A., Levine, J. H., Cogdill, A. P., Mancuso, J. J., Wargo, J. A., Pe'er, D., & Allison, J. P. (2019). Combination anti-CTLA-4 plus anti-PD-1 checkpoint blockade utilizes cellular mechanisms partially distinct from monotherapies. *Proc Natl Acad Sci U S A*, *116*(45), 22699-22709. https://doi.org/10.1073/pnas.1821218116

Wei, S. C., Duffy, C. R., & Allison, J. P. (2018). Fundamental Mechanisms of Immune Checkpoint Blockade Therapy. *Cancer Discov*, *8*(9), 1069-1086. https://doi.org/10.1158/2159-8290.CD-18-0367

Wendel, M., Galani, I. E., Suri-Payer, E., & Cerwenka, A. (2008). Natural killer cell accumulation in tumors is dependent on IFN-gamma and CXCR3 ligands. *Cancer Res*, *68*(20), 8437-8445. https://doi.org/10.1158/0008-5472.Can-08-1440

Woloschak, G. E., Shearin-Jones, P., & Chang-Liu, C. M. (1990). Effects of ionizing radiation on expression of genes encoding cytoskeletal elements: kinetics and dose effects. *Mol Carcinog*, *3*(6), 374-378. https://doi.org/10.1002/mc.2940030609

Woo, S. R., Fuertes, M. B., Corrales, L., Spranger, S., Furdyna, M. J., Leung, M. Y., Duggan, R., Wang, Y., Barber, G. N., Fitzgerald, K. A., Alegre, M. L., & Gajewski, T. F. (2014). STING-dependent cytosolic DNA sensing mediates innate immune recognition of immunogenic tumors. *Immunity*, *41*(5), 830-842. https://doi.org/10.1016/j.immuni.2014.10.017

Xin Yu, J., Hodge, J. P., Oliva, C., Neftelinov, S. T., Hubbard-Lucey, V. M., & Tang, J. (2020). Trends in clinical development for PD-1/PD-L1 inhibitors. *Nat Rev Drug Discov*, *19*(3), 163-164. https://doi.org/10.1038/d41573-019-00182-w

Xiong, H., Veedu, R. N., & Diermeier, S. D. (2021). Recent Advances in Oligonucleotide Therapeutics in Oncology. *Int J Mol Sci*, *22*(7). https://doi.org/10.3390/ijms22073295

Xiong, W., Gao, Y., Wei, W., & Zhang, J. (2021). Extracellular and nuclear PD-L1 in modulating cancer immunotherapy. *Trends Cancer*, *7*(9), 837-846. https://doi.org/10.1016/j.trecan.2021.03.003

Yamaguchi, H., Hsu, J. M., Yang, W. H., & Hung, M. C. (2022). Mechanisms regulating PD-L1 expression in cancers and associated opportunities for novel small-molecule therapeutics. *Nat Rev Clin Oncol*, *19*(5), 287-305. https://doi.org/10.1038/s41571-022-00601-9

Yanai, H., Ban, T., Wang, Z., Choi, M. K., Kawamura, T., Negishi, H., Nakasato, M., Lu, Y., Hangai, S., Koshiba, R., Savitsky, D., Ronfani, L., Akira, S., Bianchi, M. E., Honda, K., Tamura, T., Kodama, T., & Taniguchi, T.

(2009). HMGB proteins function as universal sentinels for nucleic-acid-mediated innate immune responses. *Nature*, *462*(7269), 99-103. https://doi.org/10.1038/nature08512

Yang, F., Jiang, M., Lu, M., Hu, P., Wang, H., & Jiang, J. (2018). Pharmacokinetic Behavior of Vincristine and Safety Following Intravenous Administration of Vincristine Sulfate Liposome Injection in Chinese Patients With Malignant Lymphoma. *Front Pharmacol*, *9*, 991. https://doi.org/10.3389/fphar.2018.00991

Younes, A., Bartlett, N. L., Leonard, J. P., Kennedy, D. A., Lynch, C. M., Sievers, E. L., & Forero-Torres, A. (2010). Brentuximab vedotin (SGN-35) for relapsed CD30-positive lymphomas. *N Engl J Med*, *363*(19), 1812-1821. https://doi.org/10.1056/NEJMoa1002965

Zaremba, T. G., & Irwin, R. D. (1981). Effects of ionizing radiation on the polymerization of microtubules in vitro. *Biochemistry*, *20*(5), 1323-1332. https://doi.org/10.1021/bi00508a044

Zhang, L., Li, Z., Skrzypczynska, K. M., Fang, Q., Zhang, W., O'Brien, S. A., He, Y., Wang, L., Zhang, Q., Kim, A., Gao, R., Orf, J., Wang, T., Sawant, D., Kang, J., Bhatt, D., Lu, D., Li, C. M., Rapaport, A. S., . . . Yu, X. (2020). Single-Cell Analyses Inform Mechanisms of Myeloid-Targeted Therapies in Colon Cancer. *Cell*, *181*(2), 442-459 e429. https://doi.org/10.1016/j.cell.2020.03.048

Zhang, Q., He, Y., Luo, N., Patel, S. J., Han, Y., Gao, R., Modak, M., Carotta, S., Haslinger, C., Kind, D., Peet, G. W., Zhong, G., Lu, S., Zhu, W., Mao, Y., Xiao, M., Bergmann, M., Hu, X., Kerkar, S. P., . . . Zhang, Z. (2019). Landscape and Dynamics of Single Immune Cells in Hepatocellular Carcinoma. *Cell*, *179*(4), 829-845 e820. https://doi.org/10.1016/j.cell.2019.10.003

Zhao, Y., Alonso, C., Ballester, I., Song, J. H., Chang, S. Y., Guleng, B., Arihiro, S., Murray, P. J., Xavier, R., Kobayashi, K. S., & Reinecker, H. C. (2012). Control of NOD2 and Rip2-dependent innate immune activation by GEF-H1. *Inflamm Bowel Dis*, *18*(4), 603-612. https://doi.org/10.1002/ibd.21851

Zhao, Y., Lee, C. K., Lin, C. H., Gassen, R. B., Xu, X., Huang, Z., Xiao, C., Bonorino, C., Lu, L. F., Bui, J. D., & Hui, E. (2019). PD-L1:CD80 Cis-Heterodimer Triggers the Co-stimulatory Receptor CD28 While Repressing the Inhibitory PD-1 and CTLA-4 Pathways. *Immunity*, *51*(6), 1059-1073 e1059. https://doi.org/10.1016/j.immuni.2019.11.003

Zhao, Y., Zagani, R., Park, S. M., Yoshida, N., Shah, P., & Reinecker, H. C. (2019). Microbial recognition by GEF-H1 controls IKKepsilon mediated activation of IRF5. *Nat Commun*, *10*(1), 1349. https://doi.org/10.1038/s41467-019-09283-x

Zilionis, R., Engblom, C., Pfirschke, C., Savova, V., Zemmour, D., Saatcioglu, H. D., Krishnan, I., Maroni, G., Meyerovitz, C. V., Kerwin, C. M., Choi, S., Richards, W. G., De Rienzo, A., Tenen, D. G., Bueno, R., Levantini, E., Pittet, M. J., & Klein, A. M. (2019). Single-Cell Transcriptomics of Human and Mouse Lung Cancers Reveals Conserved Myeloid Populations across Individuals and Species. *Immunity*, *50*(5), 1317-1334 e1310. https://doi.org/10.1016/j.immuni.2019.03.009

Zitvogel, L., Galluzzi, L., Smyth, M. J., & Kroemer, G. (2013). Mechanism of action of conventional and targeted anticancer therapies: reinstating immunosurveillance. *Immunity*, *39*(1), 74-88. https://doi.org/10.1016/j.immuni.2013.06.014

Zou, S., Tong, Q., Liu, B., Huang, W., Tian, Y., & Fu, X. (2020). Targeting STAT3 in Cancer Immunotherapy. *Mol Cancer*, *19*(1), 145. https://doi.org/10.1186/s12943-020-01258-7

Contributions

1. GEFH1 signaling upon microtubule destabilization is required for dendritic cell activation and specific anti-tumor responsesPD-L1 ASO

Figure 1. Microtubule destabilization, but not stabilization, induces DC maturation

D) Isolation of splenic DCs, treatment, and readout using flow cytometry. (D) represents the quantification
E) and (E) the representative dot plots.

Figure 5. Involvement of GEFH1 in microtubule destabilization-induced DC activation

C) Generation of BMDC from WT and GEFH1 KO mice, treatment and readout of activation markers using flow cytometry KO mice

D) Treatment and readout of WT and GEFH1 KO XS106 cells using flow cytometry

E) Injection of LPS, Ansamitociin P3 or DMSO in earplafs of WT and GEFH1 KO mice, harvesting, digestion, staining and readout using flow cytometry.

Figure 6. Assessment of GEF-H1 in T Cell expansion and antitumor immunity.

A,B,C) Injecton of Cell trace violet OT-I T cells in WT and GEFH1 KO mice (i.v. injections). OVA immunization and treatment of mice, dLN collection, processing, and readout using flow cytometry.

D,E) Injecton of Cell trace violet OT-I T cells in WT and GEFH1 KO mice (i.v. injections). Peptide immunization and treatment of mice, dLN collection, processing, and readout using flow cytometry.

F,G) Same as B,C and but with OT-II instead of OT-I

H) I performed the whole experiment several times from MC38 wt cell culture to MC38 cell injection in mice (s.c.), measurement of tumors, scoring of mice, sorting, treatment of mice and readout (tumor growth and survival).

Supplementary Materials

Supplementary Figure S1 (Related to Figure 1)

D) Representative histograms from Figure 1D, E.

Supplementary Figure S5 (Related to Figure 5)

A) Representative plots from Figure 5c

B) Representative plots from Figure 5d

C) Treatment and readout of WT and GEFH1 KO XS106 cells using flow cytometry

D) Representative histograms from Figure S5c

E) Representative dot plots from Figure 5e

Supplementary Figure S6 (Related to Figure 6)

A) Co-culture of BMDCs from WT and GEFH1 KO mice with OVA pulsed OT-I T cells labeled with Cell trace violet and treated with LPS or Ansamitocin P3. Readout using flow cytometry

B) Co-culture of BMDCs from WT and GEFH1 KO mice with OVA pulsed OT-II T cells Cell trace violet and treated with LPS or Ansamitocin P3. Readout using flow cytometry

In addition, I created the Key Resources table and helped with the written part of the experiemnts I performed (main text and material and methods). I also helped with the point by point reply of the revision.

2. Dual TLR9 and PD-L1 targeting unleashes dendritic cells to induce durable antitumor immunity in mice

Figure 1. Anti-PD-L1-mAb does not stimulate sufficient DC3 and T cell activation in MC38 tumors.

A) I designed and organized the experiment (number of mice, groups of treatment, doses, schedule) and supervised the experiment performed by Mélanie Buchi

B) I planned, organized and performed this experiment. Tumor cell injection, sorting of the mice, measurement, treatment and readout. I harvested, processed and stained the tumors for readout in Cytek Aurora. I then analyzed and represented the data.

C) Chiara Cianciaruso and myself planned the experiments and Chiara performed them

D)

Figure 2. IM-T9P1-ASO stimulates in vitro DC activation and IL-12 secretion while decreasing PD-L1 expression

A-G) Chiara Cianciaruso and myself planned the experiments and Chiara performed them

Figure 3. IM-T9P1-ASO therapeutic in vivo efficacy depends on both TLR9 stimulation and PD-L1 downregulation.

A) Mélanie Buchi and Elham Pishali performed these experiments

B) Mélanie Buchi and Elham Pishali performed these experiments

C) Ruben Bill performed this experiment

D) Melanie Buchi and Elham Pishali performed these experiments

E,F) I run this experiment. Cell injection, measurement of tumor in the mice, treatment, harvesting of the tumors, processing and readout using cytek aurora.

G) I planned, organized and performed this experiment. Tumor cell injection, sorting of the mice, measurement, treatment and readout (tumor growth and overall survival)

H) Performed by Chiara Cianciaruso

I) I planned, organized and performed this experiment. Tumor cell injection, sorting of the mice, measurement, treatment and readout (tumor growth and overall survival)

Fig. 4. Increased frequency of migDCs in tumor-draining lymph nodes after IM-T9P1-ASO therapy.

A,B,C,D) I planned, organized and performed this experiment. Tumor cell injection, sorting of the mice, measurement, treatment and readout. I harvested, processed and stained the dLN and non-draining lymph nodes for Cytek Aurora. I then analyzed and represented the data.

E) I planned, organized and performed this experiment. Tumor cell injection, sorting of the mice, measurement, treatment and readout (tumor growth and overall survival)

Fig. 5. IM-T9P1-ASO increases intratumoral IL-12+ DC3s.

A) I performed this experiment. Tumor cell culture, tumor cell injection, measurement, scoring, readout (tumor growth and survival)

B) I planned, organized and performed this experiment. Tumor cell injection, sorting of the mice, measurement, treatment and readout. I harvested and processed and stained the tumors for Cytek Aurora. I then analyzed and represented the data.

C) I planned and organized this experiment. Mélanie Buchi injected the cells, treated and measured the mice.

D) Performed by Chiara Cianciaruso, Ruben Bill and Rainer Kohler

E) I planned, organized and performed this experiment. Tumor cell injection, sorting of the mice, measurement, treatment and readout. I harvested and processed and stained the tumors for Cytek Aurora. I then analyzed and represented the data.

F) Chiara and I performed the experiment. Chiara generated the data on the IL-12-eYFP+ mice and I did it in WT mice. We both harvested, processed and stained the the tumors, run the samples in the cytek Aurora.

G) I planned, organized and performed this experiment. Tumor cell injection, sorting of the mice, measurement, treatment and readout. I harvested and processed and stained the tumors for Cytek Aurora. I then analyzed and represented the data.

H) I performed this experiment. Tumor cell culture, tumor cell injection, measurement, scoring, readout (tumor growth and survival)

I) Chiara Cianciaruso performed this experiment in IL-12p40 KO and WT mice

Fig. 6. *CD274* and TLR expression across human myeloid population and enrichment of IL-12 and DC signatures in melanoma patients responding to ICI

A) I looked into the datasets and generated the figures

B) I created the IL12 and the different DC signatures based on published data. Marcel Trefny run the analysis in the Riaz et al. dataset.

C) Chiara did this analysis

D) Chiara did the schematic representation

Supplementary Figures and Tables

Table 1 I generated the signatures based on public available data and created the table

Fig S1 Flow cytometry gating strategy for immune cell populations and immune cell analysis of LN in anti-PD-L1-mAb treated MC38 tumor bearing mice.

A,B) Mélanie Buchi and Elham Pishali run this experiment

C) I run this experiment and generated the gating strategy

D) I planned, organized and performed this experiment. Tumor cell injection, sorting of the mice, measurement, treatment and readout. I harvested and processed and stained the dLN for Cytek Aurora. I

E) I planned, organized and performed this experiment. Tumor cell injection, sorting of the mice, measurement, treatment and readout. I harvested and processed and stained the tumors for Cytek Aurora. I then analyzed and represented the data.

Fig. S2. TLR9 expression in MC38 tumors and *in vitro* validation of IM-T9P1-ASO.

A) Chiara Cianciaruso performed this experiment

B) Invivogen

C,D) Elhan Pishali generated these data, I analyzed and represented them

Fig. S3. Biodistribution and tolerability of IM-T9P1-ASO.

A,B,C,D) Chiara performed this experiment with the help of Rainer Kohler

E) Mélanie Buchi and Elham Pishali performed this experiment

F)
G) Chiara performed this experiment with the help of Rainer Kohler.

Fig. S4. IM-T9P1-ASO efficacy in different tumor models

A) Ruben Bill performed this experiment

B) Mélanie Buchi performed this experiment

C) I planned, organized and performed this experiment. Tumor cell injection, sorting of the mice, measurement, treatment and readout (tumor growth and overall survival)

D) Chiara generated the MC38 PDL1 KO cell line

E) I planned, organized and performed this experiment. Tumor cell injection, sorting of the mice, measurement, treatment and readout (tumor growth and overall survival)

F) I planned, organized and performed this experiment. Tumor cell injection, sorting of the mice, measurement, treatment and readout. I harvested and processed and stained the dLN for Cytek Aurora. I then analyzed and represented the data.

Fig. S5. DC3 gating strategy, pDC depletion and role of IL-12+ DC3s during IM-T9P1-ASO treatment.

A) I performed this experiment and generated the gating strategy

B) I planned, organized and performed this experiment. Tumor cell injection, sorting of the mice, measurement, treatment and readout. I harvested and processed and stained the tumors for Cytek Aurora. I then analyzed and represented the data.

C) I bleeded the mice and tested the blood for presence of pDCs using Cytek Aurora

D) I planned, organized and performed this experiment. Tumor cell injection, sorting of the mice, measurement, treatment and readout. I harvested and processed and stained the tumors for Cytek Aurora. I then analyzed and represented the data.

E) Chiara performed this experiment

F) Chiara performed this experiment

G) I performed this experiment

H) Chiara performed this experiment

Fig. S6. Enrichment of DC3 genes and TLR screening across different human tumors.

A) I generated the DC3 cell signature based on publicly available data and represented the DC3 enrichement in the Pan-cancer dataset of Cheng et al 2021

B,C) Chiara did the analysis

Movie S1: Chiara performed the intravital imaging with the help of Rainer Kohler

In addition I generated the figure outline, wrote the the first draft of the manuscript and implemented the comments and edits from Chiara, Alfred Zippelius, Mikael Pittet and other colleagues who contributed to the revision of the manuscript.